ASSESSMENT AND DEVELOPMENT OF REMOTELY SENSED EVAPOTRANSPIRATION MODELING APPROACHES

By

KUL BIKRAM KHAND

Bachelor of Science in Agricultural Engineering
Tribhuvan University
Kathmandu, Nepal
2010

Master of Science in Agricultural and Biosystems Engineering
South Dakota State University
Brookings, South Dakota
2014

Submitted to the Faculty of the
Graduate College of the
Oklahoma State University
in partial fulfillment of
the requirements for
the Degree of
DOCTOR OF PHILOSOPHY
May, 2019

ASSESSMENT AND DEVELOPMENT OF

REMOTELY SENSED EVAPOTRANSPIRATION

MODELING APPROACHES

Dissertation Approved:

Dr. Saleh Taghvaeian

Dissertation Adviser

Dr. Paul R. Weckler

Dr. Prasanna H. Gowda

Dr. Phillip Alderman

ACKNOWLEDGEMENTS

I would like to thank my advisor Dr. Saleh Taghvaeian for his guidance and encouragement throughout my studies. I would also like to thank my committee members Dr. Prasanna Gowda, Dr. Paul Weckler, and Dr. Phillip Alderman for their time and valuable suggestions to improve my research studies. Thanks to my collaborators Dr. Leila Hassan-Esfahani, Dr. George Paul, Dr. Nishan Bhattarai, and Dr. Pradeep Wagle for helping me during several phases of my research. I am grateful for the support from faculty members and staffs at the Biosystems and Agricultural Engineering Department. I acknowledge the Oklahoma Water Resources Center and all other funding agencies for supporting my research.

Thanks to my colleagues Blessing Masasi, Jacob Stivers, Ali Ajaz, Sumon Datta, Divya Handa, Mukesh Mehata, Sunil Thapa, Avinash Gupta, Prajwal Upadhaya, Nabin Paudel, and others who supported during my research and class works. Finally, I would like to thank my wife Rama Shah, sister Shanti Khand, parents Mina Kumari Khand and Tul Bahadur Khand for their love, support, and encouragement.

Name: KUL BIKRAM KHAND

Date of Degree: MAY, 2019

Title of Study: ASSESSMENT AND DEVELOPMENT OF REMOTELY SENSED EVAPOTRANSPIRATION MODELING APPROACHES

Major Field: BIOSYSTEMS AND AGRICULTURAL ENGINEERING

Abstract: Remote sensing has been a promising approach to extracting distributed evapotranspiration (ET) information at varying spatial and temporal scales. Performances of several vegetation index (VI) based and remotely sensed surface energy balance (RSEB) models were evaluated to identify simple and accurate models and apply them to study ET variations from field to regional scales. A simple VI model using a single Landsat image to estimate annual ET was evaluated and successfully captured inter-annual riparian ET variations along a section of the Colorado River, U.S. The study showed the applicability of a simple and accurate approach for annual ET estimation with fewer data and resources. A modeling framework was developed to derive daily time series of ET maps using a RSEB model, satellite imagery, and ground-based weather data. The daily and annual ET maps obtained from the modeling framework successfully captured spatial and temporal ET variations across Oklahoma, U.S. The model also identified the regions that are more susceptible to droughts. Finally, five RSEB models were evaluated for their performance in estimating daily ET of winter wheat under variable grazing and tillage practices in central Oklahoma. The surface energy balance algorithm for land (SEBAL) had the best agreement whit eddy covariance estimates. The daily ET estimates from SEBAL captured the field-scale ET variations within grazing/tillage managements. All studies conducted based on VI and RSEB models over different land covers and spatial/temporal scales identified advantages and limitations of models and developed a framework to construct time series of ET maps, which has a wide range of applications.

TABLE OF CONTENTS

Chapter Page

LIST OF TABLES

Table Page

LIST OF FIGURES

Figure Page

CHAPTER I

INTRODUCTION

1. Background

Evapotranspiration (ET) is the process of water vapor transfer from earth's surface to the atmosphere. It includes evaporation from the soil surface, waterbodies and canopy interception, and transpiration from vegetation through their stomata. ET is the largest outgoing component of the earth's surface water and energy balance, accounting for about 60% of precipitation (Brutsaert, 2005; Seckler, Amarasinghe, Molden, de Silva & Barker, 1998) and about 50% of energy (Kiehl & Trenberth, 1997; Wild et al., 2013) absorbed at the surface at global scale. Therefore, ET is an important variable to understand earth's climate system, which is largely regulated by the water and energy fluxes. Several applications in hydrology, agriculture, water resources management, meteorology, and ecology require ET information at varying spatial and temporal scales. In agricultural sector, ET information has been applied for irrigation scheduling (Allen, Pereira, Raes, & Smith, 1998), water right regulation and planning (Allen, Tasumi, Morse, & Trezza, 2005), assessing irrigation and drainage performance (Droogers & Bastiaanssen, 2002; Khand, Kjaersgaard, Hay, & Jia, 2017; Taghvaeian, Neale, Osterberg, Sritharan, & Watts, 2018), yield analysis (Cai & Sharma, 2010), assessing crop water productivity (Zwart & Bastiaanssen, 2004) and monitoring agricultural droughts (Anderson et al., 2011; Moorhead et al., 2015).

Other studies have used ET for a range of applications such as assessing vulnerability of forest to fire and drought (Nepstad et al., 2004), estimating groundwater recharge (Healy, 2010), capturing the progress of vegetation and wetland restoration (Oberg & Melesss, 2006), estimating ecosystem water balances (Sun et al., 2011), and for climate studies capturing water feedbacks associated with seasonal cycles and soil moisture deficit at regional scales (Vinukollu, Wood, Ferguson, & Fisher, 2011). While ET information have been used across multitude of applications, accurate quantification of ET is often challenging because it exhibits high spatial and temporal variability (Kustas & Norman, 1996) involving complex interactions between climate (e.g., solar radiation, air temperature, wind speed, humidity) and environmental variables (e.g., soil properties, crop characteristics, soil moisture, management practices).

The governing factors of evaporation have been explored since early 19th century (Dalton, 1802). In the mid-1990s, Penman (1948) developed an evaporation equation based on available energy and turbulent flux theory for surfaces under full water supply conditions. Later, Monteith (1964) integrated surface (or canopy) resistance component in the Penman's evaporation equation to obtain the well-known Penman-Monteith equation. During the same period, other empirical evaporation estimation approaches were introduced (Blaney & Criddle, 1950; Thornthwaite, 1948). The crop specific ET estimation method was advanced by Allen et al. (1998), as a product of reference ET and crop coefficient, to account for the reduction in potential crop ET due to limiting factors such as water and salinity stresses. Field-based instrumentation approaches such as weighing lysimeters (Daamen, Simmonds, Wallace, Laryea, & Sivakumar, 1993), sap flow (Smith & Allen, 1993), Bowen ratio energy balance (Denmead, Dunin, Wong, & Greenwood, 1993), and eddy covariance systems (Baldocchi, Hincks, & Meyers, 1998) have been also used for quantifying ET.

All of these ET estimation and measurement approaches provide information at a point scale or a few meters to a few hundred meters area and do not account for the spatial variability of ET at heterogeneous landcovers (Gowda et al., 2008). Remote sensing has proven to be a viable alternative

for capturing ET variability at varying temporal and spatial scales (Allen et al., 2011; Bastiaanssen et al., 2005; Glenn, Huete, Nagler, Hirschboeck, & Brown, 2007). Remote sensing methods for estimating ET can be broadly categorized into two major groups: empirical approaches based on vegetation indices (VI); and, physical process-based remotely sensed surface energy balance (RSEB) method. Both approaches have been applied to estimate ET from agricultural and natural ecosystems. The commonly used VI includes normalized difference vegetation index (NDVI; Tucker et al., 1979), enhanced vegetation index (EVI; Huete et al., 2002), and soil adjusted vegetation index (SAVI; Huete, 1988). These approaches are based on plant-specific VI relationship with biomass and can account the transpiration from plants, which is heavily dependent on foliage density. However, the direct evaporation from the soil or from leaves following the rainfall events is not incorporated in this approach. Further, VIs cannot quickly detect the plant stress due to limited soil moisture, diseases or pests, until the suboptimal condition last long enough to affect biomass (Nagler et al., 2005). Thus, VI approaches are more suitable to estimate ET for a longer time – over a crop cycle or annual cycle for natural vegetation (Glenn et al., 2007).

In contrast, RSEB method integrates the land surface temperature, which can reflect the impact of short-term environmental stressors on ET (Anderson, Norman, Mecikalski, Otkin, & Kustas, 2007; Bartholic, Namkem, & Wiegand, 1972; Kustas & Norman, 1999), and can be applied over diverse climatic conditions and ecosystems (Gowda et al., 2008). Numerous RSEB models have been proposed in the past. Some of the commonly used ones includes: Two-Source Energy Balance (TSEB) (Norman, Kustas, & Humes, 1995), Surface Energy Balance Algorithm for Land (SEBAL) (Bastiaanssen, Menenti, Feddes, & Holtslag, 1998), Simplified Surface Energy Balance Index (S-SEBI) (Roerink, Su, & Menenti, 2000), Surface Energy Balance System (SEBS) (Su, 2002), Mapping Evapotranspiration at high Resolution with Internalized Calibration (METRIC) (Allen, Tasumi, & Trezza, 2007), Atmosphere-Land Exchange Inverse (ALEXI) (Anderson et al., 2007), and Operational Simplified Surface Energy Balance (SSEBop) (Senay et al., 2013). Some of the RSEB

models such as SEBAL and METRIC use a manual selection of extreme pixels to compute ET, whereas, other models do not require human intervention. In general, the RSEB models are data intensive and often require multi-step processing compared to the VI approaches. The selection of an ET estimation method could vary depending on intended applications of ET information, availability of input data, and the resources (time, money, expertise) available.

2. Statement of the Problem

Simple VI approaches may be adequate when the study is focused over a specific land cover (Glenn et al., 2007), but would fail over larger and more complex terrains. The RSEB models provide an advantage over VI approaches with potential application for regional and global scale. However, these models are not widely applied for the operational decision makings and need further research and development (Amatya et al., 2016). In addition, although RSEB models have been able to provide accurate ET information for several applications (Liou & Kar, 2014), the performance evaluation of these models shows that they tend to provide good estimates under specific land cover or climatic conditions (Bhattarai, Shaw, Quackenbush, Im, & Niraula, 2016; Timmermans, Kustas, Anderson, & French, 2007). Further evaluation of these models under several hydroclimatic conditions, crop types, and management practices could help to identify a suitable model for a specific area and to assess the strength and weakness of these models for improvements. Another limitation of remote sensing methods is the need of several cloud-free satellite images to cover the study period. Thus, exploring the methods that use smaller number of satellite imagery, fewer input data, simpler formulation, and with larger temporal coverage could provide a major advancement for obtaining distributed ET information.

3. Goals and Objectives

The main goal of this research is to assess and identify suitable VI and RSEB approaches for ET estimation across agricultural and natural vegetation by addressing the shortcomings mentioned above and to develop a framework to provide distributed ET information at a regional scale. The specific objectives are:

1. To investigate the performance of a simple VI-based approach (single-satellite-scene) that requires minimal input data to estimate annual ET from riparian vegetation;

2. To develop an ET modeling framework to produce daily ET maps using a RSEB model and to analyze the applicability of this framework to study ET variations across Oklahoma; and,

3. To evaluate the performances of several RSEB models in capturing ET dynamics in response to variable tillage, grazing, and crop-rotation practices.

References

Allen, R. G., Pereira, L. S., Raes, D., & Smith, M. (1998). Crop Evapotranspiration-Guidelines for computing crop water requirements-FAO Irrigation and drainage paper 56. Fao, Rome, 300(9), D05109.

Allen, R. G., Tasumi, M., & Trezza, R. (2007). Satellite-based energy balance for mapping evapotranspiration with internalized calibration (METRIC)—Model. *Journal of irrigation and drainage engineering*, *133*(4), 380-394.

Allen, R. G., Tasumi, M., Morse, A., & Trezza, R. (2005). A Landsat-based energy balance and evapotranspiration model in Western US water rights regulation and planning. *Irrigation and Drainage systems*, *19*(3-4), 251-268.

Allen, R., Irmak, A., Trezza, R., Hendrickx, J. M., Bastiaanssen, W., & Kjaersgaard, J. (2011). Satellite- based ET estimation in agriculture using SEBAL and METRIC. *Hydrological Processes*, *25*(26), 4011-4027.

Amatya, D. M., Irmak, S., Gowda, P., Sun, G., Nettles, J. E., & Douglas-Mankin, K. R. (2016). Ecosystem evapotranspiration: challenges in measurements, estimates, and modeling. *Transactions of the ASABE*, *59*(2), 555-560.

Anderson, M. C., Hain, C., Wardlow, B., Pimstein, A., Mecikalski, J. R., & Kustas, W. P. (2011). Evaluation of drought indices based on thermal remote sensing of evapotranspiration over the continental United States. *Journal of Climate*, *24*(8), 2025-2044.

Anderson, M. C., Norman, J. M., Mecikalski, J. R., Otkin, J. A., & Kustas, W. P. (2007). A climatological study of evapotranspiration and moisture stress across the continental United States based on thermal remote sensing: 1. Model formulation. *Journal of Geophysical Research: Atmospheres*, *112*(D10).

Baldocchi, D. D., Hincks, B. B., & Meyers, T. P. (1988). Measuring biosphere- atmosphere exchanges of biologically related gases with micrometeorological methods. *Ecology*, *69*(5), 1331-1340.

Bartholic, J. F., Namkem, L. N., & Wiegand, C. L. (1972). Aerial Thermal Scanner to Determine Temperatures of Soils and of Crop Canopies Differing in Water Stress 1. *Agronomy Journal*, *64*(5), 603-608.

Bastiaanssen, W. G. M., Noordman, E. J. M., Pelgrum, H., Davids, G., Thoreson, B. P., & Allen, R. G. (2005). SEBAL model with remotely sensed data to improve water-resources management under actual field conditions. *Journal of irrigation and drainage engineering*, *131*(1), 85-93.

Bastiaanssen, W. G., Menenti, M., Feddes, R. A., & Holtslag, A. A. M. (1998). A remote sensing surface energy balance algorithm for land (SEBAL). 1. Formulation. *Journal of - hydrology*, *212*, 198-212.

Bhattarai, N., Shaw, S. B., Quackenbush, L. J., Im, J., & Niraula, R. (2016). Evaluating five remote sensing based single-source surface energy balance models for estimating daily evapotranspiration in a humid subtropical climate. *International journal of applied earth observation and geoinformation*, *49*, 75-86.

Blaney, H.F., & Criddle, W.D. (1950). Determining water requirements in irrigated areas from climatological and irrigation data. In (p. 48pp): US Department of Agriculture Soil Conservation Service.

Brutsaert, W., 2005. *Hydrology: an introduction*. Cambridge University Press, New York.

Cai, X. L., & Sharma, B. R. (2010). Integrating remote sensing, census and weather data for an assessment of rice yield, water consumption and water productivity in the Indo-Gangetic river basin. *Agricultural Water Management*, *97*(2), 309-316.

Daamen, C. C., Simmonds, L. P., Wallace, J. S., Laryea, K. B., & Sivakumar, M. V. K. (1993). Use of microlysimeters to measure evaporation from sandy soils. *Agricultural and Forest Meteorology*, *65*(3-4), 159-173.

Dalton, J. (1802). Experimental assays on the constitution of mixed gases; on the force of steam of vapor from waters and other liquids in different temperatures, both in a torricellian vacuum and in air; on evaporation; and on the expansion of gases by heat. *Memoirs of the Manchester Lit. & Phil. Soc*., 535-602.

Denmead, O. T., Dunin, F. X., Wong, S. C., & Greenwood, E. A. N. (1993). Measuring water use efficiency of eucalypt trees with chambers and micrometeorological techniques. *Journal of Hydrology*, *150*(2-4), 649-664.

Droogers, P., & Bastiaanssen, W. (2002). Irrigation performance using hydrological and remote sensing modeling. *Journal of Irrigation and Drainage Engineering*, *128*(1), 11-18.

Glenn, E. P., Huete, A. R., Nagler, P. L., Hirschboeck, K. K., & Brown, P. (2007). Integrating remote sensing and ground methods to estimate evapotranspiration. *Critical Reviews in Plant Sciences*, *26*(3), 139-168.

Gowda, P. H., Chavez, J. L., Colaizzi, P. D., Evett, S. R., Howell, T. A., & Tolk, J. A. (2008). ET mapping for agricultural water management: present status and challenges. *Irrigation science*, *26*(3), 223-237.

Healy, R. W. (2010). *Estimating groundwater recharge*. Cambridge University Press.

Huete, A. R. (1988). A soil-adjusted vegetation index (SAVI). *Remote Sensing of Environment*, *25*(3), 295-309.

Huete, A., Didan, K., Miura, T., Rodriguez, E. P., Gao, X., & Ferreira, L. G. (2002). Overview of the radiometric and biophysical performance of the MODIS vegetation indices. *Remote Sensing of Environment*, *83*(1-2), 195-213.

Khand, K., Kjaersgaard, J., Hay, C., & Jia, X. (2017). Estimating impacts of agricultural subsurface drainage on evapotranspiration using the Landsat imagery-based METRIC model. *Hydrology*, *4*(4), 49.

Kiehl, J. T., & Trenberth, K. E. (1997). Earth's annual global mean energy budget. *Bulletin of the American Meteorological Society*, *78*(2), 197-208.

Kustas, W. P., & Norman, J. M. (1996). Use of remote sensing for evapotranspiration monitoring over land surfaces. *Hydrological Sciences Journal*, *41*(4), 495-516.

Kustas, W. P., & Norman, J. M. (1999). Evaluation of soil and vegetation heat flux predictions using a simple two-source model with radiometric temperatures for partial canopy cover. *Agricultural and Forest Meteorology*, *94*(1), 13-29.

Liou, Y. A., & Kar, S. K. (2014). Evapotranspiration estimation with remote sensing and various surface energy balance algorithms—A review. *Energies*, *7*(5), 2821-2849.

Monteith, J.L. (1964). The state of movement of water in living organisms. *In, Evaporation and environment* (pp. 205-234). Cambridge: Cambridge Univ. Press.

Moorhead, J. E., Gowda, P. H., Singh, V. P., Porter, D. O., Marek, T. H., Howell, T. A., & Stewart, B. A. (2015). Identifying and evaluating a suitable index for agricultural drought monitoring in the Texas high plains. JAWRA Journal of the American Water Resources Association, 51(3), 807-820.

Nagler, P. L., Scott, R. L., Westenburg, C., Cleverly, J. R., Glenn, E. P., & Huete, A. R. (2005). Evapotranspiration on western US rivers estimated using the Enhanced Vegetation Index from MODIS and data from eddy covariance and Bowen ratio flux towers. *Remote Sensing of Environment*, 97(3), 337-351.

Nepstad, D., Lefebvre, P., Lopes da Silva, U., Tomasella, J., Schlesinger, P., Solórzano, L., Moutinho, P., Ray, D., & Guerreira Benito, J. (2004). Amazon drought and its

implications for forest flammability and tree growth: A basin- wide analysis. *Global change biology*, *10*(5), 704-717.

Norman, J. M., Kustas, W. P., & Humes, K. S. (1995). Source approach for estimating soil and vegetation energy fluxes in observations of directional radiometric surface temperature. *Agricultural and Forest Meteorology*, *77*(3-4), 263-293.

Oberg, J. W., & Melesss, A. M. (2006). Evapotranspiration dynamics at an ecohydrological restoration site: An energy balance and remote sensing approach1. *Journal of the American Water Resources Association*, *42*(3), 565-582.

Penman, H. L. (1948). Natural evaporation from open water, bare soil and grass. *Proc. R. Soc. Lond. A*, *193*(1032), 120-145.

Roerink, G. J., Su, Z., & Menenti, M. (2000). S-SEBI: A simple remote sensing algorithm to estimate the surface energy balance. *Physics and Chemistry of the Earth, Part B: Hydrology, Oceans and Atmosphere*, *25*(2), 147-157.

Seckler, D., Amarasinghe, U., Molden, D., de Silva, R., & Barker, R. (1998). World Water Demand and Supply, 1990–2025: Scenarios and Issues. Research Report 19. International Water Management Institute, Colombo, Sri Lanka.

Senay, G. B., Bohms, S., Singh, R. K., Gowda, P. H., Velpuri, N. M., Alemu, H., & Verdin, J. P. (2013). Operational evapotranspiration mapping using remote sensing and weather datasets: A new parameterization for the SSEB approach. *JAWRA Journal of the American Water Resources Association*, *49*(3), 577-591.

Smith, D. M., & Allen, S. J. (1996). Measurement of sap flow in plant stems. *Journal of Experimental Botany*, 1833-1844.

Su, Z. (2002). The Surface Energy Balance System (SEBS) for estimation of turbulent heat fluxes. *Hydrology and earth system sciences*, *6*(1), 85-100.

Sun, G., Alstad, K., Chen, J., Chen, S., Ford, C. R., Lin, G., Liu, C., McNulty, S. G., Miao, H., Noormets, A., Vose, J. M., Wilske, B., Zeppel, M., Zhang, Y., & Zhang, Z. (2011). A general predictive model for estimating monthly ecosystem evapotranspiration. *Ecohydrology*, *4*(2), 245-255.

Taghvaeian, S., Neale, C. M., Osterberg, J. C., Sritharan, S. I., & Watts, D. R. (2018). Remote Sensing and GIS Techniques for Assessing Irrigation Performance: Case Study in Southern California. *Journal of Irrigation and Drainage Engineering*, *144*(6), 05018002.

Thornthwaite, C. W. (1948). An approach toward a rational classification of climate. *Geographical review*, *38*(1), 55-94.

Timmermans, W. J., Kustas, W. P., Anderson, M. C., & French, A. N. (2007). An intercomparison of the surface energy balance algorithm for land (SEBAL) and the two-source energy balance (TSEB) modeling schemes. *Remote Sensing of Environment*, *108*(4), 369-384.

Tucker, C. J. (1979). Red and photographic infrared linear combinations for monitoring vegetation. *Remote Sensing of Environment*, *8*(2), 127-150.

Vinukollu, R. K., Wood, E. F., Ferguson, C. R., & Fisher, J. B. (2011). Global estimates of evapotranspiration for climate studies using multi-sensor remote sensing data: Evaluation of three process-based approaches. *Remote Sensing of Environment*, *115*(3), 801-823.

Wild, M., Folini, D., Schär, C., Loeb, N., Dutton, E. G., & König-Langlo, G. (2013). The global energy balance from a surface perspective. *Climate dynamics*, *40*(11-12), 3107-3134.

Zwart, S. J., & Bastiaanssen, W. G. (2004). Review of measured crop water productivity values for irrigated wheat, rice, cotton and maize. *Agricultural water management*, *69*(2), 115-133.

CHAPTER II

MAPPING ANNUAL RIPARIAN WATER USE BASED ON THE SINGLE-SATELLITE-SCENE APPROACH

Abstract: The accurate estimation of water use by groundwater-dependent riparian vegetation is of great importance to sustainable water resource management in arid/semi-arid regions. Remote sensing methods can be effective in this regard, as they capture the inherent spatial variability in riparian ecosystems. The single-satellite-scene (SSS) method uses a derivation of the Normalized Difference Vegetation Index (NDVI) from a single space-borne image during the peak growing season and minimal ground-based meteorological data to estimate the annual riparian water use on a distributed basis. This method was applied to a riparian ecosystem dominated by tamarisk along a section of the lower Colorado River in southern California. The results were compared against the estimates of a previously validated remotely sensed energy balance model for the year 2008 at two different spatial scales. A pixel-wide comparison showed good correlation (R^2 = 0.86), with a mean residual error of less than 104 mm·year^{-1} (18%). This error reduced to less than 95 mm·year^{-1} (15%) when larger areas were used in comparisons. In addition, the accuracy improved significantly when areas with no and low vegetation cover were excluded from the analysis. The SSS method was then applied to estimate the riparian water use for a 23-year period (1988–2010). The average annual water use over this period was 748 mm·year^{-1} for the entire study area, with large spatial variability depending on vegetation density. Comparisons with two

independent water use estimates showed significant differences. The MODIS evapotranspiration product (MOD16) was 82% smaller, and the crop-coefficient approach employed by the US Bureau of Reclamation was 96% larger, than that from the SSS method on average.

1. Introduction

Large extents of the Colorado River floodplain are currently occupied by invasive species, such as tamarisk or salt cedar (*Tamarix* spp.) and Russian olive (*Eleagnus angustifolia*), that have replaced the native species, such as cottonwood (*Populus* spp.) and willow (*Salix* spp.). Tamarisk, in particular, has invaded millions of hectares of riparian floodplain in western U.S. (Owens & Moore, 2007), particularly in the dry southwestern states of Arizona, New Mexico, Texas, Nevada, Utah, and California (Zavaleta, 2000). Glenn and Nagler (2005) reported that tamarisk spreads at rates exceeding 20 $km \cdot year^{-1}$, becoming a dominant plant on the banks of rivers, streams, and ponds from eastern Oklahoma to northwestern California, and from western Montana to Sonora, Mexico. In addition, tamarisk has a high tolerance to salinity (Glenn et al., 1998; Vandersande, Glenn, & Walworth, 2001) and drought (Cleverly, Smith, Sala, & Devitt, 1997). The negative impacts of tamarisk invasion include, but are not limited to: displacing native vegetation (Glenn & Nagler, 2005; Stromberg, 1998), increasing fire frequency (Busch & Smith, 1993), degrading wildlife habitat (Bailey, Schweitzer, & Whitham, 2001), reducing biodiversity (Harms & Hiebert, 2006), and increasing water consumption (Di Tomaso, 1998; Zavaleta, 2000). The impact of tamarisk on water availability has been the subject of numerous studies, such as the one by Zavaleta (2000), who reported that the financial burden of high tamarisk water use on water supplies, hydropower generation, and flood control could reach $285 million U.S. dollars per year. Other researchers have found lower rates of tamarisk water use (Murray, Nagler, Morino, & Glenn, 2009; Nagler et al., 2009a; Taghvaeian, Neale, Osterberg, Sritharan, & Watts,

2014). Since millions of dollars are spent annually on removal and restoration projects, it is crucial for decision-makers and water managers, especially in water-scarce areas, to have access to tools that can provide accurate estimates of water use by invasive species with reasonable financial, computational, and human resources requirements.

Among the different methods available for quantifying riparian water use, remote sensing approaches have the advantage of capturing the high spatial variability common in riparian ecosystems. Existing methods for the remote sensing of riparian water use or evapotranspiration (ET) can be broadly grouped into two major categories: empirical approaches based on vegetation indices (VI); and physically based, remotely sensed energy balance (RSEB) models. The RSEB models rely on land surface temperature derived from the thermal bands of air- and space-borne imagery to compute ET as the residual of the surface energy balance. On the other hand, VI approaches are based on the plant-specific relationships between VIs and ET. An advantage of the RSEB models is their potential to detect variations in ET caused by short-term environmental stressors (due to the use of land surface temperature), while VI approaches may fail to do so unless the suboptimal conditions last long enough to affect biomass (Nagler et al., 2005a, 2009a). Another advantage is that RSEB models can be applied over diverse climatic conditions and ecosystems (Scott et al., 2008). In contrast, VI approaches may not be easily transferred to geographic areas different from the one where they were developed (Murray et al., 2009). On the other hand, RSEB models require numerous inputs (Gowda et al., 2008) and depend on a complex iterative process to accurately compute surface energy balance components (Irmak et al., 2012; Kalma, McVIcar, & McCabe, 2008; Morton et al., 2013). The iterative process requires selection of end-member pixels with a manual checkup by an experienced operator to ensure the calibration accuracy (Morton et al., 2013), and to minimize the constraints associated with directional radiometric surface temperature or vegetation fraction cover (Gowda et al., 2008). An additional challenge in validating the RSEB models with ground-based measurements is the

closure of energy balance, which may not be achieved (Gowda et al., 2008; Kalma et al., 2008). The VI approaches benefit from significantly smaller computational costs to run. As a result, they are usually preferred in studying inter-annual variations of ET across a region with similar hydro-climatic conditions, providing similar levels of uncertainty compared to RSEB models (Glenn, Huete, Nagler, Hirschboeck, & Brown, 2007; Gonzalez-Dugo et al., 2009; Kalma et al., 2008).

The RSEB models have been implemented before to estimate riparian ET at the Middle Rio Grande Basin in New Mexico (Bawazir, Samani, Bleiweiss, Skaggs, & Schmugge, 2009), along the North Plate River in the Nebraska Panhandle (Kamble et al., 2013), over the Lower Virgin River in Nevada (Liebert, Huntington, Morton, Sueki, & Acharya, 2016), and along the Lower Colorado River in southern California (Taghvaeian et al., 2014). Multiple VI-based approaches have also been developed and applied to estimate riparian ET. For example, the Modified Soil Adjusted Vegetation Index (MSAVI: Qi, Chehbouni, Huete, Kerr, & Sorooshian, 1994) has been empirically related to ET from groundwater-dependent riparian vegetation (Nicholas, 2000). The Enhanced Vegetation Index (EVI: Huete et al., 2002) derived from Moderate Resolution Imaging Spectroradiometer (MODIS) has been also used in several previous studies (Murray et al., 2009; Nagler et al., 2005a; Scott et al., 2008; Taghvaeian et al., 2014; Tillman, Callegary, Nagler, & Glenn, 2012). Nagler et al. (2005a, 2005b) developed a method to compute riparian ET using MODIS-EVI and maximum daily air temperature (T_{air}), and reported an error of ±25% when compared with flux tower observations from three western U.S. river corridors. This empirical relationship was modified by Scott et al. (2008), showing the potential application of MODIS land-surface temperature instead of ground-based maximum T_{air}. Later, Nagler et al. (2009b) developed a new linear relation between scaled EVI from MODIS and the Blaney–Criddle reference ET ($ET_{o\text{-}BC}$: Brouwer, 1986). This new model had reduced error (within 20%) when applied to riparian and agricultural areas along the Lower Colorado River in the southwestern U.S. In a more recent study, Nagler, Glenn, Nguyen, Scott, and Doody (2013)

replaced $ET_{o\text{-}BC}$ with the Penman–Monteith ET_o (Allen, Clemmens, Burt, Solomon, & O'Halloran, 2005), and developed an exponential relation. This newer method had a better performance in predicting ET, with an error of 10% when compared with flux tower and water balance data from riparian zones and irrigation districts at multiple locations from western U.S., Spain, and Australia (Nagler et al., 2013).

Among all VI approaches developed in the past, the single-satellite-scene (SSS) method developed by (Groeneveld and Baugh, 2007a; Groeneveld, Baugh, Sanderson, & Cooper, 2007b) has the least computational costs, as it requires only one image during peak vegetation growth to map the annual riparian ET. The SSS method relies on Normalized Difference Vegetation Index (NDVI) estimates, scaled from zero to one using two NDVI extremes representing zero and full-cover vegetation obtained from within the selected scene. The scaled NDVI was found to be highly correlated with riparian ET estimates from flux towers in California, Colorado, and New Mexico, with errors between −45 and 40 $mm \cdot year^{-1}$ (less than 13%) (Groeneveld et al., 2007b). Similar errors were reported when Landsat derived EVI was used in the SSS method (Beamer, Huntington, Morton, & Pohll, 2013). This method has been also applied to study ET and groundwater dynamics (Glenn, Jarchow, & Waugh, 2016; Groeneveld, 2008), a cost/benefit analysis of tamarisk control (Barz, Watson, Kanney, Roberts, & Groeneveld, 2009), the sustainability of vegetation, hydrology, and habitat value (Mexicano et al., 2013), tamarisk leaf beetles' impact on water availability (Nagler et al., 2012), and impacts of Colorado River delta pulse flow on riparian water use (Jarchow, Nagler, & Glenn, 2017). To the best of our knowledge, no independent study has assessed the performance of the SSS method in the past. Considering the potential of this method, evaluating its performance under variable hydro-ecological conditions would be beneficial to water managers and other potential users. The main objective of this study was to evaluate the performance of the SSS method using previously validated RSEB results, and to apply it over a 23-year period (1988–2010) to investigate inter-

annual riparian ET variations across parts of the Cibola National Wildlife Refuge in the Lower Colorado River Basin.

2. Materials and Methods

2.1 Study Area

The study area included parts of the Cibola National Wildlife Refuge (CNWR), which occupies about 70 square kilometers in the floodplains of the lower Colorado River, about 150 river km downstream of the Parker Dam. The CNWR was established in 1964 by the U.S. Bureau of Reclamation (USBR) to serve as a refuge and breeding area for migratory birds and wildlife, and to mitigate flooding by the Colorado River. The average annual rainfall is less than 100 mm in this low-desert environment (Nagler et al., 2009a). Most of the rainfall occurs in July and August with occasional winter rains. The average air temperature ranges from 4.0 °C in December to 38.0 °C in August (Nagler et al., 2009a). More than 90% of CNWR is covered by tamarisk (*Tamarix* spp.), followed by mesquite (*Prosopis velutina*), cottonwood, willow, arrowweed (*Pluchea sericea*), qualibush, and fourwing saltbush (Nagler et al., 2009a; Taghvaeian et al., 2014).

The location of the study area within the Colorado River basin is presented in Figure 2.1 (left panel). The new and old Colorado River channels are specified in the satellite image (right panel) along with six subareas used in analyzing ET signals in this study. The old river channel serves as the border between California (CA) and Arizona (AZ). Subareas 2, 3, and 4 are located in AZ, while subareas 1, 5, and 6 are in CA. Since 1964, when most of the river flow was diverted to the new channel, the old channel has been carrying agricultural return flows from the Palo Verde Irrigation District (PVID) upstream of CNWR, as well as a small, regulated flow to support the wildlife.

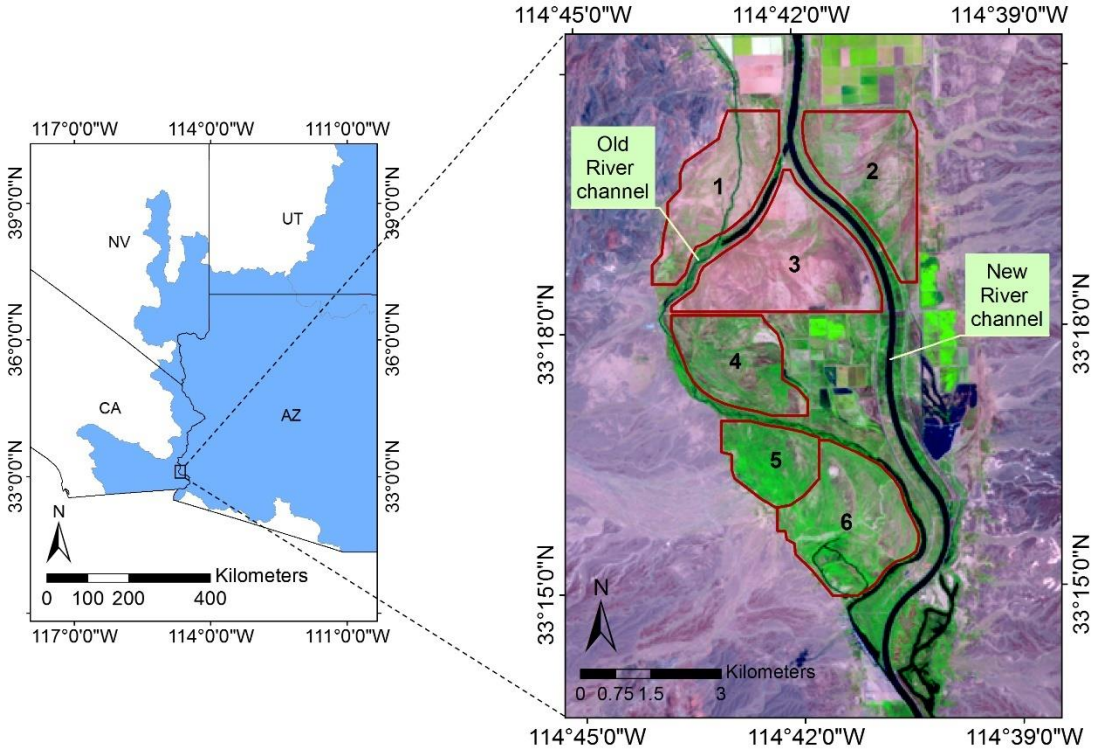

Figure 2.1. Location of the study area in the Lower Colorado River Basin (left). The six subareas in the right panel indicate parts of the Cibola National Wildlife Refuge (CNWF) included in this study.

2.2 Single-Satellite-Scene (SSS) Approach

The Single-Satellite-Scene (SSS) is a simple method of estimating annual riparian ET based on just one mid-summer satellite image and some ground-based meteorological data (Groeneveld et al., 2007a, 2007b). In this method, the annual riparian ET is a function of NDVI*, reference ET (ET_o), and precipitation as:

$$ET = (ET_o - \text{Precipitation}) \times NDVI^* + \text{Precipitation} \quad (2.1)$$

where NDVI* is a scaled NDVI, computed using the relationship presented in [36] as:

$$NDVI^* = (NDVI - NDVI_o) / (NDVI_s - NDVI_o) \quad (2.2)$$

where $NDVI_o$ is NDVI at zero vegetation cover and $NDVI_s$ is NDVI at saturation, both extracted from the same satellite scene to be used in ET estimation. The conversion of NDVI to NDVI* is performed to remove the variations inherent in this parameter caused by atmospheric, soil, and vegetation factors (Groeneveld et al., 2007a; Huete & Liu, 1994; Liu & Huete, 1995), making it possible to use NDVI estimated by different sensors at different times and locations. The selection of $NDVI_o$ and $NDVI_s$ is a critical step. These parameters are estimated by developing a cumulative frequency distribution graph of NDVI values for the selected scene (Groeneveld et al., 2007a). At the low end of this graph, the relationship (NDVI vs. cumulative pixel count) becomes asymptotic and choosing an appropriate $NDVI_o$ becomes subjective (Groeneveld et al., 2007a). To minimize such subjectivity, a line is fitted to the near-linear lower portion of the NDVI cumulative frequency distribution and the x-intercept of the fitted line is taken as $NDVI_o$. $NDVI_s$ is chosen from a region with the maximum possible NDVI (e.g., irrigated crops with full-cover or thick riparian forests). Further details of this method are presented in Groeneveld et al. (2007a) and Groeneveld et al. (2007b). The main assumptions of the SSS method are the presence of shallow groundwater, arid/semi-arid environments, and similar conditions before and after (homeostasis) the mid-summer satellite image (Groeneveld et al., 2007b).

A major question for potential users of the SSS method could be the selection of the single scene to be used in the analysis. The sensitivity of estimated annual riparian ET to the selected image was investigated by applying the method to three Landsat images from mid-summer 2008. The three NDVI maps used in this study were processed by the Landsat Ecosystem Disturbance Adaptive Processing System (LEDAPS) (Masek et al., 2012), which applies the Second Simulation of a Satellite Signal in the Solar Spectrum (6S) radiative transfer models to minimize the radiometric errors. The performance of the SSS method was then assessed on a distributed basis through comparing its result with that obtained from a previously validated remotely sensed energy balance (RSEB) model. This RSEB model was a modified Surface

Energy Balance Algorithm for Land (SEBAL) model (Taghvaeian et al., 2014). SEBAL has been extensively validated before under variable land covers and hydro-climatic settings (Bastiaanssen et al., 1998; Bastiaanssen et al., 2005). The land surface energy balance components considered in SEBAL are presented in equation 2.3, assuming energy consumed in photosynthesis and energy stored in the canopy are insignificant.

$$LE = Rn - G - H \tag{2.3}$$

where LE is the latent heat flux, and is estimated as a residual of net radiation (Rn), soil heat flux (G), and sensible heat flux (H). The LE estimated based on equation 2.3 represents the instantaneous flux at the time of satellite overpass. Extrapolation of this instantaneous flux to daily ET in SEBAL is accomplished by using evaporative fraction (EF), estimated as the ratio of instantaneous LE to instantaneous available energy (Rn - G). Instantaneous EF is assumed to be the same as the 24-h (daily) EF, representing the ratio of daily LE to Rn (Alllen, Tasumi, & Trezza, 2007; Bastiaanssen et al., 1998). Details on the computational steps of SEBAL are presented in Bastiaanssen et al. (1998).

Taghvaeian et al. (2014) applied the modified SEBAL model over the study area (CNWR), using 21 Landsat TM images acquired in 2008. In the modified SEBAL application at CNWR, an adjustment coefficient was adopted to account for the canopy temperature contamination caused by shadows of tall riparian vegetation (Taghvaeian et al., 2014). The results were compared against the estimates of two independent methods: the Bowen ratio flux tower and the White method, which is based on the diurnal fluctuations of groundwater (White, 1932). On a seasonal basis, ET estimates of the modified SEBAL were within 2% and 10% of those from the White method and Bowen ratio, respectively (Taghvaeian et al., 2014). This difference was less than the expected error of each method, giving confidence to the accuracy of this RSEB model.

Hence, the modified SEBAL was used as the reference to evaluate the performance of the SSS method.

Comparisons were made at two scales: pixel-based and area-wide. At the pixel-based scale, ET values were extracted for each method using a randomly scattered collection of 1571 circular sampling features with a diameter of 120 m. At the area-wide scale, comparisons were made for the six subareas demonstrated in Figure 2.1, with average and total areas of 5.12 and 30.74 km^2, respectively. After obtaining the ET data from each method, the residual and percent error were calculated as:

$$\text{Residual error} = \text{SSS-ET} - \text{RSEB-ET} \tag{2.4}$$

$$\text{Percent error} = \frac{\text{Residual Error}}{\text{RSEB}-\text{ET}} \times 100 \tag{2.5}$$

where SSS-ET is the ET estimated by the SSS method, and RSEB-ET is the ET from the modified SEBAL model.

2.3 Long-Term Estimates

After evaluating the performance of the SSS method, long-term ET estimates were obtained over a 23-year period from 1988 to 2010. The meteorological data were obtained from the Palo Verde weather station, which is operated and maintained by the California Irrigation Management Information System (CIMIS). This weather station is located about 4.5 km north of the study area, and is the closest weather station in the region. A mid-summer Landsat image was selected in each study year and used for computing $NDVI_o$, $NDVI_s$, and NDVI*, which was integrated with annual grass-based reference ET (ET_o) (ASCE-EWRI, 2005) and precipitation to map annual riparian ET based on equation 2.1. The average annual ET was estimated for the subareas in CA (1, 5, 6) and the subareas in AZ (2, 3, 4), and was compared with two independent ET estimates: the remotely sensed MODIS ET product known as MOD16 (Mu, Heinsch, Zhao, &

Running, 2007; Mu, Zhao, & Running, 2011) averaged over the same subareas, and the crop-coefficient approach implemented by USBR in the Lower Colorado River Accounting System (LCRAS) and reported for the CA and AZ sections of the study area.

The MOD16-ET was downloaded from the University of Montana's Numerical Terradynamic Simulation Group data archive (http://www.ntsg.umt.edu). The MOD16 global ET dataset is primarily based on the Penman–Montheith equation (Monteith, 1965; Mu et al., 2007, 2011), and has a spatial resolution of 1.0 km. Although this resolution was much coarser than the resolution of the SSS estimates used in this study, MOD16 was included in the comparison because it is available to water managers at no cost. A comparison of the MOD16-ET and the SSS-ET was made only for the 11-year period of 2000 to 2010 due to the unavailability of MOD16 before the year 2000.

In the USBR LCRAS approach, daily riparian ET is estimated as a product of ET_o and crop coefficients (Kc) and summed to obtain the annual ET. Climatological data from the California Irrigation Management Information System (CIMIS) and the Arizona Meteorological Network (AZMET) are used for these ET estimations. The details on ET estimation methods and procedures, as well as annual riparian ET from the CA and AZ areas of CNWR, are presented in the LCRAS reports (USBR, 2007, 2014). For comparison with SSS estimation, LCRAS-ET estimates in acre-feet were divided by the CNWR area at each state (provided in the same report) to obtain the annual ET in units of water depth. The spatial extent of the CA and AZ regions in the LCRAS and SSS methods were not exactly the same, but similar enough to warrant a comparison between the two approaches. The LCRAS reports are available from 1995 to 2011. However, to be consistent with MOD16 data, a LCRAS–SSS comparison was conducted for the period from 2000 to 2010.

3. Results and Discussion

3.1 SSS Evaluation

The SSS method requires only a single satellite image during peak riparian growth to estimate ET. Figure 2.2 demonstrates the evolution of NDVI, averaged over the study area, for all cloud-free Landsat TM5 scenes acquired in 2008. The average NDVI varied from 0.22 in March to 0.49 in September. The maximum NDVI over the CNWR occurred during summer, with the highest values of 0.49, 0.47, and 0.49 observed on day of year (DOY) 195 (13 July), 227 (14 August), and 259 (15 September), respectively. To examine the sensitivity of the SSS method to the selection of a Landsat scene, each of these three dates was used separately in estimation of the annual ET.

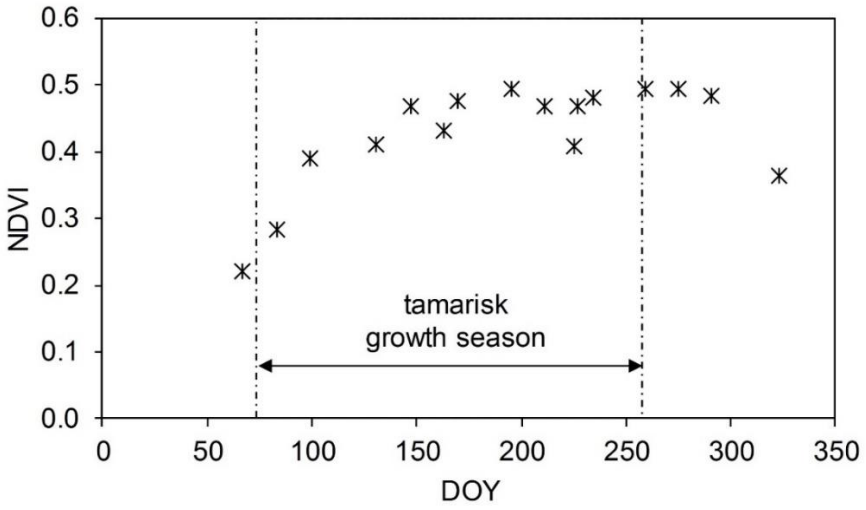

Figure 2.2. Average Normalized Difference Vegetation Index (NDVI) of the study area for all cloud-free Landsat scenes in 2008. DOY, day of year.

The selection of $NDVI_o$ and $NDVI_s$ for each of the three scenes was facilitated by plotting cumulative NDVI frequency graphs with the x-intercept ($NDVI_o$) of the fitted line to the near-linear lower portion of the cumulative frequency graph and the maximum possible NDVI

($NDVI_s$). The $NDVI_o$ was 0.07, 0.05, and 0.07, for DOYs 195, 227, and 259, respectively, and the $NDVI_s$ was 0.90, 0.84, and 0.94 for the same DOYs (Figure 2.3). This information was used in mapping NDVI* and eventually the SSS-ET. The annual SSS-ET averaged over the entire study area was 677, 676, and 658 mm·year^{-1} for DOYs 195, 227, and 259, respectively. The average annual RSEB-ET was smaller, at 571 mm·year^{-1}.

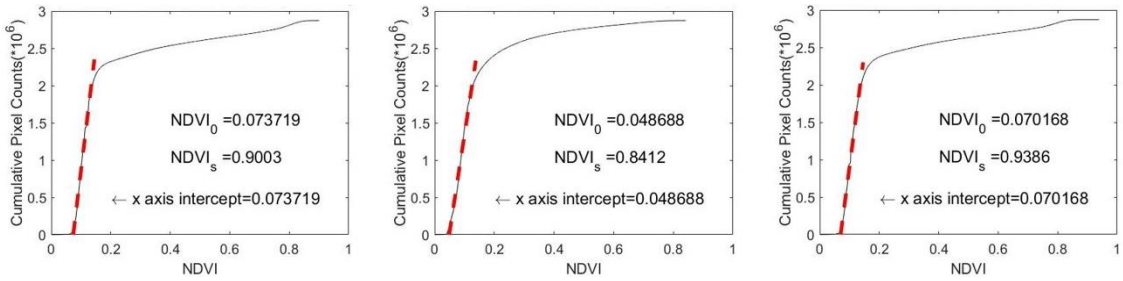

Figure 2.3. Cumulative NDVI frequency distribution for DOYs 195 (a); 227 (b); and 259 (c).

For the pixel-based evaluation, both the SSS-ET and RSEB-ET estimates were extracted using 1571 randomly located samples. In general, the pixel-based comparison showed good correlation between the two methods, with a coefficient of determination (R^2) larger than 0.86. The residual error varied between 84 and 104 mm·year^{-1} for the three DOYs (Table 2.1). This translated to percent errors from 14.3 to 17.7%. Figure 2.4 demonstrates a scatterplot of ET estimates and how they populate around the 1:1 line. Two distinct areas can be observed in the scatterplot with higher densities of points. The majority of points in the lower-left cluster in Figure 2.4 were from subareas 1, 2, and 3, where vegetation was sparse, with average NDVI less than 0.31 for all three DOYs. The overestimation of the SSS-ET over the low-vegetation areas (lower-left cluster in Figure 2.4) can be attributed to the inclusion/exclusion of surface temperature in the RSEB model and SSS method. Due to the exclusion of surface temperature, the reduced ET from the low vegetation and bare soil is not fully accounted for by the SSS method. However, a minimum NDVI threshold can be set based on local vegetation and weather data to minimize the errors while applying the SSS method under low-vegetation conditions. The

higher ET cluster mostly contained samples from subareas 4, 5, and 6, with average NDVI ranging from 0.37 to 0.55.

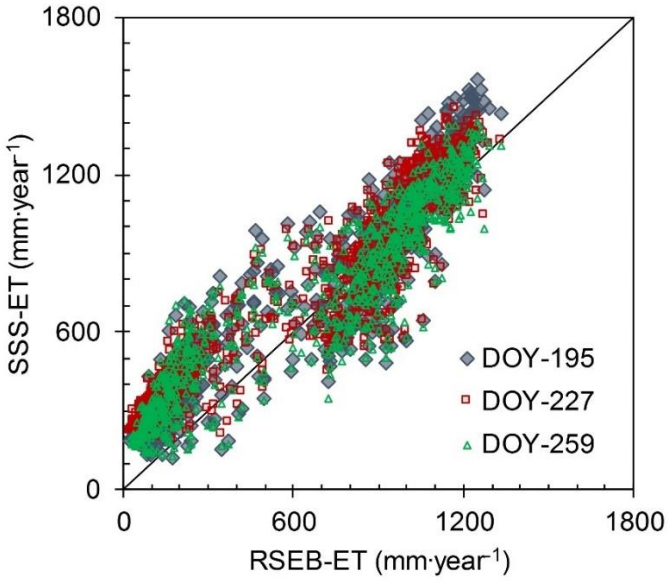

Figure 2.4. Comparison of annual single-satellite-scene evapotranspiration (SSS-ET) and remotely sensed energy balance evapotranspiration (RSEB-ET) for randomly selected samples within the CNWR.

Table 2.1. Summary of pixel-based and area-wide comparison of SSS-ET and RSEB-ET

Scale	DOY	SSS-ET ($mm \cdot year^{-1}$)	RSEB-ET ($mm \cdot year^{-1}$)	R^2	Residual Error ($mm \cdot year^{-1}$)	Percent Error
Pixel-based	195	693	589	0.86	104	17.7
	227	692	589	0.87	103	17.5
	259	673	589	0.86	84	14.3
Area-wide	195	732	637	0.97	95	14.9
	227	727	637	0.96	90	14.1
	259	708	637	0.98	71	11.1

R^2 = coefficient of determination

The evaluation of SSS performance was also conducted at the area-wide scale, where a comparison of the SSS-ET and RSEB-ET was made on all DOYs (195, 227, 259) over the six

subareas within the CNWR. The reason behind performing an area-wide comparison was that the SSS method will most likely be implemented by water managers to obtain estimates over larger areas and to use the information in making decisions, as opposed to research applications that may require more details. Similar to the pixel-based comparison, the area-wide results had good agreement ($R^2 \geq 0.96$) with RSEB-ET estimates (Figure 2.5). The residual errors were smaller at 95, 90, and 71 mm·year^{-1} for DOYs 195, 227, and 259, respectively. The percent errors were 14.9, 14.1, and 11.1% for the same DOYs, respectively.

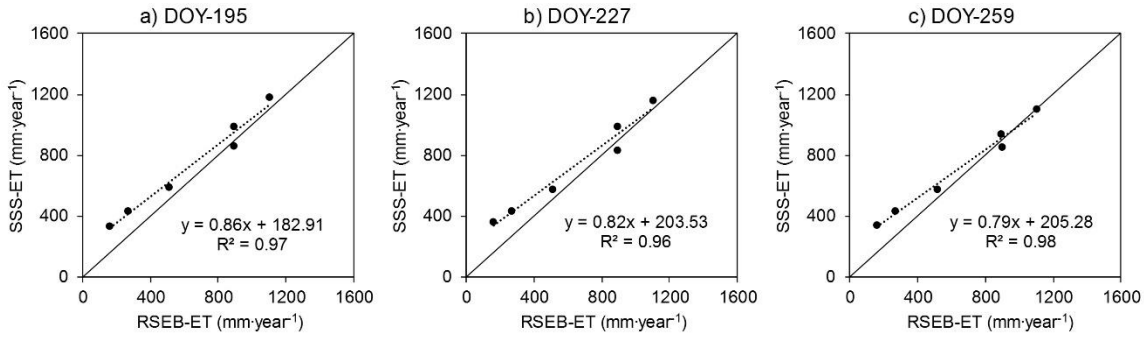

Figure 2.5. (a-c) Comparison of annual SSS-ET and RSEB-ET for six subareas within the CNWR.

The percent errors found in this study for the pixel-based (<17.7%) and area-wide (<14.9%) comparisons are promising, since they are within typical ranges of errors in the measurements of other water balance components in riparian ecosystems. These errors are also close to the lower end of errors of VI approaches, which typically range from 15% to 40% (Allen, Pereira, Howell, & Jensen, 2011) depending on the knowledge and experience of an operator. Based on this metric, the estimated error of the SSS method is acceptable considering the fact that it requires minimal operator knowledge and that the entire process can be automated using computer programming.

The area-wide comparison revealed a potential relationship between the magnitude of SSS-ET error and the vegetation density. The greatest difference between the two methods was

206 mm·year^{-1} from subarea 3 for DOY 227. This subarea had the smallest average NDVI of 0.18. In contrast, the smallest difference in annual ET estimates was 4 mm·year^{-1} from subarea 5 for DOY 259. The average NDVI was 0.54 over this subarea. To further investigate this relationship, the differences between the SSS-ET and RSEB-ET were plotted against the average NDVI of each subarea (Figure 2.6). The differences were greatest for NDVI values smaller than 0.25, but were reduced significantly and remained insensitive beyond this NDVI threshold. Subareas 1 and 3 had average NDVI values less than 0.25 for all three DOYs. Removing these subareas from the analysis resulted in a significant reduction in average residual errors to 58, 42, and 20 mm·year^{-1} for DOYs 195, 227, and 259, respectively. The percent errors were also smaller, at 6.8%, 5.0%, and 2.4% for the same DOYs, respectively. The inverse relationship between the SSS-ET error and NDVI is expected, as this method was developed and calibrated to estimate the water use of riparian species. Thus, it underperforms over bare soil and low-vegetation areas.

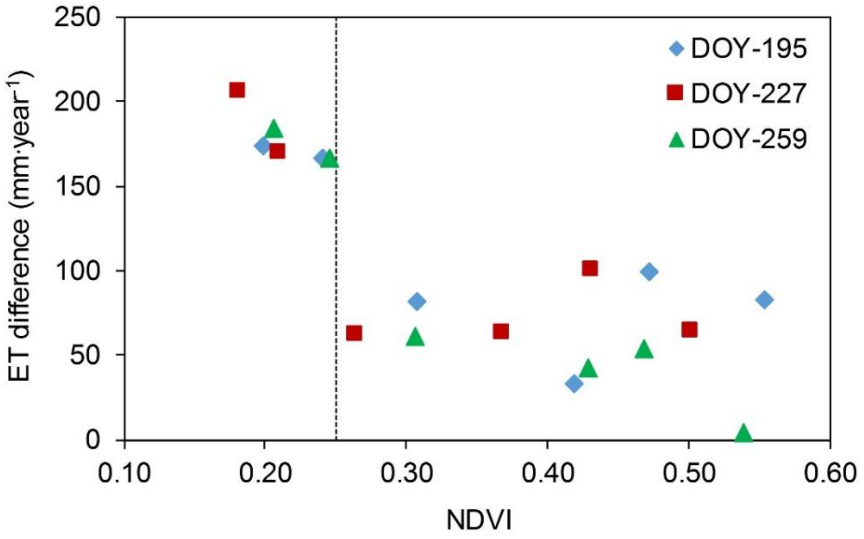

Figure 2.6. Evapotranspiration (ET) differences (SSS-RSEB) versus NDVI for the three DOYs in 2008. Each point represents a subarea within the CNWR.

No significant differences in SSS-ET estimates were found among the three selected scenes, and all performed satisfactorily based on acceptable errors for VI approaches. The Landsat image of 17 August (DOY 227) was selected for the annual ET estimation for the validation year 2008. Previous studies (Allander, Smith, & Johnson, 2009; Gooeneveld et al., 2007b; Smith, Laczniak, Moreo, & Welborn, 2007) have suggested June to August as a representative period to characterize peak biomass and water use of riparian vegetation in western U.S. A visual representation of annual ET estimated by SSS, RSEB, and MOD16 for the year 2008 is shown in Figure 2.7. Missing pixels in the MOD16 map represent barren or sparsely vegetated areas where ET values are not estimated.

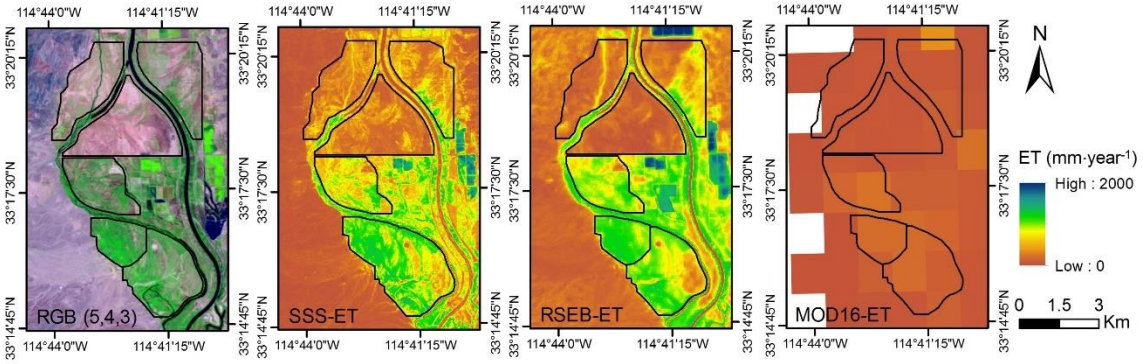

Figure 2.7. Annual ET based on SSS, RSEB, and MOD16 for the year 2008.

3.2 Inter-Annual Variation of Water Use

Annual riparian water use was mapped over the study area for a 23-year period from 1988 to 2010, after the selection of an appropriate mid-summer Landsat image. For most of the studied years (18 out of 23), the selected scene was from August, and the remaining scenes were from July and September. The procedure explained in previous sections was followed for estimating $NDVI_o$ and $NDVI_s$. $NDVI_o$ had a range of 0.06 to 0.10, and $NDVI_s$ varied between 0.83 and 1.0 (Table 2.2). Comparatively, lower variation (0.04) was observed in $NDVI_o$ than in $NDVI_s$ (0.17). The reference ET (ET_o) values were between 1644 mm·year^{-1} to 2015 mm·year^{-1},

with an average of 1785 mm·year^{-1} (Table 2.2). Annual precipitation varied from 1 mm·year^{-1} to 177 mm·year^{-1}, with an average of 66 mm·year^{-1} during the study period.

Table 2.2. Day of year (DOY) of selected Landsat images, their respective $NDVI_o$ and $NDVI_s$, reference ET (ET_o), precipitation, and estimated annual SSS-ET for 23 years of study.

Year	DOY	$NDVI_o$	$NDVI_s$	ET_o (mm·year^{-1})	Precipitation (mm·year^{-1})	SSS-ET (mm·year^{-1})
1988	220	0.08	1.00	1836	129	762
1989	238	0.07	0.92	1752	39	762
1990	241	0.06	0.94	1855	53	854
1991	244	0.07	0.88	1746	78	793
1992	215	0.08	0.83	1790	161	769
1993	217	0.09	1.00	1960	126	783
1994	236	0.08	0.89	2015	40	915
1995	223	0.09	0.88	1866	144	826
1996	226	0.08	0.95	1868	53	898
1997	212	0.08	0.93	1732	80	787
1998	215	0.09	0.96	1738	89	762
1999	218	0.08	1.00	1793	55	816
2000	221	0.07	0.87	1748	6	750
2001	223	0.07	0.87	1754	80	851
2002	226	0.08	0.87	1805	1	746
2003	229	0.07	0.92	1709	177	849
2004	248	0.08	1.00	1696	80	677
2005	218	0.10	0.90	1668	72	754

2006	237	0.07	0.91	1768	10	NA
2007	224	0.08	0.91	1774	10	508
2008	227	0.05	0.84	1815	1	598
2009	229	0.09	0.88	1728	19	524
2010	232	0.10	0.91	1644	19	483

NA = Not applicable due to wildfire

The long-term (1988–2010) average annual ET over the CNWR was 748 mm·year^{-1}, with the smallest value observed in 2010 at 483 mm·year^{-1} and the largest in 1994 at 915 mm·year^{-1}. This annual average SSS-ET (748 mm·year^{-1}) was about 42% of long-term average ET_o. The annual average precipitation was 66 mm·year^{-1}, only about 9% of the average SSS-ET during the study period. The annual ET for the year 2006 was excluded due to the violation of a major assumption in the SSS method. Based on this assumption, the conditions before and after the single satellite scene should be similar (homeostasis conditions) (Groeneveld et al., 2007b), which was not fulfilled for the year 2006 due to a massive wildfire. This wildfire, which occurred in mid-July 2006, can also explain the considerable (33%) reduction in riparian water use after 2006. The average values of SSS-ET were 754 and 508 mm·year^{-1} before and after 2006, respectively. Another factor that may have played a role is the release of tamarisk leaf beetles (*Diaorhabda carinulata*), which started in 2001 in some riparian forests upstream of the study area (Nagler et al., 2012). Pre- and post-beetle studies in the western U.S. have reported a 50% reduction in daily midsummer ET (Nagler et al., 2014) and a 16% (204 mm·year^{-1}) reduction on an annual basis (Liebert et al., 2016). A graphical representation of inter-annual variations of SSS-ET during the study years and the impact of the 2006 wildfire on tamarisk ET over the CNWR is shown in Figure 2.8.

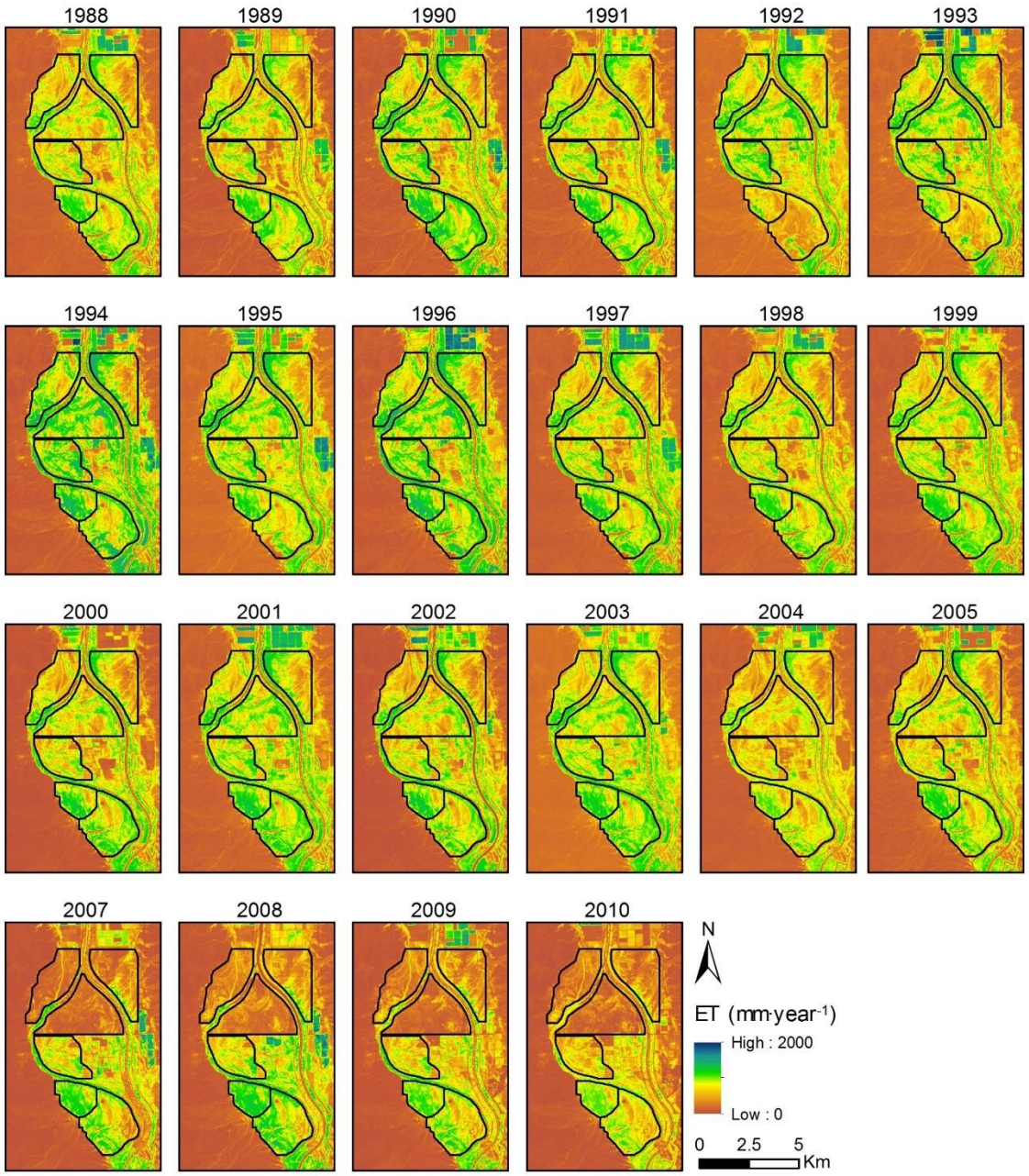

Figure 2.8. Annual ET from the CNWR obtained by the SSS method from 1988 to 2010.

The average annual tamarisk ET was 748 mm·year^{-1}. If the entire tamarisk monoculture area of 182 × 10^6 m^2 (18,200 ha) (Nagler et al., 2009a) in the lower Colorado River Basin is similar to that of the CNWR, the annual water loss would be about 136.3 × 10^6 m^3 (110,514 acre-foot). This amount of water consumed by tamarisk would be less than 1.5% of the long-term

(1988–2010) average annual flow (1.12×10^{10} m^3) of the Colorado River measured at Lee's Ferry, AZ and about 18% of the long-term (1991–2010) average annual water use (620,835 acre-foot: LADWP, 2015) by the city of Los Angeles, CA.

The annual riparian water use estimates in this study were within the range of ET rates reported by previous studies. Murray et al. (2009) reported annual ET from 608 to 1005 $mm \cdot year^{-1}$, with an average of 825 $mm \cdot year^{-1}$ from the entire CNWR during the study period 2000 to 2008 based on MODIS EVI. However, Nagler, et al. (2008) found an average annual ET of 1110 $mm \cdot year^{-1}$ from the CNWR for the period of 2000 to 2006. This is significantly larger (44%) than the results of this study, with a maximum annual ET of 851 $mm \cdot year^{-1}$ during the same period. Potential reasons for the observed differences include, but are not limited to, differences in implemented methods, possible differences in the weather parameters used in analysis (weather station selected), and differences in space-born imagery. The studies by (Murray et al., 2009; Nagler et al., 2008) applied MODIS imagery with a 250 m ground resolution, which can potentially include non-target or multiple land covers within a pixel (Murray et al., 2009), whereas the present study used finer resolution (30 m) Landsat imagery.

3.3 Comparison with MOD16 and LCRAS

The comparison between SSS, MOD16, and LCRAS water use estimates was conducted for 10 years from 2000 to 2010, excluding the year 2006 due to the wildfire that occurred in the study area. The annual ET estimates from MOD16 were significantly smaller than those based on the SSS method, with a minimum and maximum of 92 and 187 $mm \cdot year^{-1}$ during the comparison period, respectively. On average, the MOD16 estimate of riparian water use over the study area was 122 $mm \cdot year^{-1}$ (excluding 2006), which is about 82% smaller than the average SSS-ET for the same period (674 $mm \cdot year^{-1}$). This difference could be due to the MOD12 land cover product (Friedl et al., 2002; Friedl et al., 2010) used in estimating MOD16, which has a coarse spatial

resolution (500 m) and classifies most of the CNWR as croplands with some open/closed shrublands. In addition, MOD16 has a spatial resolution of 1 km, much coarser than the 30 m resolution of Landsat imagery used in the SSS. This introduces a significant contamination from nearby desert areas. The finer spatial resolution of Landsat is achieved at the cost of coarser temporal resolution. Nevertheless, most riparian corridors in western U.S. are narrow in extent and do not experience rapid temporal variations. This makes Landsat a better option than MODIS when it comes to studying spatially heterogeneous riparian water consumption. The underestimation of MOD16 has been reported for croplands in previous studies (Biggs, Marshall, & Messina, 216; Ruhoff et al., 2013; Velpuri, Senay, Singh, Bohms, & Verdin, 2013). The MOD16-ET from the CA portion was 34% greater than the AZ areas. Similar to the MOD16-ET, the SSS method estimated greater (24%) ET from CA.

In contrast to MOD16, the annual riparian ET estimates reported in LCRAS were greater than the SSS-ET estimates (Figure 2.9). The annual ET based on LCRAS varied between 787 $mm \cdot year^{-1}$ (2010) and 1530 $mm \cdot year^{-1}$ (2001), with an average of 1320 $mm \cdot year^{-1}$ during the comparison period (excluding 2006). This was 96% larger than the average SSS-ET (674 $mm \cdot year^{-1}$) during the same period. The difference between the LCRAS and SSS estimates of ET was greater than 600 $mm \cdot year^{-1}$ for the years from 2000 to 2009. However, the difference was significantly reduced to 304 $mm \cdot year^{-1}$ in 2010. For the year 2010, LCRAS reported an annual ET of 787 $mm \cdot year^{-1}$, which was about 56% lower compared to the 2009 ET of 1231 $mm \cdot year^{-1}$. This abrupt decrease can be attributed to an adjustment made in 2010 on crop coefficients (Kc), which reduced riparian ET by 30 to 40% (USBR, 2014). In the original LCRAS method, the maximum Kc (mid-season stage) was 1.15 (Jensen, 2003), which was reduced to 0.76 (Westenberg, Harper, & DeMeo, 2006) in the 2010 estimation. The updated Kc values in LCRAS are consistent with those reported by (Taghvaeian et al., 2014) over dense tamarisk stands within

the CNWR based on the RSEB model and the groundwater-based method. The overestimation error of LCRAS has been also reported in Murray et al. (2009) and Nagler et al. (2009a).

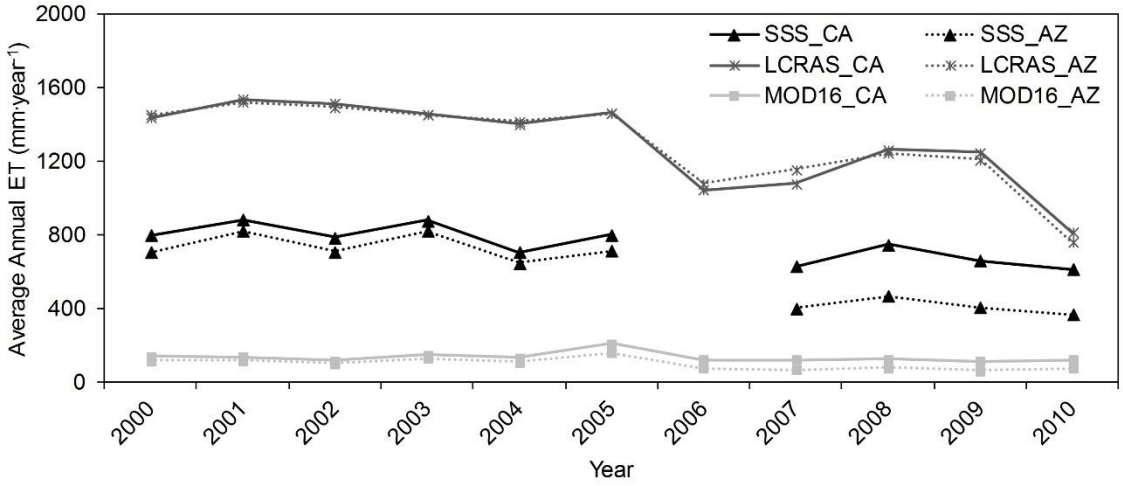

Figure 2.9. Comparison of annual ET over the California (CA) (solid) and Arizona (AZ) (dotted) regions of the CNWR. SSS-ET was not estimated for 2006 due to wildfire.

While both of the remotely estimated ET products (SSS and MOD16) were able to capture ET differences between CA and AZ, the Kc-based LCRAS was not able to account for those ET variations. After the wildfire of 2006, the 4-year (2007–2010) average SSS-ET from the CA portion was 60% greater compared to the AZ portion. This difference was 10% on average during the 4 years before the wildfire (2002–2005). However, the Kc-based LCRAS reported only 1% greater ET from CA after the 2006 wildfire, and no difference before the wildfire.

3.4 Impact of Wildfire on Water Use

The massive wildfire of 2006 in the CNWR had a significant impact on riparian water use. The 4-year average annual SSS-ET after the wildfire (2007–2010) was 528 mm·year^{-1}, 30% smaller than the average (797 mm·year^{-1}) for the 4-year period before the fire (2002–2005). The wildfire had a greater impact in the northern parts of the CNWR (subareas 1, 2, and 3) as shown in Figure 2.10. The largest ET reduction was observed in subarea 3, where the ET reduced from

738 mm·year^{-1} in 2005 to 227 mm·year^{-1} in 2007 (69% reduction). Similarly, the annual ET over subareas 1 and 2 was reduced by 64% and 43%, respectively. Subareas 4, 5, and 6 showed a small reduction (3%), no change, and a small increase (6%) in water use between 2005 and 2007, respectively (Figure 2.11). This indicates that ET reductions in the northern subareas can be mainly attributed to the wildfire and not water stress caused by declines in groundwater levels. The potential impact of variable atmospheric demand was also ruled out, since ET_o was 1774 mm·year^{-1} in 2007, only 6% larger compared to ET_o in 2005 (1668 mm·year^{-1}). The average 4-year ET_o before and after the wildfire was 1720 mm·year^{-1} and 1740 mm·year^{-1}, respectively. The lower ET rates over the northern parts of the CNWR due to wildfire of 2006 were also reported by Nagler et al. (2009a).

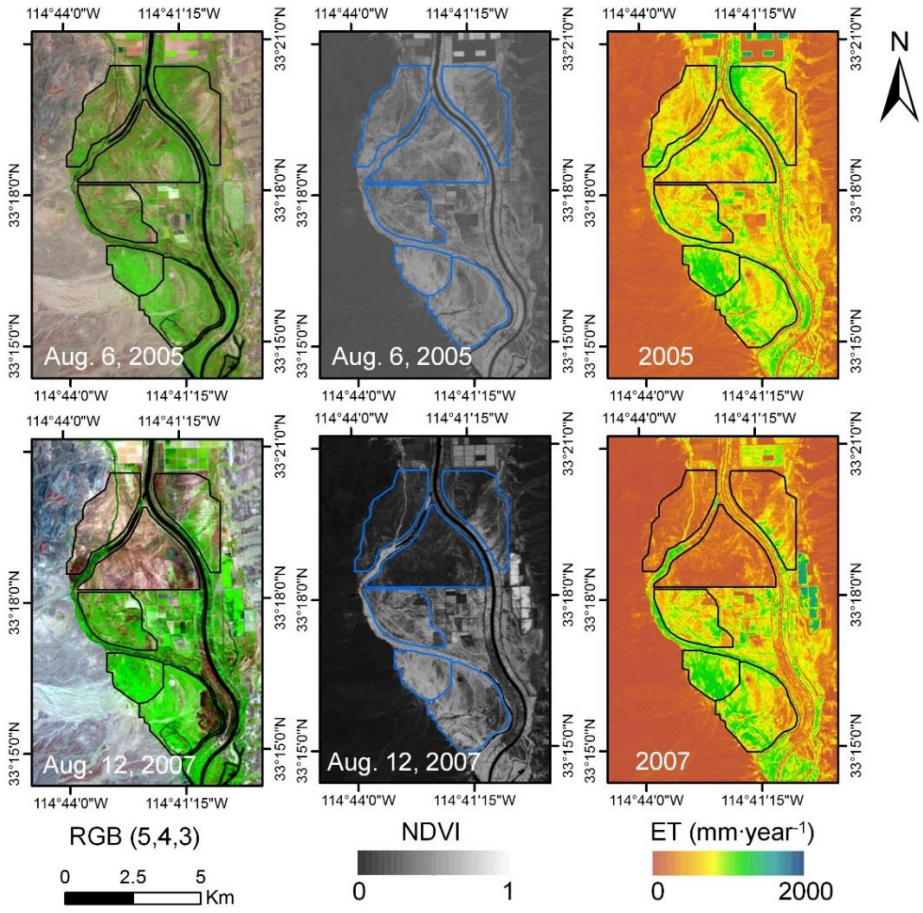

Figure 2.10. Landsat false color composite, NDVI, and annual ET before (top) and after (bottom) the wildfire of 2006.

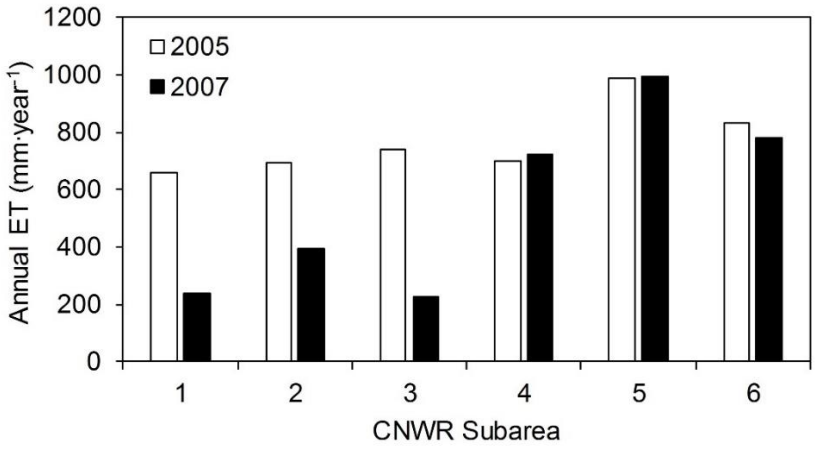

Figure 2.11. Annual SSS-ET for each CNWR subarea before and after the wildfire of 2006.

Another wildfire occurred in the southern part of the CNWR in August 2011. Lewis (2016) used a groundwater-based method to investigate changes in riparian water use pre- and post-fire at three locations in southern CNWR, and found both increases and decreases in ET after the wildfire of 2011. They reported that, after the wildfire, riparian ET decreased by 59% and 31% at two of the locations and increased by 8% at the third location. The study found groundwater depth was an important factor for defining ET rates before wildfire, whereas it was not a limiting factor after the wildfire, and that frequent burns in the CNWR most likely reduce annual ET rates. A wildfire's impact on riparian water use may vary depending on multiple factors (Devitt et al., 1998), including water availability, canopy development after wildfire, and advection of energy along riparian zones. In the short-term, riparian water use could increase by the abundance of sprouting shoots (Busch et al., 1993). In the long-term, however, changes in forest composition by shifts in tree-age structure may reduce the forest leaf area compared to a pre-fire condition, ultimately decreasing the ET rates (Stormberg & Rychener, 2010).

4. Conclusions

The single-satellite-scene (SSS) approach was applied to estimate the annual riparian water use over parts of the Cibola National Wildlife Refuge (CNWR) using Landsat TM5 imagery. The performance of the SSS method was assessed through comparing its results with those of a previously validated remotely sensed energy balance model at two distributed scales. At the pixel-based scale (comparisons for 1571 samples), the mean residual error was less than 104 mm·year^{-1} (18%). The area-wide comparison was similar, showing an error of less than 95 mm·year^{-1} (15%). The errors reduced by more than a half to less than 58 mm·year^{-1} (7%) after excluding the areas with no to low vegetation from the analysis. These errors are in agreement with the reported errors of similar remote sensing approaches. In addition, they are within the error ranges of other major components of water balance for riparian ecosystems. Moreover, the results were not sensitive to the single image selected for analysis as long as that image was acquired during the peak vegetation cover. Hence, the SSS method can be used effectively to map annual water use over heterogeneous riparian forests.

The method was then applied to estimate riparian ET over a 23-year period from 1988 to 2010. The average annual ET varied from 483 to 915 mm·year^{-1} during the study period, with an average of 748 mm·year^{-1}. A comparison with two readily available, independent sources of water use information revealed significant differences. The ET from the MODIS product (MOD16) was on average 82% smaller than the result of the SSS method. On the other hand, the U.S. Bureau of Reclamation's Lower Colorado River Accounting System estimates were almost double that of the ET from the SSS method. Considering the simplicity and accuracy of the SSS approach, it has great potential to be the method of choice in estimating riparian ET and making informed water management decisions, especially in arid/semi-arid regions.

Despite significant advantages, the SSS method has three main limitations that must be considered before any application. As this method relies on remotely sensed NDVI and meteorological information, it may not able to account for factors that are not accounted for by NDVI. For example, water stresses that limit the ET rates are not instantly reflected in NDVI (Nagler et al., 2005a, 2009a). The second limitation is that this method requires homeostasis conditions, and thus will not provide accurate estimates if disturbances with significant impact on water use (e.g., wildfires, floods, and disease outbreaks) occur during part of the study year. Finally, the SSS method cannot account for direct evaporation from shallow groundwater.

References

Allander, K. K., Smith, J. L., Johnson, M. J. (2009). *Evapotranspiration from the Lower Walker River Basin, West-Central Nevada, Water Years 2005–07*. *United States Geological Survey Scientific Investigations Report 2009-5079. United States Geological Survey.*

Allen, R. G., Clemmens, A. J., Burt, C. M., Solomon, K., & O'Halloran, T. (2005). Prediction accuracy for projectwide evapotranspiration using crop coefficients and reference evapotranspiration. *Journal of Irrigation and Drainage Engineering*, *131*(1), 24-36.

Allen, R. G., Pereira, L. S., Howell, T. A., & Jensen, M. E. (2011). Evapotranspiration information reporting: I. Factors governing measurement accuracy. *Agricultural Water Management*, *98*(6), 899-920.

Allen, R. G., Tasumi, M., & Trezza, R. (2007). Satellite-based energy balance for mapping evapotranspiration with internalized calibration (METRIC)—Model. *Journal of irrigation and drainage engineering*, *133*(4), 380-394.

Allen, R. G., Walter, I. A., Elliott, R. L., Howell, T. A., Itenfisu, D., Jensen, M. E., & Snyder, R. L. (2005). The ASCE standardized reference evapotranspiration equation. (2005). *Technical Committee report to the Environmental and Water Resources Institute of the American Society of Civil Engineers from the Task Committee on Standardization of Reference Evapotranspiration, ASCE*.

Bailey, J. K., Schweitzer, J. A., & Whitham, T. G. (2001). Salt cedar negatively affects biodiversity of aquatic macroinvertebrates. *Wetlands*, *21*(3), 442-447.

Barz, D., Watson, R. P., Kanney, J. F., Roberts, J. D., & Groeneveld, D. P. (2009). Cost/benefit considerations for recent saltcedar control, Middle Pecos River, New Mexico. *Environmental management*, *43*(2), 282.

Bastiaanssen, W. G. M., Noordman, E. J. M., Pelgrum, H., Davids, G., Thoreson, B. P., & Allen,

R. G. (2005). SEBAL model with remotely sensed data to improve water-resources management under actual field conditions. *Journal of irrigation and drainage engineering*, *131*(1), 85-93.

Bastiaanssen, W. G., Menenti, M., Feddes, R. A., & Holtslag, A. A. M. (1998). A remote sensing surface energy balance algorithm for land (SEBAL). 1. Formulation. *Journal of hydrology*, *212*, 198-212.

Bawazir, A. S., Samani, Z., Bleiweiss, M., Skaggs, R., & Schmugge, T. (2009). Using ASTER satellite data to calculate riparian evapotranspiration in the Middle Rio Grande, New Mexico. *International journal of remote sensing*, *30*(21), 5593-5603.

Beamer, J. P., Huntington, J. L., Morton, C. G., & Pohll, G. M. (2013). Estimating annual groundwater evapotranspiration from phreatophytes in the great basin using landsat and flux tower measurements. *JAWRA Journal of the American Water Resources Association*, *49*(3), 518-533.

Biggs, T. W., Marshall, M., & Messina, A. (2016). Mapping daily and seasonal evapotranspiration from irrigated crops using global climate grids and satellite imagery: Automation and methods comparison. *Water Resources Research*, *52*(9), 7311-7326.

Brouwer, C., & Heibloem, M. (2010). Irrigation water management. Training manual no. 3. FAO Land and Water. *Development Division. FAO, Rome, Italy*.

Busch, D. E., & Smith, S. D. (1993). Effects of fire on water and salinity relations of riparian woody taxa. *Oecologia*, *94*(2), 186-194.

Cleverly, J. R., Smith, S. D., Sala, A., & Devitt, D. A. (1997). Invasive capacity of Tamarix ramosissima in a Mojave Desert floodplain: the role of drought. *Oecologia*, *111*(1), 12-18.

Devitt, D. A., Sala, A., Smith, S. D., Cleverly, J., Shaulis, L. K., & Hammett, R. (1998). Bowen

ratio estimates of evapotranspiration for Tamarix ramosissima stands on the Virgin River in southern Nevada. *Water Resources Research*, *34*(9), 2407-2414.

Di Tomaso, J. M. (1998). Impact, biology, and ecology of saltcedar (Tamarix spp.) in the southwestern United States. *Weed technology*, 326-336.

Friedl, M. A., McIver, D. K., Hodges, J. C., Zhang, X. Y., Muchoney, D., Strahler, A. H., ... & Baccini, A. (2002). Global land cover mapping from MODIS: algorithms and early results. *Remote sensing of Environment*, *83*(1-2), 287-302.

Friedl, M. A., Sulla-Menashe, D., Tan, B., Schneider, A., Ramankutty, N., Sibley, A., & Huang, X. (2010). MODIS Collection 5 global land cover: Algorithm refinements and characterization of new datasets. *Remote sensing of Environment*, *114*(1), 168-182.

Glenn, E. P., & Nagler, P. L. (2005). Comparative ecophysiology of Tamarix ramosissima and native trees in western US riparian zones. *Journal of Arid Environments*, *61*(3), 419-446.

Glenn, E. P., Huete, A. R., Nagler, P. L., Hirschboeck, K. K., & Brown, P. (2007). Integrating remote sensing and ground methods to estimate evapotranspiration. *Critical Reviews in Plant Sciences*, *26*(3), 139-168.

Glenn, E. P., Jarchow, C. J., & Waugh, W. J. (2016). Evapotranspiration dynamics and effects on groundwater recharge and discharge at an arid waste disposal site. *Journal of Arid Environments*, *133*, 1-9.

Glenn, E., Tanner, R., Mendez, S., Kehret, T., Moore, D., Garcia, J., & Valdes, C. (1998). Growth rates, salt tolerance and water use characteristics of native and invasive riparian plants from the delta of the Colorado River, Mexico. *Journal of Arid Environments*, *40*(3), 281-294.

Gonzalez-Dugo, M. P., Neale, C. M. U., Mateos, L., Kustas, W. P., Prueger, J. H., Anderson, M. C., & Li, F. (2009). A comparison of operational remote sensing-based models for

estimating crop evapotranspiration. *Agricultural and Forest Meteorology*, *149*(11), 1843-1853.

Gowda, P. H., Chavez, J. L., Colaizzi, P. D., Evett, S. R., Howell, T. A., & Tolk, J. A. (2008). ET mapping for agricultural water management: present status and challenges. *Irrigation science*, *26*(3), 223-237.

Groeneveld, D. P. (2008). Remotely-sensed groundwater evapotranspiration from alkali scrub affected by declining water table. *Journal of hydrology*, *358*(3-4), 294-303.

Groeneveld, D. P., & Baugh, W. M. (2007a). Correcting satellite data to detect vegetation signal for eco-hydrologic analyses. *Journal of Hydrology*, *344*(1-2), 135-145.

Groeneveld, D. P., Baugh, W. M., Sanderson, J. S., & Cooper, D. J. (2007b). Annual groundwater evapotranspiration mapped from single satellite scenes. *Journal of Hydrology*, *344*(1-2), 146-156.

Harms, R. S., & Hiebert, R. D. (2006). Vegetation response following invasive tamarisk (Tamarix spp.) removal and implications for riparian restoration. *Restoration Ecology*, *14*(3), 461-472.

Huete, A. R., & Liu, H. Q. (1994). An error and sensitivity analysis of the atmospheric-and soil-correcting variants of the NDVI for the MODIS-EOS. *IEEE Transactions on Geoscience and Remote sensing*, *32*(4), 897-905.

Huete, A., Didan, K., Miura, T., Rodriguez, E. P., Gao, X., & Ferreira, L. G. (2002). Overview of the radiometric and biophysical performance of the MODIS vegetation indices. *Remote sensing of environment*, *83*(1-2), 195-213.

Irmak, A., Allen, R. G., Kjaersgaard, J., Huntington, J., Kamble, B., Trezza, R., & Ratcliffe, I. (2012). Operational remote sensing of ET and challenges. In *Evapotranspiration-remote sensing and modeling*. InTech.

Jarchow, C. J., Nagler, P. L., & Glenn, E. P. (2017). Greenup and evapotranspiration following the Minute 319 pulse flow to Mexico: An analysis using Landsat 8 Normalized Difference Vegetation Index (NDVI) data. *Ecological engineering*, *106*, 776-783.

Jensen, M. E. (2003). *Vegetative and Open Water Coefficients for the Lower Colorado River Accounting System (Addendum to the 1998 Report). United States Bureau of Reclamation.*

Kalma, J. D., McVicar, T. R., & McCabe, M. F. (2008). Estimating land surface evaporation: A review of methods using remotely sensed surface temperature data. *Surveys in Geophysics*, *29*(4-5), 421-469.

Kamble, B., Irmak, A., Martin, D. L., Hubbard, K. G., Ratcliffe, I., Hergert, G., Narumalani, S., & Oglesby, R. J. (2013). Satellite-Based energy balance approach to assess riparian water use. In *Evapotranspiration-An Overview*. InTech.

Lewis, C. S. (2016). *Evapotranspiration Estimation: A Study of Methods in the Western United States* (Doctoral Dissertation).

Liebert, R., Huntington, J., Morton, C., Sueki, S., & Acharya, K. (2016). Reduced evapotranspiration from leaf beetle induced tamarisk defoliation in the Lower Virgin River using satellite- based energy balance. *Ecohydrology*, *9*(1), 179-193.

Liu, H. Q., & Huete, A. (1995). A feedback based modification of the NDVI to minimize canopy background and atmospheric noise. *IEEE Transactions on Geoscience and Remote Sensing*, *33*(2), 457-465.

Los Angeles Department of Water and Power (LADWP). (2015). *Urban Water management Plan, Arcadis U.S. Inc.*

Lower Colorado River Accounting System. (2007). *Evapotranspiration and Evaporation Calculations, Calendar Year 2005. United States Bureau of Reclamation, USA.*

Lower Colorado River Accounting System. (2014). *Evapotranspiration and Evaporation Calculations, Calendar Year 2010. United States Bureau of Reclamation, USA.*

Masek, J. G., Vermote, E. F., Saleous, N., Wolfe, R., Hall, F. G., Huemmrich, K. F., Gao, F., Kutler, J., & Lim, T. K. (2012). LEDAPS Landsat calibration, reflectance, atmospheric correction preprocessing code. *ORNL DAAC*.

Mexicano, L., Glenn, E. P., Hinojosa-Huerta, O., Garcia-Hernandez, J., Flessa, K., & Hinojosa-Corona, A. (2013). Long-term sustainability of the hydrology and vegetation of Cienega de Santa Clara, an anthropogenic wetland created by disposal of agricultural drain water in the delta of the Colorado River, Mexico. *Ecological engineering*, *59*, 111-120.

Monteith, J. L. (1965, July). Evaporation and environment. In *Symp. Soc. Exp. Biol* (Vol. 19, No. 205-23, p. 4).

Morton, C. G., Huntington, J. L., Pohll, G. M., Allen, R. G., McGwire, K. C., & Bassett, S. D. (2013). Assessing calibration uncertainty and automation for estimating evapotranspiration from agricultural areas using METRIC. *JAWRA Journal of the American Water Resources Association*, *49*(3), 549-562.

Mu, Q., Heinsch, F. A., Zhao, M., & Running, S. W. (2007). Development of a global evapotranspiration algorithm based on MODIS and global meteorology data. *Remote sensing of Environment*, *111*(4), 519-536.

Mu, Q., Zhao, M., & Running, S. W. (2011). Improvements to a MODIS global terrestrial evapotranspiration algorithm. *Remote Sensing of Environment*, *115*(8), 1781-1800.

Murray, R. S., Nagler, P. L., Morino, K., & Glenn, E. P. (2009). An empirical algorithm for estimating agricultural and riparian evapotranspiration using MODIS Enhanced Vegetation Index and ground measurements of ET. II. Application to the Lower Colorado River, US. *Remote Sensing*, *1*(4), 1125-1138.

Nagler, P. L., Brown, T., Hultine, K. R., Bean, D. W., Dennison, P. E., Murray, R. S., & Glenn, E. P. (2012). Regional scale impacts of Tamarix leaf beetles (Diorhabda carinulata) on the water availability of western US rivers as determined by multi-scale remote sensing methods. *Remote Sensing of Environment, 118,* 227-240.

Nagler, P. L., Cleverly, J., Glenn, E., Lampkin, D., Huete, A., & Wan, Z. (2005b). Predicting riparian evapotranspiration from MODIS vegetation indices and meteorological data. *Remote Sensing of Environment*, *94*(1), 17-30.

Nagler, P. L., Glenn, E. P., Didan, K., Osterberg, J., Jordan, F., & Cunningham, J. (2008). Wide-area estimates of stand structure and water use of Tamarix spp. on the Lower Colorado River: Implications for restoration and water management projects. *Restoration Ecology, 16*(1), 136-145.

Nagler, P. L., Glenn, E. P., Nguyen, U., Scott, R. L., & Doody, T. (2013). Estimating riparian and agricultural actual evapotranspiration by reference evapotranspiration and MODIS enhanced vegetation index. *Remote Sensing*, *5*(8), 3849-3871.

Nagler, P. L., Morino, K., Didan, K., Erker, J., Osterberg, J., Hultine, K. R., & Glenn, E. P. (2009a). Wide- area estimates of saltcedar (Tamarix spp.) evapotranspiration on the lower Colorado River measured by heat balance and remote sensing methods. *Ecohydrology: Ecosystems, Land and Water Process Interactions, Ecohydrogeomorphology*, *2*(1), 18-33.

Nagler, P. L., Morino, K., Murray, R. S., Osterberg, J., & Glenn, E. P. (2009b). An empirical algorithm for estimating agricultural and riparian evapotranspiration using MODIS enhanced vegetation index and ground measurements of ET. I. Description of method. *Remote Sensing*, *1*(4), 1273-1297.

Nagler, P. L., Pearlstein, S., Glenn, E. P., Brown, T. B., Bateman, H. L., Bean, D. W., & Hultine,

K. R. (2014). Rapid dispersal of saltcedar (Tamarix spp.) biocontrol beetles (Diorhabda carinulata) on a desert river detected by phenocams, MODIS imagery and ground observations. *Remote Sensing of Environment*, *140*, 206-219.

Nagler, P. L., Scott, R. L., Westenburg, C., Cleverly, J. R., Glenn, E. P., & Huete, A. R. (2005a). Evapotranspiration on western US rivers estimated using the Enhanced Vegetation Index from MODIS and data from eddy covariance and Bowen ratio flux towers. *Remote sensing of environment*, *97*(3), 337-351.

Nichols, W. D. (2000). *Regional ground-water evapotranspiration and ground-water budgets, Great Basin, Nevada* (No. 1628). US Geological Survey.

Owens, M. K., & Moore, G. W. (2007). Saltcedar water use: realistic and unrealistic expectations. *Rangeland Ecology & Management*, *60*(5), 553-557.

Qi, J., Chehbouni, A., Huete, A. R., Kerr, Y. H., & Sorooshian, S. (1994). A modified soil adjusted vegetation index. *Remote sensing of environment*, *48*(2), 119-126.

Ruhoff, A. L., Paz, A. R., Aragao, L. E. O. C., Mu, Q., Malhi, Y., Collischonn, W., ... & Running, S. W. (2013). Assessment of the MODIS global evapotranspiration algorithm using eddy covariance measurements and hydrological modelling in the Rio Grande basin. *Hydrological Sciences Journal*, *58*(8), 1658-1676.

Scott, R. L., Cable, W. L., Huxman, T. E., Nagler, P. L., Hernandez, M., & Goodrich, D. C. (2008). Multiyear riparian evapotranspiration and groundwater use for a semiarid watershed. *Journal of Arid Environments*, *72*(7), 1232-1246.

Smith, J., Laczniak, R. J., Moreo, M. T., & Welborn, T. L. (2007). *Mapping Evapotranspiration Units in the Basin and Range Carbonate-Rock Aquifer System, White Pine County, Nevada, and Adjacent Areas in Nevada and Utah*. *United States Geological Survey.*

Stromberg, J. C. (1998). Functional equivalency of saltcedar (Tamarix chinensis) and fremont

cottonwood (Populus fremonth) along a free-flowing river. *Wetlands*, *18*(4), 675-686.

Stromberg, J. C., & Rychener, T. J. (2010). Effects of fire on riparian forests along a free-flowing dryland river. *Wetlands*, *30*(1), 75-86.

Taghvaeian, S., Neale, C. M., Osterberg, J., Sritharan, S. I., & Watts, D. R. (2014). Water use and stream-aquifer-phreatophyte interaction along a Tamarisk-dominated segment of the Lower Colorado River. *Remote Sensing of the Terrestrial Water Cycle; John & Sons, Inc.: Hoboken, NJ, USA*, 95-113.

Tillman, F. D., Callegary, J. B., Nagler, P. L., & Glenn, E. P. (2012). A simple method for estimating basin-scale groundwater discharge by vegetation in the basin and range province of Arizona using remote sensing information and geographic information systems. *Journal of arid environments*, *82*, 44-52.

Vandersande, M. W., Glenn, E. P., & Walworth, J. L. (2001). Tolerance of five riparian plants from the lower Colorado River to salinity drought and inundation. *Journal of Arid Environments*, *49*(1), 147-159.

Velpuri, N. M., Senay, G. B., Singh, R. K., Bohms, S., & Verdin, J. P. (2013). A comprehensive evaluation of two MODIS evapotranspiration products over the conterminous United States: Using point and gridded FLUXNET and water balance ET. *Remote Sensing of Environment*, *139*, 35-49.

Westenberg, C., Harper, D., DeMeo, G. (2006). *Evapotranspiration by Phreatophytes Along the Lower Colorado River at Havasu National Wildlife Refuge, Arizona. United States Geological Survey Scientific Investigations Report, 2006-5043. United States Geological Survey.*

White, W. N. (1932). *A method of estimating ground-water supplies based on discharge by plants and evaporation from soil: Results of investigations in Escalante Valley, Utah* (Vol. 659).

US Government Printing Office.

Zavaleta, E. (2000). Valuing ecosystem services lost to Tamarix invasion in the United States. *Invasive species in a changing world*, 261-300.

CHAPTER III

A MODELING FRAMEWORK FOR DERIVING DAILY TIME SERIES OF EVAPOTRANSPIRATION MAPS USING A SURFACE ENERGY BALANCE MODEL

Abstract: Surface energy balance models have been one of the most widely used approaches to estimate spatially distributed evapotranspiration (ET) at varying landscape scales. However, more research is required to develop and test an operational framework that can address all challenges related to processing and gap filling of non-continuous satellite data to generate time series of ET at regional scale. In this study, an automated modeling framework was developed to construct daily time series of ET maps using MODIS imagery and the Surface Energy Balance System model. The ET estimates generated from this modeling framework were validated against observations of three eddy-covariance towers in Oklahoma, United States during a two-year period at each site. The modeling framework overestimated ET but captured its spatial and temporal variability. The overall performance was good with mean bias errors less than 30 W m^{-2} and root mean square errors less than 50 W m^{-2}. The model was then applied for a 14-year period (2001–2014) to study ET variations across Oklahoma. The statewide annual ET varied from 841 to 1100 mm yr^{-1}, with an average of 994 mm yr^{-1}. The results were also analyzed to estimate the ratio of estimated ET to reference ET, which is an indicator of water scarcity. The potential applications and challenges of the ET modeling framework are discussed and the future direction for the improvement and development of similar automated approaches are highlighted.

1. Introduction

Time series of remotely sensed evapotranspiration (ET) maps have extensive applications in agricultural, hydrological, and environmental studies as they capture the spatiotemporal variability of vegetation consumptive use from field to continental scales. For example, spatial ET data have been used in agriculture sector for water right regulation, planning, and monitoring (Allen, Tasumi, Morse, & Trezza, 2005), assessing irrigation and drainage performance (Droogers & Bastiaanssen, 2002; Santos, Lorite, Tasumi, Allen, & Fereres, 2010; Taghvaeian, Neale, Osterberg, Sritharan, & Watts, 2018), closing water balance at irrigation scheme levels (Taghvaeian & Neale, 2011), and managing agricultural water resources (Anderson et al., 2012; Bastiaanssen et al., 2005; Folhes, Rennó, & Soares, 2009). Recent studies have shown that remotely sensed ET can be used effectively for monitoring agricultural droughts (Anderson et al., 2011; Yao, Liang, Qin, & Wang, 2010; Zhang & Mu, 2016) with the future potential of improving the performance of ET-integrated agricultural drought indices (Moorhead et al., 2015). ET maps have been also used in assessing crop water productivity (Ahmad, Turral, & Nazeer, 2009; Li et al., 2008; Teixeira, Bastiaanssen, Ahmad, & Bos, 2009) and crop yield analysis (Anderson et al., 2016; Cai & Sharma, 2010). Numerous studies have demonstrated the use of time series ET maps for ecological applications, such as capturing the progress of vegetation and wetland restoration (Oberg & Melesss, 2006), assessing the vulnerability of forest to fire and drought (Nepstad et al., 2004), and accounting water use from riparian vegetation and invasive species (Bawazir, Samani, Bleiweiss, Skaggs, & Schmugge, 2009; Khand, Taghvaeian, & Hassan-Esfahani, 2017; Nagler, Glenn, Nguyen, Scott, & Doody, 2013; Taghvaeian, Neale, Osterberg, Sritharan, & Watts, 2014). Remote sensing based ET products have also been applied in improving the performances of hydrological models (Chen, Chen, Ju, & Geng, 2005; Herman et al., 2018; Immerzeel, Gaur, & Zwart, 2008) and for climate studies to capture water feedbacks

associated with seasonal cycles and soil moisture deficit at regional scales (Vinukollu, Wood, Ferguson, & Fischer, 2011).

Among different approaches developed for mapping ET, the remotely sensed surface energy balance (RSEB) approach has been widely used to acquire distributed ET at varying geographical scales (Gowda et al., 2007, Kalma, McVicar, & McCabe, 2008; Li et al., 2009; Liou & Kar, 2014). Numerous RSEB models have been proposed, including but not limited to Surface Energy Balance Index (SEBI) (Menenti & Choudhary, 1993), Two-Source Energy Balance (TSEB) (Norman & Becker, 1995; Kustas & Norman, 1999), Surface Energy Balance Algorithm for Land (SEBAL) (Bastiaanssen, Menenti, Feddes & Holtslag, 1998), Simplified Surface Energy Balance Index (S-SEBI) (Roerink, Su, & Menenti, 2000), Surface Energy Balance System (SEBS) (Su, 2002), Mapping Evapotranspiration at high Resolution with Internalized Calibration (METRIC) (Allen, Tasumi & Trezza, 2007), Atmosphere-Land Exchange Inverse (ALEXI) (Anderson, Norman, Mecikalski, Otkin, & Kustas, 2007), Regional ET Estimation Model (REEM) (Saman & Bawzir, 2007), Remote Sensing Evapotranspiration model (ReSET) (Elhaddad & Garcia, 2008), Operational Simplified Surface Energy Balance (SSEBop) (Senay et al., 2013), and Hybrid Dual-Source Scheme and Surface Energy Framework-Based Evapotranspiration Model (HTEM) (Yang & Shang, 2013). Some of these models such as SEBAL and METRIC use manual selection of extreme pixels to compute sensible heat flux, which could result in variations in estimated ET (Timmermans, Kustas, Anderson & French, 2007) and may add uncertainty and errors based on the user's experience (Allen, Pereira, Howell & Jensen, 2011). Other models such as TSEB, SEBS, and SSEBop do not require human intervention so that the associated uncertainties are minimized. The selection of the RSEB model and the quality of input data are likely key factors to determine the accuracy of modeled ET (Fisher, Whittaker, & Malhi, 2011).

Developing time series of ET maps requires complex, multi-step analyses to deal with issues associated with pre-processing of remote sensing data and post-processing of resulting ET products. The choice of the RSEB model and satellite data could vary depending on intended applications of ET maps, availability and requirements of input data, and availability of resources (time, money, and expertise) to run the model. In general, the RSEB-based ET estimation process can be divided into six steps: i) collection of remotely sensed and ground-based input data, ii) quality assessment of collected datasets and preparation of all necessary inputs for the selected RSEB model, iii) running the RSEB model (including all modules and algorithms) to obtain the instantaneous ET at the time of satellite overpass, iv) extrapolation of instantaneous ET to daily estimates, v) filling the gaps due to cloud coverage over a portion of the map, and vi) interpolation of daily ET between image acquisition dates to obtain ET for longer time scales.

The first two steps are performed to ensure the quality of input data, a critical requirement for any remote sensing data analysis. A thorough QA/QC procedure for weather data as presented in Allen (1996) and ASCE-EWRI (2005) is necessary as the accuracy of final ET product depends on the quality of these datasets. The quality assurance of weather dataset is more critical in case of RSEB models as they are sensitive to weather parameters. For example, Webster, Ramp, and Kingsford (2016) found air temperature and wind speed as influential inputs for HTEM and SEBS models, whereas, S-SEBI was less sensitive to meteorological inputs.

For small-scale applications with similar climatic conditions, weather data from a single ground station are usually used as input in most RSEB models. However, for regional applications with varying climatic conditions, gridded datasets are required. Several recent studies (Biggs, Marshall, & Messina, 2016; Senay, Friedrichs, Singh & Velpuri, 2016) have applied gridded weather datasets for mapping daily ET due to the ease of their application for regional studies. However, users need to confirm the integrity of the datasets before processing the RSEB model. A study (Moorhead et al., 2015) found overestimation of reference ET due to

biases in air temperature and wind speed in the widely used reanalysis data – North American Land Data Assimilation System when compared to reference ET estimates from the Texas High Plains ET Network (Porter et al., 2012). The study recommended using weather station datasets within agricultural settings, whenever possible, for precise applications of time series ET information such as in irrigation scheduling. A few studies have explored the applicability of developing distributed weather data from the point measurements of a network of ground stations to account for the spatial variability of weather parameters (Elhaddad & Garcia, 2011).

The third step is to run the selected RSEB model, which involves several sub-models to solve the RSEB equation as shown in equation 3.1.

$$LE = Rn - G - H \tag{3.1}$$

where LE is the latent heat flux, Rn is net radiation, G is soil heat flux, and H is sensible heat flux. All parameters are in units of W m^{-2}. Based on the sensible heat flux computation approach, RSEB models can be categorized into single-source and two-source models. The sensible heat fluxes for soil and vegetation are computed separately in two-source models, while a single value for each pixel is computed in single-source models. Each approach has its own advantages and caveats. In theory, two-source models could provide more accurate ET over sparse vegetation as they close the energy balance separately for soil and vegetation. Timmermans, Kustas, Anderson and French (2007) found better accuracy from a TSEB model compared to SEBS across sparsely vegetated grasslands in the Southern Great Plains. Kustas, Humes, Norman, and Moran (1996) reported that two-source performed better in sub-humid tallgrass prairie, whereas greater accuracy was found for a single-source model in semiarid rangeland.

As mentioned before, some single-source models require an additional step in running the model, which involves the manual selection of extreme hot and cold pixels by user. To remove the subjectivity in the selection of extreme pixels in SEBAL, Long and Singh (2012) introduced a trapezoidal approach to define boundary conditions for the selection of these pixels based on the

relationship between vegetation fraction and surface temperature. Automated approaches have been proposed in Allen et al. (2013), Bhattarai, Quackenbush, Im, and Shaw (2017), and Kjaersgaard, Allen, Garcia, Kramber, and Trezza (2009) to replace human intervention. Alternative approaches are also applied by Trezza, Allen, and Tasumi (2013) and Khand, Numata, Kjaersgaard, and Vourlitis (2017) to estimate ET from a cold pixel as a function normalized difference vegetation index when an ideal cold pixel is difficult to find within a satellite image.

The fourth step is to extrapolate the instantaneous ET to daily values. Evaporative fraction (Λ) (Brutsaert and Sugita, 1992; Bastiaanssen et al., 1998; Su, 2002; Kustas et al., 1994) and ETrF (fraction of reference ET) (Allen et al., 2007; Terezza, 2002) are the common methods to obtain daily ET. Both of these methods assume the instantaneous Λ or ETrF is the same as for the daily Λ or ETrF. However, a study (Gentine, Entekhabi, Chehouni, Boulet, & Duchemin, 2007) reported that this assumption was not satisfied when the fractional vegetation cover was close to a maximum. In the Texas Panhandle, Colaizzi, Evitt, Howell, and Tolk (2006) found a better agreement of ETrF method for cropland and Λ method for bare soil when compared with lysimeter measurements. Chávez, Beale, Prueger, and Kustas (2008) evaluated six extrapolation approaches on corn and soybean fields and found smaller error from Λ method when compared with eddy covariance measurements. Another study (Delogu et al., 2012) found Λ method advantageous during several water stress events, whereas ETrF approach performed better under advective conditions (Allen et al., 2007; Trezza, 2002), which could be significant in arid environments.

The fifth step is to fill the gaps caused by cloud coverage over a portion of the daily ET maps. One approach is to apply linear interpolation of nearest reliable values within an image (Senay et al., 2016). This method is suitable when the nearest pixels are under the same land cover as that of missing pixels. However, it may not be appropriate when the area with data gap is

large and encompasses heterogeneous terrain. Another approach includes the use of time-weighted interpolation of preceding and following images (Kjaersgaard et al., 2010). This method adjusts the vegetation development using normalized difference vegetation index (NDVI) across vegetated areas and residual soil moisture differences for the areas with bare soil surface. Anderson et al. (2007) applied the available water for the root zone and soil surface layer to fill the gaps. The available water for the clear and cloudy days are used to estimate the daily water depletion due to ET from the root zone and soil surface layer, and the fraction of available water is used to fill the gaps (Anderson et al., 2007).

The final step is the interpolation of daily ET maps between consecutive satellite overpass dates to construct daily ET time series. Several Interpolation and data-fusion approaches have been implemented for this purpose. A common approach is to apply linear interpolation of Λ or ETrF images between consecutive satellite overpass dates (Singh, Liu, Tieszen, Suyker, & Verma, 2012). Another approach is to apply a curvilinear function using more than two Λ or ETrF images. For example, at least one cloud-free image for each month was used for spline interpolation within METRIC to obtain monthly and seasonal ET (Allen et al., 2007; Khand, Kjaersgaard, Hay, & Jia, 2017; Kjaersgaard, Allen, & Irmak, 2011). Singh, Liu, Tieszen, Suyker, and Verma (2012) evaluated the performance of several interpolation methods and found no significant difference in seasonal ET among cubic spline, fixed ETrF, and linear interpolations. A backward-average iterative approach has been also proposed to estimate ET in between Landsat overpass dates (Dhungel, Allen, Trezza, & Robinson, 2016).

While numerous studies have been conducted to address the issues related to specific steps involved in generating remotely sensed ET time series based on SEB models, only a few have focused on developing automated modeling frameworks, covering all hierarchical steps mentioned above. Such modeling frameworks, if validated, could have significant value in providing end-users with daily ET time series for practical applications in improving land and

water management. Furthermore, a comprehensive and detailed documentation of the entire process of deriving daily ET maps at regional scales could be a useful resource to potential end-users who currently need to understand and select appropriate approaches for each of the six steps from many sources. Developing and documenting a comprehensive framework that generates complete ET time series from raw input data enables potential users outside the research community to utilize this framework for making more informed decisions and policies. The main goal of this study was to develop and document a modeling framework to construct daily time series of ET maps for the entire state of Oklahoma, USA. The performance of this framework was also evaluated by comparing its results with ET estimates of flux towers in Oklahoma. Finally, long-term variations in ET across Oklahoma were investigated.

2. Materials and Methods

2.1 Study Area

The study area covered the entire state of Oklahoma, USA, with an area of about 181,200 km^2 (Figure 3.1). Oklahoma Climate is classified as humid subtropical at most parts of the state and cold semi-arid at far west (Kottek, Grieser, Beck, Rudolf, & Rubel, 2006). The state has nine climate divisions (CD) delineated based on precipitation and temperature gradients. The normal (1981-2010) annual precipitation is about 925 mm yr^{-1}, with significant spatial variation across CDs. While southeast (CD9) receives the largest amount of 1,301 mm yr^{-1} on average, the Panhandle (CD1) holds the smallest record of 520 mm yr^{-1}. The normal annual mean air temperature is 15.6 ºC, with July and January being the hottest and coldest months, respectively. The southcentral (CD8) has the highest mean annual temperature of 16.7 ºC, whereas the Panhandle region has the lowest value at 13.6 ºC. The top two land cover categories in Oklahoma are grassland (36.4%) and pastureland (11.3%) (Homer et al., 2015). The elevation varies

between 88 m above mean sea level at the southeast border with Arkansas and 1516 m at far-west border with New Mexico.

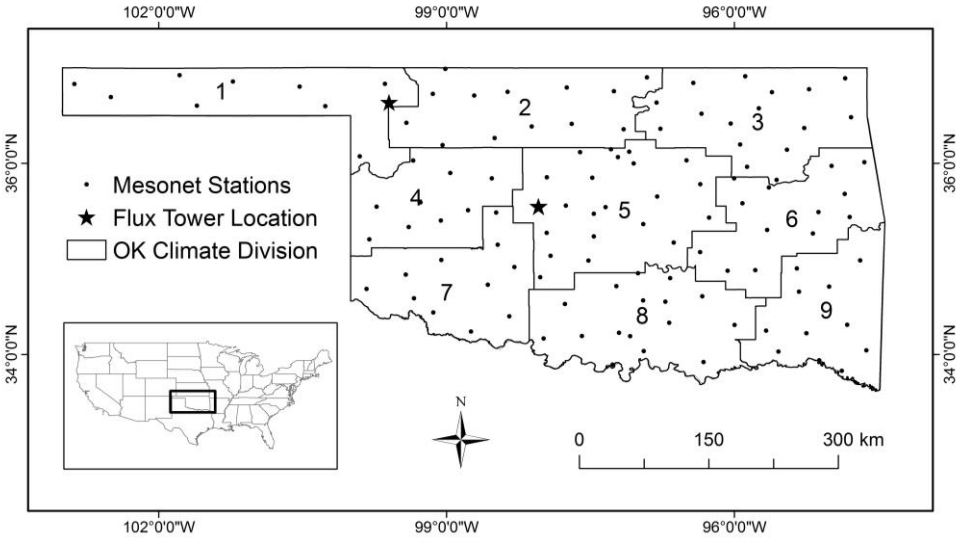

Figure 3.1. Map of Oklahoma and its nine climate divisions. The locations of Mesonet stations and flux towers are also specified.

2.2 Modeling Framework

The modeling framework was designed to use daily images from the MODIS Terra satellite as input data. The single-source SEBS model (Su, 2002) was selected as the SEB model for estimating energy fluxes. The main reason for the selection of SEBS over other SEB models was its applicability over large areas with heterogeneous surfaces (Liou & Kar, 2014). In addition, this model does not require intermittent human intervention, which facilitates the automation process. A graphical illustration of the proposed framework is shown in Figure 3.2, followed by detailed explanation of specific approaches selected for each of the six computational steps mentioned before.

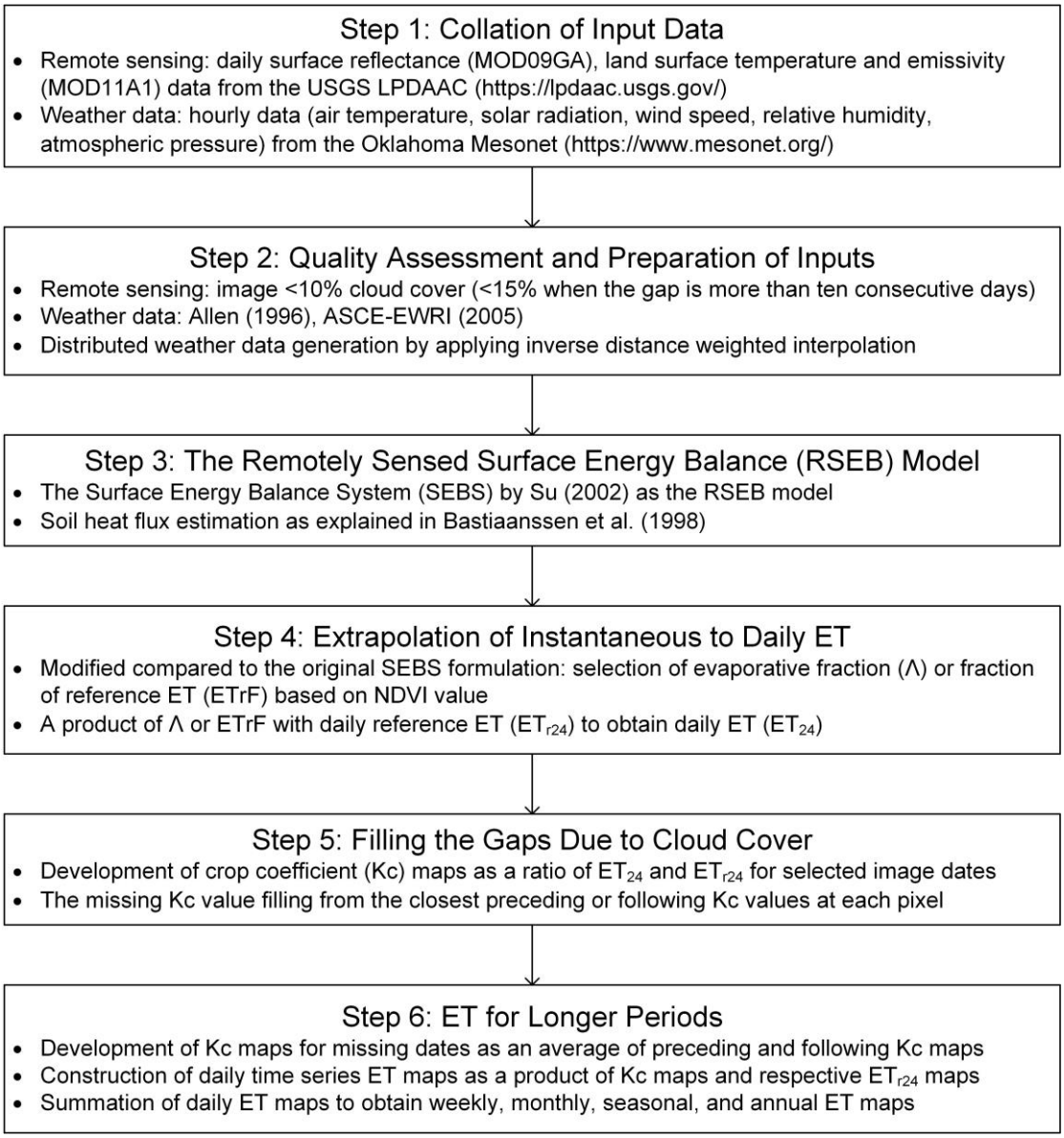

Figure 3.2. A descriptive flow diagram of the daily time series of evapotranspiration (ET) modeling framework

2.2.1 Collation of Input Data

The daily surface reflectance (MOD09GA, Vermote & Wolfe, 2015), daily land surface temperature (LST) and emissivity (MDO11A1, Wan, Hook, & Hulley, 2015) data were downloaded from the US Geological Survey Land Processes Distributed Active Archive Center

(https://lpdaac.usgs.gov/). Ground-based meteorological data included hourly air temperature, relative humidity, incoming shortwave solar radiation, wind speed and atmospheric pressure. These data were obtained from the Oklahoma Mesonet (Brock et al., 2015; McPherson et al., 2007) weather stations installed across the state (Figure 3.1). The Oklahoma Mesonet is a world-class environmental monitoring network (https://www.mesonet.org/) consisting of 120 active stations with at least one station at each of the 77 counties in Oklahoma.

2.2.2 Quality Assessment and Preparation of Inputs

The initial quality assessment of suitable MODIS images was based on cloud coverage. Images with less than 10% cloud cover were selected for further processing. Hence, any day when the cloud coverage was above 10% was assumed as a day with missing remotely sensed data. When the period of missing imagery was more than 10 consecutive days, images with less than 15% cloud cover were also included as acceptable quality. Then, cloud-covered pixels in each selected image were masked by applying a threshold of LST smaller than 250 K. These steps were repeated for all selected reflectance, LST and emissivity images. Since a single MODIS image tile was not sufficient to cover the entire state of Oklahoma, two image tiles (h09v05 and h10v05) were merged.

The quality assessment of each weather variables was performed as described in Allen (1996) and ASCE-EWRI (2005). The solar radiation was checked against the upper limit under clear sky condition. Daily average temperature was compared against the average extreme temperatures to ensure the difference between them was within the acceptable range (2 ºC) (ASCE-EWRI, 2005). The quality of wind speed was maintained by considering gust factor threshold of more than 1. Relative humidity data were considered when the values were less than 100%. The missing weather data were filled by an average value of that parameter from four nearest Mesonet stations. Hourly alfalfa reference ET (ET_r) (ASCE-EWRI, 2005) was then computed at each

station during the study period using the Bushland ET Calculator (Gowda, Ennis, Howell, Marek, & Porter, 2012). Daily ET_r estimates were obtained by summing 24-hour ET_r values. To incorporate the weather variability between the weather stations, spatial input data were generated by applying inverse distance weighted interpolation for all weather variables, including hourly and daily ET_r. As mentioned in the previous section, the Oklahoma Mesonet is a densely distributed weather station network, with about 1,510 km^2 per station. This is a significantly finer spatial resolution than the 5,000 km^2 per station value recommended by the World Meteorological Organization for evaporation stations on interior plains (WMO, 2008). Hence, the adjustment of meteorological parameters with elevation was not considered during interpolation.

2.2.3 The RSEB Model

As mentioned before, the Surface Energy Balance System (SEBS) model of Su (2002) was selected as the SEB model in the present study. However, other SEB models such as those reviewed in the Introduction section can be used in this step based on user resources, availability of input data and desired accuracy. Like other SEB models, SEBS estimates the latent heat flux (LE) as a residual of the land surface energy balance as shown in equation 3.1. The Rn was calculated by applying the surface radiation balance equation:

$$\mathrm{Rn} = (1 - \alpha)\mathrm{R_s} + \varepsilon_s\, \varepsilon_a\, \sigma\, \mathrm{T_A^4} - \varepsilon_s\, \sigma \tag{3.2}$$

where R_S is incoming shortwave solar radiation, α is surface albedo (dimensionless) estimated following (Linag, 2001), ε_a and ε_s are emissivities (dimensionless) of atmosphere and surface, estimated following (Brutsaert, 1982) and (Liang, 2005), respectively. σ is the Stefan-Boltzmann constant (5.67×10^{-8} W m^{-2} K^{-4}), T_A is air temperature (K) and T_s is the surface temperature (K), estimated as a ratio of brightness temperature to $\varepsilon_s^{-0.25}$. The G was estimated by applying the relationship developed by [35]:

$$\frac{\mathrm{G}}{\mathrm{Rn}} = \frac{(\mathrm{T_s} - 273.15)}{100\,\alpha}(c_1\,\alpha + c_2\,\alpha^2)(1 - 0.98\,\mathrm{NDVI}^4) \tag{3.3}$$

where c_1 and c_2 are calibration coefficients and were considered as 0.24 and 0.46, respectively.

SEBS uses similarity theories to estimate H: the bulk atmospheric similarity (BAS) theory for atmospheric boundary layer (ABL) scaling (Brutsaert, 1999) and the Monin-Obukhov similarity (MOS) for atmospheric surface layer (ASL) scaling (Monin, & Obukhov, 1954). The ABL is a part of the atmosphere that is directly impacted by earth's surface and responds to surface forcing with a timescale of an hour or less, whereas ASL is usually the bottom 10% of ABL (Su, 2002). During unstable conditions, an appropriate atmospheric (BAS or MOS) scaling is determined as presented in Brutsaert (1982). For stable conditions, functions given by Brutsaert (1982) and Beljaars and Holtslag (1991) are used for ABL and ASL scaling, respectively. In the ASL, the similarity relationships for mean wind speed (u) and the difference between potential temperature profiles are derived using the MOS theory as:

$$u = \frac{u_*}{k}\left[\ln\left(\frac{z-d_0}{z_{0m}}\right) - \psi_m\left(\frac{z-d_0}{L}\right) + \psi_m\left(\frac{z_{0m}}{L}\right)\right] \tag{3.4}$$

$$\theta_0 - \theta_a = \frac{H}{k\,u_*\,\rho_a\,C_p}\left[\ln\left(\frac{z-d_0}{z_{0h}}\right) - \psi_h\left(\frac{z-d_0}{L}\right) + \psi_h\left(\frac{z_{0h}}{L}\right)\right] \tag{3.5}$$

$$L = -\frac{\rho_a C_p u_*^3 \theta_v}{kgH} \tag{3.6}$$

where u_* is the friction velocity (m s^{-1}), k is the von Karman's constant (0.41), z is the height above the surface (m), d_0 is the zero plane displacement height (m), z_{0m} is the roughness height for momentum transfer (m) estimated using an empirical relationship with NDVI (Gupta, Prasad, & Vijayan, 2002), z_{0h} is roughness height for heat transfer (m), θ_0 is the potential air temperature at surface (K), θ_a is the potential air temperature at z (K), θ_v is the potential virtual temperature near the surface (K), ρ_a is the air density (kg m^{-3}), C_p is the specific heat capacity of air (1,013 J kg^{-1} K^{-1}) and g is the gravitational acceleration (9.8 m s^{-2}). ψ_m and ψ_h are the stability correction functions for momentum and sensible heat transfer, respectively and L is the Monin–Obukhov length (m).

The scalar roughness height for heat transfer, z_{0h}, is an important parameter to regulate the heat transfer between the land surface and the atmosphere and estimated as:

$$z_{0h} = \frac{z_{0m}}{\exp(kB^{-1})} \tag{3.7}$$

where kB^{-1} is the Stanton number, a dimensionless heat transfer coefficient, estimated using a formulation from Su, Schmugge, Kustas, and Massman (2001) as:

$$kB^{-1} = \frac{kC_d}{4C_t \frac{u_*}{u(h)}\left(1-e^{\frac{-n_{ec}}{2}}\right)} f_c^2 + 2\, f_c\, f_s \frac{k\left(\frac{u_*}{u(h)}\right)\left(\frac{z_{0m}}{h}\right)}{C_t^*} + kB_s^{-1} f_s^2 \tag{3.8}$$

The heat transfer coefficient in equation 3.8 was formulated to account for three different land surface conditions. The first term follows the Choudhury and Monteith (Choudhary & Monteith, 1988) model for full canopy, the second term accounts for the interaction between the vegetation and soil surface and the third term is for the bare soil surface given (Brutsaert, 1982). In this equation, f_c and f_s are canopy and soil fraction coverage, respectively, C_d is the drag coefficient for the foliage with a value of 0.2; C_t and C_t^* are the heat transfer coefficients of the leaf and soil, respectively. The value of C_t was taken as 0.03 and C_t^* was computed from Prandtl number and roughness Reynolds number (Re_*) (Su, 2002). The u(h) in equation 3.8 is the horizontal wind speed at the canopy top (m s^{-1}) and h is canopy height (m) estimated as a ratio of z_{0m} to 0.136 (Su, 2002). The n_{ec} (within-canopy wind speed profile extinction coefficient) and Brutsaert term kB_S^{-1} (for bare soil surface) were calculated as:

$$n_{ec} = \frac{C_d\, LAI}{\frac{2u_*^2}{u(h)^2}} \tag{3.9}$$

$$kB_s^{-1} = 2.46(Re_*)^{0.25} - \ln(7.4) \tag{3.10}$$

where LAI is the leaf area index and estimated as a functional relation with NDVI (Gowda et al., 2007).

SEBS requires estimation of H for dry (H_{dry}) and wet (H_{wet}) boundary conditions. Under dry conditions, the H_{dry} is equivalent to the available energy ($R_n - G$) as there is no evaporation

due to the limitation of water availability and H_{wet} is calculated using the Penman-Monteith equation (Monteith, 1965, 1981). After computing H for boundary conditions, the relative evaporative fraction (Λ_r), the evaporative fraction (Λ) and ET are estimated. The steps and explanation are detailed in Su (2002).

2.2.4 Extrapolation of Instantaneous to Daily ET

The SEBS uses the Λ approach for scaling instantaneous ET to daily ET, assuming the Λ at the time of overpass is equal to the daily Λ. In this study, a modified approach was implemented where either Λ or ETrF is used for extrapolation of each pixel based on its NDVI value as shown in equation 3.15.

$$\Lambda_r = 1 - \frac{H - H_{wet}}{H_{dry} - H_{wet}} \quad (3.11)$$

$$\Lambda = \frac{\Lambda_r (R_n - G - H_{wet})}{R_n - G} \quad (3.12)$$

$$ET_{inst} = \left(\frac{R_n - H - G}{\lambda}\right) \text{ x } 3600 \quad (3.13)$$

$$ETrF = \frac{ET_{inst}}{ET_r} \quad (3.14)$$

$$ET_{24} = [\Lambda \times ET_{r24} \text{ for NDVI} < 0.30] \text{ or } [ETrF \times ET_{r24} \text{ for NDVI} \geq 0.30] \quad (3.15)$$

where ET_{inst} and ET_r are the actual and reference ET at the hour of satellite overpass (mm hr^{-1}), λ is the latent heat of vaporization (~2.45 MJ kg^{-1}). ET_{r24} is the daily reference ET and ET_{24} is the daily actual ET (mm d^{-1}). This modification was made to take the advantage of Λ and ETrF approach to better represent the water limited and energy limited conditions, respectively. The ETrF was estimated as a ratio of ET obtained from Step 3 to reference ET at the satellite overpass time (MODIS Terra satellite overpass local time around 10:30 AM).

2.2.5 Filling the Gaps Due to Cloud Cover

Data-gaps due to cloud cover is a common issue in all space-borne satellites. In this study, crop coefficient (Kc) was used to fill the data-gaps. The Kc maps were created for all

images as the ratio of ET_{24} and respective daily ET_r. To fill the Kc of a cloud covered (missing) pixel for a specific image date, the Kc value of the same pixel from the preceding image date was first used. If the same pixel was missing in the preceding image, the Kc value was obtained from the next Kc map. The latter step was repeated if the next day was missing until a date was found with a Kc value estimated for the same pixel. This interpolation method was suitable to fill the data gaps as most of the selected images were less than 10 days apart during the crop growing season (April to October).

2.2.6 ET for Longer Periods

After filling the data gaps in daily ET maps due to clouds, the ET maps needed to be created for days when the cloud coverage was more than 10% (or 15%) and thus no input imagery was available. To fill these gaps, the average Kc of the preceding and following images closest to the image date of interest was used. The Kc images were then multiplied with respective daily ET_r to obtain complete time series of daily ET maps. Construction of weekly, monthly, seasonal and annual ET maps was accomplished by summation of daily ET maps over corresponding periods. The processing of all steps was executed in Python language within the ArcGIS environment.

2.3 Comparison with Flux Tower Data

Daily ET time series from the modeling framework explained above were compared against observed ET from three flux towers: US-ARc (35.5464 N, 98.0400 W), US-ARb (35.5497 N, 98.0402 W) (Fischer et al., 2012) and US-AR2 (36.6358 N, 99.5975 W) (Billesbach et al., 2015). The US-ARc and US-ARb were located close to each other over native grassland in central Oklahoma. The US-AR2 was located over planted switchgrass in northwest Oklahoma. The 30-minute flux data from the towers were downloaded from the AmeriFlux data archive (http://ameriflux.lbl.gov/) for years 2005 and 2006 for US-ARc and US-ARb sites and years 2010

and 2011 for the US-AR2 site. The flux tower data usually have the issue with energy balance closure, therefore, the closure error was corrected by maintaining constant Bowen-ratio following (Twine et al., 2000). The corrected 30-min data were averaged to obtain daily data. The daily observed ET was then compared with the average values of 3 × 3 pixels (~1390 m x 1390 m) from the SEBS ET at the flux tower locations. It should be noted that the three flux towers used for validating the performance of the modeling framework in this study represent only two land covers (native and managed grassland). Hence, the performance of the framework may be different from what is documented here over different types of land covers not included in the present analysis.

For statistical analysis, correlation coefficient (r), the coefficient of determination (R^2), mean absolute error (MAE), mean bias error (MBE) and root mean square error (RMSE) were used:

$$\mathrm{MAE} = \frac{1}{n}\sum_{i=1}^{n} |\text{SEBS-ET} - \text{FT-ET}| \tag{3.16}$$

$$\mathrm{MBE} = \frac{1}{n}\sum_{i=1}^{n} (\text{SEBS-ET} - \text{FT-ET}) \tag{3.17}$$

$$\mathrm{RMSE} = \sqrt{\frac{1}{n}\sum_{i=1}^{n} (\text{SEBS-ET} - \text{FT-ET})^2} \tag{3.18}$$

where FT-ET is the observed flux tower daily ET and SEBS-ET is the estimated daily ET from the SEBS model.

2.4 Application of the Modeling Framework

After evaluating the accuracy of the modeling framework, it was used to estimate annual ET maps over the entire state of Oklahoma during the 2001–2014 period. The annual ET were also compared with publicly available MOD16 ET dataset (Mu, Heinsch, Zhao, & Running, 2007; Mu, Zhao, & Running, 2011) over the same period, which covers the most recent drought episode of 2011–2014. The degree of water availability for each pixel and CD within Oklahoma was assessed by estimating the ratio of annual ET from the modeling framework and the

reference ET. This ratio is an indication of the portion of the atmospheric demand that is supplied at each pixel and CD. Areas with smaller ratios represent water scarcity since the actual ET from the model is far from the potential limits of ET. The information on annual ET variations and water availability across Oklahoma can assist state water managers with making critical decisions based on long-term objective data from the implemented framework. As mentioned before, the validation dataset only represented native and managed grassland. About half (47%) of all lands in Oklahoma are under rangeland and grassland. With winter wheat being the most dominant crop, the majority of croplands have similar canopy characteristics. Nevertheless, the lack of representation of other land covers (e.g. 21% of forest in Oklahoma) should be considered in applications and interpretations of the results of the modeling framework.

3. Results and Discussion

3.1 Comparison with Flux Tower Data

The comparison with flux tower data showed good agreement between daily SEBS-ET and FT-ET. The modeling approach captured the spatial and temporal variations in ET. However, the model overestimated ET at all sites and years (Figure 3.3), with average MBE of 20.1 W m^{-2}. The range of MBE was between 1.7 W m^{-2} at US-AR2 in 2011 and 29.3 W m^{-2} at US-ARb in 2006 (Table 3.1). The mean MAE and RMSE were 33.0 W m^{-2} and 42.7 W m^{-2}, respectively. The correlation coefficients varied from 0.61 to 0.81 and R^2 from 0.37 to 0.66.

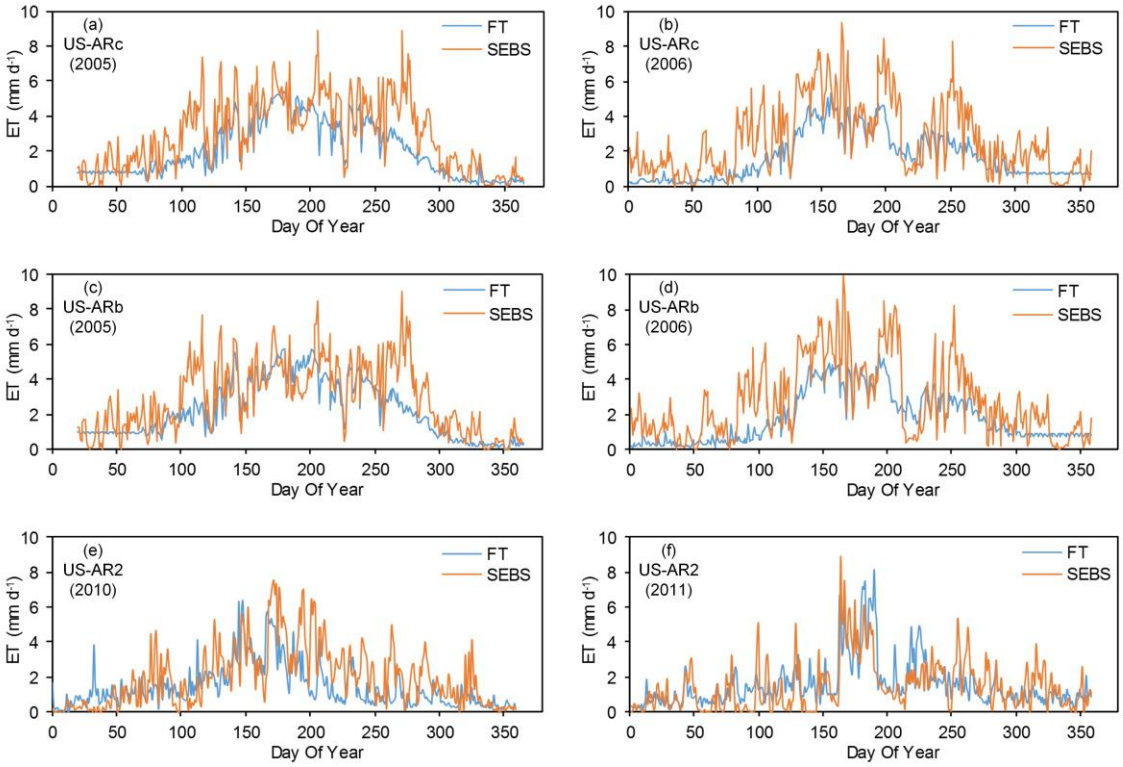

Figure 3.3. Comparison of daily ET from surface energy balances (SEBS) and flux tower (FT).

Table 3.1. Statistical indicators between SEBS and flux tower ET.

Site	Year	r	R^2	MAE (W m^{-2})	MBE (W m^{-2})	RMSE (W m^{-2})
US-ARc	2005	0.78	0.61	39.6	19.1	40.1
	2006	0.77	0.59	36.7	27.5	49.2
US-ARb	2005	0.81	0.66	31.9	26.6	43.3
	2006	0.78	0.61	35.9	29.3	47.7
US-AR2	2010	0.61	0.37	29.4	16.4	41.7
	2011	0.62	0.39	24.7	1.7	34.1

The errors in the ET estimates of the modeling framework are due to errors generated in each of the six steps outlined in previous section. A major step for error introduction is step three,

that is, the surface energy balance model. Previous studies have reported uncertain characterization of kB^{-1} in water limited environments (Bhattarai, Mallick, Brunsell, Sun, & Jain, 2018; Gibson, 2013; Gokmen et al., 2012; Paul et al., 2014) and in low vegetation cover conditions (Bhattarai et al., 2018). Overestimating kB^{-1} under these conditions would lead to overestimating z_{0h}, underestimating H and consequently overestimating ET (Gokmen et al., 2012). The overestimation errors observed in this study were within the range of errors in previous studies when using MODIS as the input imagery to SEBS model. For example, Khan, Hong, Vieux, and Liu (2010) reported ET overestimation with MBE of 6.1 W m^{-2}; Liaqat and Choi (2017) found MBE of 20.1 W m^{-2} and RMSE of 34.7 W m^{-2}; Yang, Zhang, Yang, Hao, and Zhang (2016) reported MBE of 144.9 W m^{-2} when comparing SEBS-ET from cropland and grassland with flux tower estimates; Li et al. (106) found overall MBE of 31 W m^{-2} and RMSE of 76 W m^{-2}; and, Huang, Li, Gu, Lu, and Li (2015) reported MBE of 95.1 W m^{-2} and RMSE of 122.2 W m^{-2} across several land covers and climatic conditions. While several studies have reported overestimation error from SEBS, the mean absolute error from the current study was smaller than the threshold of 50 W m^{-2} suggested by Kustas and Norman (2000).

Errors in other steps of the framework can contribute to biases in final ET estimates. A common source of error in estimating ET from satellite imagery is due to cloud contamination. A thin layer of cloud or a shaded area due to cloud presence over nearby pixels can result in underestimation of LST and consequently, overestimation of ET. In practical applications, it is impossible to remove all these contaminated pixels from the entire image even after applying the LST thresholds during quality control. In this study, there were days with underestimated LST due to cloud presence. For example, the LST at the flux tower pixel area dropped by 10.6 K from Day of Year (DOY) 113 to 114, while both DOYs were identified as cloud-free and no precipitation was recorded. The instantaneous T_A increased by 3.2 K over the same period. The

smaller LST on DOY 114 affected ET estimation for this day and the following days until another cloud-free image was obtained for DOY 117 (Figure 3.3a).

A sensitivity analysis study (Van der Kwast et al., 2009) on SEBS model reported LST as the most sensitive parameter, with up to 70% error in H from irrigated fields expected with 0.5 K bias in LST. Another study (Liaqat, Choi, & Awan, 2015) found that error in H varied between −41% and 152% when LST bias ranged from -4 K to 10 K. These studies show that a small bias in LST can significantly impact H and ultimately ET. The magnitude of error may depend upon the sensitivity of SEBS to LST, including other parameters such as T_A, u, Δt (Wang, Li, & Tang, 2013) and could vary depending on whether the wet or dry limits have been reached (Gibson, Munch, & Engelbrecht, 2011; Liaqat et al., 2015).

In this study, the filtering criteria of less than 15% cloud cover limited the availability of cloud-free images. Applying this filter resulted in 125 and 154 cloud-free images for processing during 2005 and 2006, respectively. For the days with no cloud-free images, the ET estimate was dependent on the Kc approach explained before. However, the Kc approach may fail to account for the variability in pixel conditions, especially if land and weather conditions change dramatically during long periods of gaps in imagery. In this study, 10 to 15 cloud-free images each month were available for most months, which was assumed sufficient to capture general daily soil moisture and weather variations. In other periods, however, it was not possible to keep the length of gap periods short. For example, cloud-free images were not available for 17 consecutive days from DOY 270 to 286 in 2005, when larger differences between FT-ET and SEBS-ET were observed (Figure 3.3a and c).

The combined impact of LST bias due to cloud contamination and unavailability of cloud-free images significantly increase biases in ET estimation. The 15% cloud cover filter could be reduced to reduce cloud contamination issue but this would come at the cost of

increasing the length of periods with no imagery at all. Increasing the filtering limit will have an opposite effect (more available imagery with larger cloud contamination within each image). Another solution is to manually inspect and select images. However, this increases the processing time and interrupts the automated nature of the ET modeling framework. Another factor that could play a significant role in increasing ET errors is the availability and quality of input weather data. Su, Wood, McCabe, and Su (2007) reported about 40% increase in RMSE (from 73 W m^{-2} to 102 W m^{-2}) when using reanalysis dataset - Global Land Data Assimilation System within SEBS instead of ground-based weather data. In this study, the impact of this source of error is expected to be minimal since rigorous quality control was conducted on ground-based data and only less than 2% of data were missing during the study period.

As highlighted before, the daily ET results, uncertainty and potential biases of the proposed ET modeling framework were evaluated and discussed based on flux tower measurements over native and managed grassland at central and northwest Oklahoma. Flux tower data across other land covers were not available for comparison, thus the results from the framework may need further assessment to warrant the similar level of accuracy and uncertainty while applying the results to different land covers and climates across the state. In particular, the analysis and interpretation of results from current study may differ for vegetation with different canopy structure compared to grassland.

3.2 Application of the Modeling Framework

The automated operational ET modeling framework proposed in this study was used to create annual ET maps covering the entire state of Oklahoma for the period from 2001 to 2014. As expected, the annual ET followed the precipitation pattern and increased from southeast to Panhandle (Figure 3.4). When averaged over the entire 14 years, the southeast climate division (CD9) had the largest annual ET of 1,272 mm yr^{-1} and the Panhandle climate division (CD1) had

the smallest annual ET of 588 mm yr^{-1} (Table 3.2). The reference ET (ET_r) had an opposite pattern, with CD1 having the largest amount at 2,140 mm yr^{-1} and CD9 the smallest (1,360 mm yr^{-1}). This means that on average, about 94% of atmospheric demand was fulfilled at southeast, compared to only 27% in the Panhandle during the study period. In other words, water scarcity is a larger issue in CD1 compared to CD9 as available resources were not sufficient to keep up with atmospheric demand. The statewide average annual ET was 994 mm yr^{-1}, about 57% of the average annual ET_r of 1,755 mm yr^{-1}.

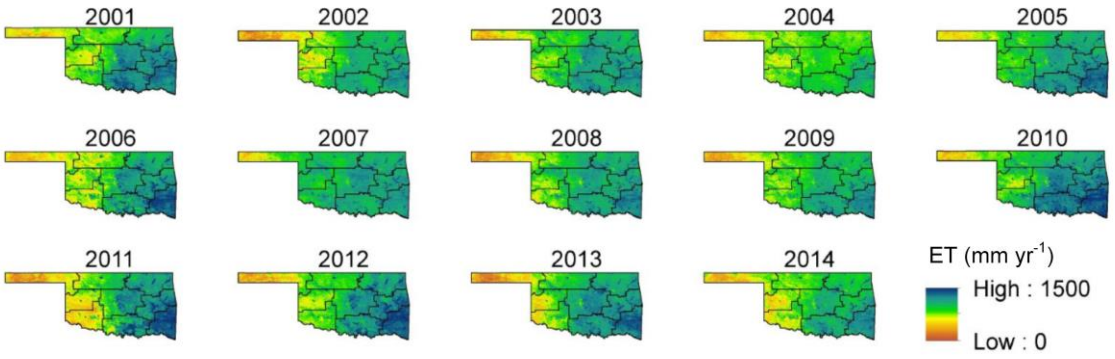

Figure 3.4. Annual ET maps (SEBS-ET) of Oklahoma from 2001 to 2014. The solid lines represent boundaries of the nine climate divisions. It should be noted that CDs 6 and 9 in southeast have a forested area of more than 29%. Hence, their ET estimates may not be accurate since the flux towers used in validation did not include forest land cover.

Table 3.2. Average annual SEBS-ET, MOD16-ET, ET_r and the ratio of SEBS-ET to ET_r for all Oklahoma climate divisions (CD) during the 2001–2014 period.

Climate Division	SEBS-ET (mm yr^{-1})	MOD16-ET (mm yr^{-1})	ET_r (mm yr^{-1})	SEBS-ET ET_r^{-1}
CD1 (Panhandle)	588	259	2140	0.27

CD2 (North Central)	918	364	1871	0.49
CD3 (Northeast)	1098	657	1521	0.72
CD4 (West Central)	790	338	2018	0.39
CD5 (Central)	1095	531	1700	0.64
CD6 (East Central)*	1175	736	1492	0.79
CD7 (Southwest)	845	363	2009	0.42
CD8 (South Central)	1163	599	1683	0.69
CD9 (Southeast)*	1272	798	1360	0.94
Oklahoma	994	516	1755	0.57

* These CDs have a forested area of more than 29%. The results presented in this table may not be accurate for these CDs since the flux towers used in validation did not include forest land cover.

The average annual ET comparison between MOD16 and SEBS indicated large differences across all Oklahoma CDs (Table 3.2). The differences between MOD16-ET and SEBS-ET varied between 37% at CD9 to 60% at CD2, with an average of 48% lower ET rates from MOD16. Three eastern humid CDs (CD3, CD6, CD9) had smaller differences between MOD16-ET and SEBS-ET compared to three western CDs (CD1, CD4, CD7). The difference between SEBS-ET and MOD16-ET is possibly due to a combination of overestimations from SEBS and underestimation from MOD16. The underestimation of ET from MOD16 has been reported in previous studies, particularly in semi-arid and arid climates (Feng et al., 2012; Hu, Jia, & Menenti, 2015).

The ratio of SEBS-ET to ET_r can be estimated on a pixel wise basis to provide information on water scarcity at a finer resolution for local water management and planning. This ratio is mapped in Figure 3.5. The general patterns are similar to those presented in Table 3.2, with western parts of the state under relatively larger water scarcity compared to the eastern parts. However, significant variability can be observed within some CDs. In CD1, for example, the western half of CD (Cimarron and Texas counties) had smaller ratios compared to the eastern half, suggesting a more severe water scarcity. CD2 was similar in terms of variations in the ET ratios across the CD. The surface water resources in western Oklahoma were visible in regions with a ratio value of more than 0.5. Examples include the riparian areas of Cimarron and North Canadian rivers in southwest of CD2, as well as Canton Lake and Foss reservoir in CD4 and the five reservoirs in CD7 (Lugert-Altus, Tom Steed, Lawtonka, Ellsworth and Fort Cobb). Maps similar to the one in Figure 3.5 can be developed at varying temporal and spatial scales to monitor changes in water availability more closely. The ratio of actual ET to reference or potential ET has been used in the past in monitoring water stress and drought, such as in the Evaporative Stress Index (Anderson et al., 2016).

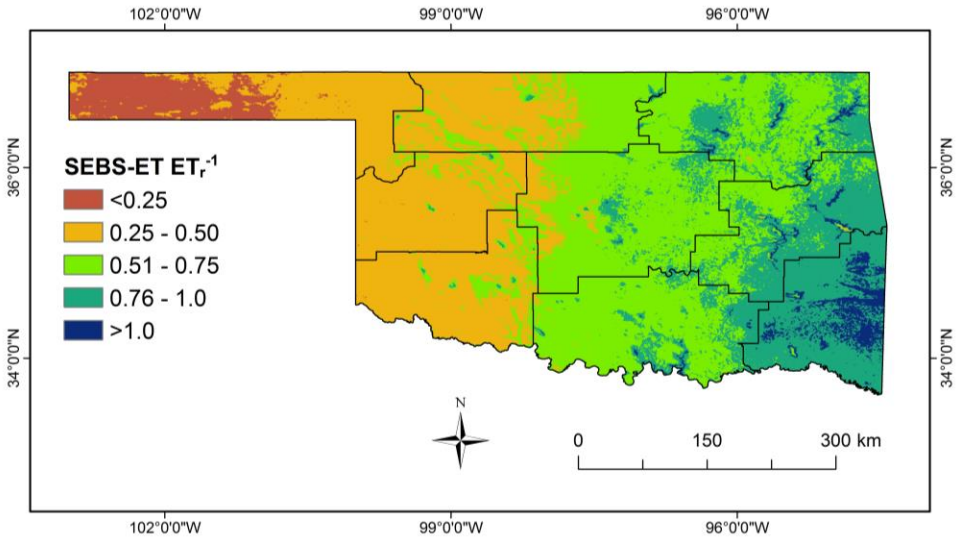

Figure 3.5. The ratio of average annual SEBS-ET to ET_r across Oklahoma during the period 2001–2014. It should be noted that CDs 6 and 9 in southeast have a forested area of more than 29%. Hence, their ET estimates may not be accurate since the flux towers used in validation did not include forest land cover.

The inter-annual variations in ET were also examined for each CD and for the entire state. Figure 3.6 demonstrates deviations in SEBS-ET as percentage of the average annual ET during the 2001–2014 period. The impact of the 2011–2014 drought in western Oklahoma can be observed in this graph, with the maximum reduction in ET occurring in 2011 for the three western CDs of CD1, CD4 and CD7. The percent deviations from average was −22%, −21% and −33% for the same CDs, respectively. According to the U.S. Drought Monitor (USDM) (Svobada et al., 2002), more than 80% of the three CDs was under extreme drought (D3 category) from June. The drought condition worsened in July and remained under D4 category until December 2011. The three eastern CDs of CD3, CD6 and CD9 were above average in 2011, with percent deviations of 9%, 8% and 10%, respectively. The USDM indicated almost no drought at CD3 in 2011, whereas CD6 and CD9 had less than 40% of their area under extreme drought from August to November 2011. The middle three CDs registered close to long-term average ET. The largest positive deviations for the three western CDs occurred in 2007, a year that was characterized by above normal precipitation.

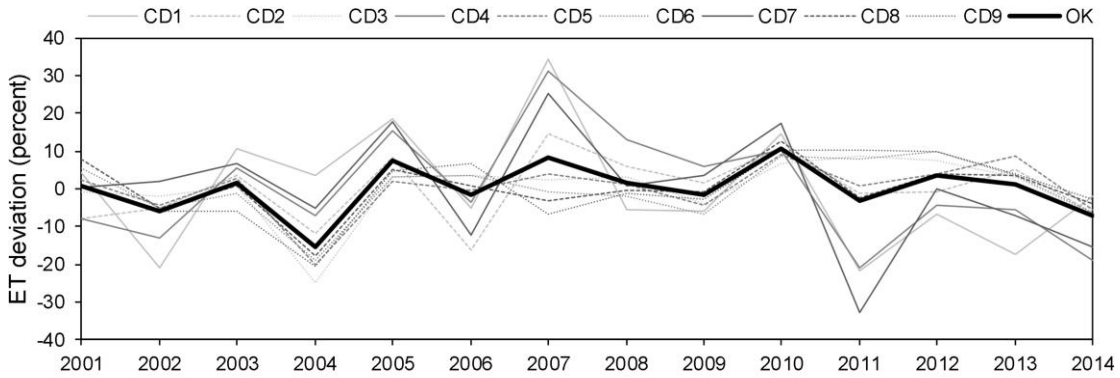

Figure 3.6. Annual ET deviation across climate divisions of Oklahoma from 2001 to 2014.

The ET modeling framework proposed in this study can automatically generate time series of daily ET maps on a continuous basis, with several applications beyond those mentioned in previous sections. For example, ET maps over agricultural areas can be analyzed in conjunction with yield data to evaluate the water use efficiency. However, this modeling framework has some limitations that must be considered and improved in future applications. One limitation is the size of MODIS pixels, which practically hinders the possibility of using the ET data at field scale. This limitation can be overcome by modifying the framework to use satellite imagery at finer resolution (e.g., Landsat). Another challenge is identifying and removing cloud contaminated pixels. The filters used in this study were not always effective in identifying pixels that were covered by thin layers of cloud or were in the shadow of a cloud. Thus, further investigation and application of robust methods to examine cloud contamination are needed. Finally, there were periods when no images were available for several days due to clouds covering the entire scene. This negatively affects the ability to capture ET fluctuations during those periods. Data-fusion approaches can be implemented in the modeling framework as a potential solution to improving ET interpolation for days with missing images.

4. Conclusions

An ET modeling framework was proposed to automatically construct daily time series of ET maps across Oklahoma by integrating MODIS imagery, ground-based weather data and surface energy balance model. The comparison of the results with daily observations at three flux towers (two years of data at each site) showed good performance of the modeling framework with mean bias errors less than 30 W m^{-2} and root mean squared errors less than 50 W m^{-2}. The results were then used to investigate spatial and temporal variations in ET across the state and its nine

climate divisions (CD). The statewide annual ET varied between 841 and 1100 mm yr^{-1} during the period from 2001 to 2014, with an average of 994 mm yr^{-1}. A large difference in ET was observed among CDs, with Oklahoma Panhandle (CD1) having the smallest and southeast (CD9) the largest average annual ET of 588 and 1272 mm yr^{-1}, respectively. The ratio of estimated ET to reference ET was used as an indicator of water scarcity at pixel and CD levels. The deviations in annual ET from the 2001–2014 average ET were also studied and found to be in good agreement with temporal and spatial variations in drought. The proposed ET modeling framework provided a pathway to construct daily time series of ET maps with potential for a range of applications. However, further improvements are necessary to resolve the issues highlighted in the current study.

References

Ahmad, M. U. D., Turral, H., & Nazeer, A. (2009). Diagnosing irrigation performance and water productivity through satellite remote sensing and secondary data in a large irrigation system of Pakistan. *Agricultural Water Management*, *96*(4), 551-564.

Allen, R. G. (1996). Assessing integrity of weather data for reference evapotranspiration estimation. *Journal of Irrigation and Drainage Engineering*, *122*(2), 97-106.

Allen, R. G., Burnett, B., Kramber, W., Huntington, J., Kjaersgaard, J., Kilic, A., ... & Trezza, R. (2013). Automated calibration of the metric-landsat evapotranspiration process. *JAWRA Journal of the American Water Resources Association*, *49*(3), 563-576.

Allen, R. G., Pereira, L. S., Howell, T. A., & Jensen, M. E. (2011). Evapotranspiration information reporting: I. Factors governing measurement accuracy. *Agricultural Water Management*, *98*(6), 899-920.

Allen, R. G., Tasumi, M., & Trezza, R. (2007). Satellite-based energy balance for mapping evapotranspiration with internalized calibration (METRIC)—Model. *Journal of irrigation and drainage engineering*, *133*(4), 380-394.

Allen, R. G., Tasumi, M., Morse, A., & Trezza, R. (2005). A Landsat-based energy balance and evapotranspiration model in Western US water rights regulation and planning. *Irrigation and Drainage systems*, *19*(3-4), 251-268.

Anderson, M. C., Allen, R. G., Morse, A., & Kustas, W. P. (2012). Use of Landsat thermal imagery in monitoring evapotranspiration and managing water resources. *Remote Sensing of Environment*, *122*, 50-65.

Anderson, M. C., Hain, C., Wardlow, B., Pimstein, A., Mecikalski, J. R., & Kustas, W. P. (2011). Evaluation of drought indices based on thermal remote sensing of evapotranspiration over the continental United States. *Journal of Climate*, *24*(8), 2025-2044.

Anderson, M. C., Norman, J. M., Mecikalski, J. R., Otkin, J. A., & Kustas, W. P. (2007). A climatological study of evapotranspiration and moisture stress across the continental United States based on thermal remote sensing: 1. Model formulation. *Journal of Geophysical Research: Atmospheres*, *112*(D10).

Anderson, M. C., Zolin, C. A., Sentelhas, P. C., Hain, C. R., Semmens, K., Yilmaz, M. T., ... & Tetrault, R. (2016). The Evaporative Stress Index as an indicator of agricultural drought in Brazil: An assessment based on crop yield impacts. *Remote Sensing of Environment*, *174*, 82-99.

Bastiaanssen, W. G. M., Noordman, E. J. M., Pelgrum, H., Davids, G., Thoreson, B. P., & Allen, R. G. (2005). SEBAL model with remotely sensed data to improve water-resources management under actual field conditions. *Journal of irrigation and drainage engineering*, *131*(1), 85-93.

Bastiaanssen, W. G., Menenti, M., Feddes, R. A., & Holtslag, A. A. M. (1998). A remote sensing surface energy balance algorithm for land (SEBAL). 1. Formulation. *Journal of hydrology*, *212*, 198-212.

Bawazir, A. S., Samani, Z., Bleiweiss, M., Skaggs, R., & Schmugge, T. (2009). Using ASTER satellite data to calculate riparian evapotranspiration in the Middle Rio Grande, New Mexico. *International journal of remote sensing*, *30*(21), 5593-5603.

Beljaars, A. C. M., & Holtslag, A. A. M. (1991). Flux parameterization over land surfaces for atmospheric models. *Journal of Applied Meteorology*, *30*(3), 327-341.

Bhattarai, N., Mallick, K., Brunsell, N. A., Sun, G., & Jain, M. (2018). Regional evapotranspiration from an image-based implementation of the Surface Temperature Initiated Closure (STIC1. 2) model and its validation across an aridity gradient in the conterminous US. *Hydrology and Earth System Sciences*, *22*(4), 2311-2341.

Bhattarai, N., Quackenbush, L. J., Im, J., & Shaw, S. B. (2017). A new optimized algorithm for automating endmember pixel selection in the SEBAL and METRIC models. *Remote sensing of environment*, *196*, 178-192.

Biggs, T. W., Marshall, M., & Messina, A. (2016). Mapping daily and seasonal evapotranspiration from irrigated crops using global climate grids and satellite imagery: Automation and methods comparison. *Water Resources Research*, *52*(9), 7311-7326.

Billesbach, D., Bradford, J., & Margaret, T. (2015). *AmeriFlux US-AR2 ARM USDA UNL OSU Woodward Switchgrass 2*; U.S. Department of Agriculture: Washington, DC, USA; University of Nebraska: Lincoln, NE, USA.

Brock, F. V., Crawford, K. C., Elliott, R. L., Cuperus, G. W., Stadler, S. J., Johnson, H. L., & Eilts, M. D. (1995). The Oklahoma Mesonet: a technical overview. *Journal of Atmospheric and Oceanic Technology*, *12*(1), 5-19.

Brutsaert, W. (2013). *Evaporation into the atmosphere: theory, history and applications* (Vol. 1). Springer Science & Business Media.

Brutsaert, W., & Sugita, M. (1992). Application of self-preservation in the diurnal evolution of the surface energy budget to determine daily evaporation. *Journal of Geophysical Research: Atmospheres*, *97*(D17), 18377-18382.

Cai, X. L., & Sharma, B. R. (2010). Integrating remote sensing, census and weather data for an assessment of rice yield, water consumption and water productivity in the Indo-Gangetic river basin. *Agricultural Water Management*, *97*(2), 309-316.

Chávez, J. L., Neale, C. M., Prueger, J. H., & Kustas, W. P. (2008). Daily evapotranspiration estimates from extrapolating instantaneous airborne remote sensing ET values. *Irrigation Science*, *27*(1), 67-81.

Chen, J. M., Chen, X., Ju, W., & Geng, X. (2005). Distributed hydrological model for mapping evapotranspiration using remote sensing inputs. *Journal of Hydrology*, *305*(1-4), 15-39.

Choudhury, B. J., & Monteith, J. L. (1988). A four- layer model for the heat budget of homogeneous land surfaces. *Quarterly Journal of the Royal Meteorological Society*, *114*(480), 373-398.

Colaizzi, P. D., Evett, S. R., Howell, T. A., & Tolk, J. A. (2006). Comparison of five models to scale daily evapotranspiration from one-time-of-day measurements. *Transactions of the ASABE*, *49*(5), 1409-1417.

Delogu, E., Boulet, G., Olioso, A., Coudert, B., Chirouze, J., Ceschia, E., Le Dantec, V., Marloie, O., Chehbouni, G., & Lagouarde, J. P. (2012). Reconstruction of temporal variations of evapotranspiration using instantaneous estimates at the time of satellite overpass. *Hydrology and Earth System Sciences*, *16*(8), 2995-3010.

Dhungel, R., Allen, R. G., Trezza, R., & Robison, C. W. (2016). Evapotranspiration between satellite overpasses: methodology and case study in agricultural dominant semi-arid areas. *Meteorological Applications*, *23*(4), 714-730.

Droogers, P., & Bastiaanssen, W. (2002). Irrigation performance using hydrological and remote sensing modeling. *Journal of Irrigation and Drainage Engineering*, *128*(1), 11-18.

Elhaddad, A., & Garcia, L. A. (2008). Surface energy balance-based model for estimating evapotranspiration taking into account spatial variability in weather. *Journal of irrigation and drainage engineering*, *134*(6), 681-689.

Elhaddad, A., & Garcia, L. A. (2011). ReSET-raster: surface energy balance model for calculating evapotranspiration using a raster approach. *Journal of Irrigation and Drainage Engineering*, *137*(4), 203-210.

Environmental and Water Resources Institute for the American Society of Civil Engineers (ASCE-EWRI) (2005). *The ASCE Standardized Reference Evapotranspiration Equation*. Report of the ASCE-EWRI Task Committee on 566 Standardization of Reference Evapotranspiration.

Feng, X. M., Sun, G., Fu, B. J., Su, C. H., Liu, Y., & Lamparski, H. (2012). Regional effects of vegetation restoration on water yield across the Loess Plateau, China. *Hydrology and Earth System Sciences*, *16*(8), 2617-2628.

Fischer, M. L., Torn, M. S., Billesbach, D. P., Doyle, G., Northup, B., & Biraud, S. C. (2012). Carbon, water, and heat flux responses to experimental burning and drought in a tallgrass prairie. *Agricultural and forest meteorology*, *166*, 169-174.

Fisher, J. B., Whittaker, R. J., & Malhi, Y. (2011). ET come home: potential evapotranspiration in geographical ecology. *Global Ecology and Biogeography*, *20*(1), 1-18.

Folhes, M. T., Rennó, C. D., & Soares, J. V. (2009). Remote sensing for irrigation water management in the semi-arid Northeast of Brazil. *Agricultural Water Management*, *96*(10), 1398-1408.

Gentine, P., Entekhabi, D., Chehbouni, A., Boulet, G., & Duchemin, B. (2007). Analysis of evaporative fraction diurnal behaviour. *Agricultural and forest meteorology*, *143*(1-2), 13-29.

Gibson, L. A. (2013). *The application of the surface energy balance system model to estimate evapotranspiration in South Africa* (Doctoral dissertation, University of Cape Town).

Gibson, L. A., Münch, Z., & Engelbrecht, J. (2011). Particular uncertainties encountered in using a pre-packaged SEBS model to derive evapotranspiration in a heterogeneous study area in South Africa. *Hydrology and earth system sciences*, *15*(1), 295-310.

Gokmen, M., Vekerdy, Z., Verhoef, A., Verhoef, W., Batelaan, O., & Van der Tol, C. (2012). Integration of soil moisture in SEBS for improving evapotranspiration estimation under water stress conditions. *Remote sensing of environment*, *121*, 261-274.

Gowda, P. H., Chavez, J. L., Colaizzi, P. D., Evett, S. R., Howell, T. A., & Tolk, J. A. (2007). Remote sensing based energy balance algorithms for mapping ET: Current status and future challenges. *Transactions of the ASABE*, *50*(5), 1639-1644.

Gowda, P. H., Chavez, J. L., Colaizzi, P. D., Howell, T. A., Schwartz, R. C., & Marek, T. H. (2007). Relationship between LAI and Landsat TM spectral vegetation indices in the Texas Panhandle. In *2007 ASAE Annual Meeting* (p. 1). American Society of Agricultural and Biological Engineers.

Gowda, P. H., Ennis, J., Howell, T. A., Marek, T. H., & Porter, D. O. (2012). The ASCE Standardized Equation-Based Bushland Reference ET Calculator. In *World Environmental and Water Resources Congress 2012: Crossing Boundaries*(pp. 2198-2205).

Gupta, R. K., Prasad, T. S., & Vijayan, D. (2002). Estimation of roughness length and sensible heat flux from WiFS and NOAA AVHRR data. *Advances in Space Research*, *29*(1), 33-38.

Herman, M. R., Nejadhashemi, A. P., Abouali, M., Hernandez-Suarez, J. S., Daneshvar, F., Zhang, Z., Anderson, M. C., Sadeghi, A. M., Hain, C. R., & Sharifi, A. (2018). Evaluating the role of evapotranspiration remote sensing data in improving hydrological modeling predictability. *Journal of Hydrology*, *556*, 39-49.

Homer, C., Dewitz, J., Yang, L., Jin, S., Danielson, P., Xian, G., Coulston, J., Herold, N., Wickham, J, & Megown, K. (2015). Completion of the 2011 National Land Cover

Database for the conterminous United States–representing a decade of land cover change information. *Photogrammetric Engineering & Remote Sensing*, *81*(5), 345-354.

Hu, G., Jia, L., & Menenti, M. (2015). Comparison of MOD16 and LSA-SAF MSG evapotranspiration products over Europe for 2011. *Remote Sensing of Environment*, *156*, 510-526.

Huang, C., Li, Y., Gu, J., Lu, L., & Li, X. (2015). Improving estimation of evapotranspiration under water-limited conditions based on SEBS and MODIS data in arid regions. *Remote Sensing*, *7*(12), 16795-16814.

Immerzeel, W. W., Gaur, A., & Zwart, S. J. (2008). Integrating remote sensing and a process-based hydrological model to evaluate water use and productivity in a south Indian catchment. *Agricultural Water Management*, *95*(1), 11-24.

Kalma, J. D., McVicar, T. R., & McCabe, M. F. (2008). Estimating land surface evaporation: A review of methods using remotely sensed surface temperature data. *Surveys in Geophysics*, *29*(4-5), 421-469.

Khan, I. S., Hong, Y., Vieux, B., & Liu, W. (2010). Developmentevaluation of an actual evapotranspiration estimation algorithm using satellite remote sensingmeteorological observational network in Oklahoma. *International Journal of Remote Sensing*, *31*(14), 3799-3819.

Khand, K., Kjaersgaard, J., Hay, C., & Jia, X. (2017). Estimating impacts of agricultural subsurface drainage on evapotranspiration using the Landsat imagery-based METRIC model. *Hydrology*, *4*(4), 49.

Khand, K., Numata, I., Kjaersgaard, J., & Vourlitis, G. L. (2017). Dry Season Evapotranspiration Dynamics over Human-Impacted Landscapes in the Southern Amazon Using the Landsat-Based METRIC Model. *Remote Sensing*, *9*(7), 706.

Khand, K., Taghvaeian, S., & Hassan-Esfahani, L. (2017). Mapping Annual Riparian Water Use Based on the Single-Satellite-Scene Approach. *Remote Sensing*, *9*(8), 832.

Kjaersgaard, J. H., Allen, R. G., Garcia, M., Kramber, W., & Trezza, R. (2009). Automated selection of anchor pixels for landsat based evapotranspiration estimation. In *World Environmental and Water Resources Congress 2009: Great Rivers* (pp. 1-11).

Kjaersgaard, J., Allen, R., & Irmak, A. (2011). Improved methods for estimating monthly and growing season ET using METRIC applied to moderate resolution satellite imagery. *Hydrological Processes*, *25*(26), 4028-4036.

Kjaersgaard, J., Allen, R., Trezza, R., Robison, C., Oliveira, A., Dhungel, R., & Kra, E. (2012). Filling satellite image cloud gaps to create complete images of evapotranspiration. *IAHS Publ*, *2012*, 102-105.

Kottek, M., Grieser, J., Beck, C., Rudolf, B., & Rubel, F. (2006). World map of the Köppen-Geiger climate classification updated. *Meteorologische Zeitschrift*, *15*(3), 259-263.

Kustas, W. P., & Norman, J. M. (1999). Evaluation of soil and vegetation heat flux predictions using a simple two-source model with radiometric temperatures for partial canopy cover. *Agricultural and Forest Meteorology*, *94*(1), 13-29.

Kustas, W. P., & Norman, J. M. (2000). Evaluating the effects of subpixel heterogeneity on pixel average fluxes. *Remote Sensing of Environment*, *74*(3), 327-342.

Kustas, W. P., Humes, K. S., Norman, J. M., & Moran, M. S. (1996). Single-and dual-source modeling of surface energy fluxes with radiometric surface temperature. *Journal of Applied Meteorology*, *35*(1), 110-121.

Kustas, W. P., Perry, E. M., Doraiswamy, P. C., & Moran, M. S. (1994). Using satellite remote sensing to extrapolate evapotranspiration estimates in time and space over a semiarid rangeland basin. *Remote sensing of environment*, *49*(3), 275-286.

Li, H., Zheng, L., Lei, Y., Li, C., Liu, Z., & Zhang, S. (2008). Estimation of water consumption and crop water productivity of winter wheat in North China Plain using remote sensing technology. *Agricultural Water Management*, *95*(11), 1271-1278.

Li, Y., Huang, C., Hou, J., Gu, J., Zhu, G., & Li, X. (2017). Mapping daily evapotranspiration based on spatiotemporal fusion of ASTER and MODIS images over irrigated agricultural areas in the Heihe River Basin, Northwest China. *Agricultural and Forest Meteorology*, *244*, 82-97.

Li, Z. L., Tang, R., Wan, Z., Bi, Y., Zhou, C., Tang, B., Yan, G., & Zhang, X. (2009). A review of current methodologies for regional evapotranspiration estimation from remotely sensed data. *Sensors*, *9*(5), 3801-3853.

Liang, S. (2001). Narrowband to broadband conversions of land surface albedo I: Algorithms. *Remote sensing of environment*, *76*(2), 213-238.

Liang, S. (2005). *Quantitative remote sensing of land surfaces*(Vol. 30). John Wiley & Sons.

Liaqat, U. W., & Choi, M. (2017). Accuracy comparison of remotely sensed evapotranspiration products and their associated water stress footprints under different land cover types in Korean peninsula. *Journal of cleaner production*, *155*, 93-104.

Liaqat, U. W., Choi, M., & Awan, U. K. (2015). Spatio- temporal distribution of actual evapotranspiration in the Indus Basin Irrigation System. *Hydrological processes*, *29*(11), 2613-2627.

Liou, Y. A., & Kar, S. (2014). Evapotranspiration estimation with remote sensing and various surface energy balance algorithms—A review. *Energies*, *7*(5), 2821-2849.

Long, D., & Singh, V. P. (2012). A modified surface energy balance algorithm for land (M-SEBAL) based on a trapezoidal framework. *Water Resources Research*, *48*(2).

McPherson, R. A., Fiebrich, C. A., Crawford, K. C., Kilby, J. R., Grimsley, D. L., Martinez, J. E., ... & Melvin, A. D. (2007). Statewide monitoring of the mesoscale environment: A technical update on the Oklahoma Mesonet. *Journal of Atmospheric and Oceanic Technology*, *24*(3), 301-321.

Menenti, M., & Choudhary, B. (1993). Parameteraization of land surface evaporation by means of location dependent potential evaporation and surface temperature range. *Proceedings of IAHS conference on Land Surface Processes.*

Monin, A. S., & Obukhov, A. M. (1954). Basic laws of turbulent mixing in the surface layer of the atmosphere. *Contrib. Geophys. Inst. Acad. Sci. USSR*, *151*(163), e187.

Monin, A. S., & Obukhov, A. M. (1954). Basic laws of turbulent mixing in the surface layer of the atmosphere. *Contrib. Geophys. Inst. Acad. Sci. USSR*, *151*(163), e187.

Monteith, J. L. (1965). Evaporation and Environment. The state and movement of water in living organism. Symposium of the Society for the Experimental Biology 19.

Monteith, J. L. (1981). Evaporation and surface temperature. *Quarterly Journal of the Royal Meteorological Society*, *107*(451), 1-27.

Moorhead, J. E., Gowda, P. H., Singh, V. P., Porter, D. O., Marek, T. H., Howell, T. A., & Stewart, B. A. (2015). Identifying and evaluating a suitable index for agricultural drought monitoring in the Texas high plains. *JAWRA Journal of the American Water Resources Association*, *51*(3), 807-820.

Moorhead, J., Gowda, P., Hobbins, M., Senay, G., Paul, G., Marek, T., & Porter, D. (2015). Accuracy assessment of NOAA gridded daily reference evapotranspiration for the Texas High Plains. *JAWRA Journal of the American Water Resources Association*, *51*(5), 1262-1271.

Mu, Q., Heinsch, F. A., Zhao, M., & Running, S. W. (2007). Development of a global evapotranspiration algorithm based on MODIS and global meteorology data. *Remote sensing of Environment*, *111*(4), 519-536.

Mu, Q., Zhao, M., & Running, S. W. (2011). Improvements to a MODIS global terrestrial evapotranspiration algorithm. *Remote Sensing of Environment*, *115*(8), 1781-1800.

Nagler, P. L., Glenn, E. P., Nguyen, U., Scott, R. L., & Doody, T. (2013). Estimating riparian and agricultural actual evapotranspiration by reference evapotranspiration and MODIS enhanced vegetation index. *Remote Sensing*, *5*(8), 3849-3871.

Nepstad, D., Lefebvre, P., Lopes da Silva, U., Tomasella, J., Schlesinger, P., Solórzano, L., Moutinho, P., Ray, D., & Guerreira Benito, J. (2004). Amazon drought and its implications for forest flammability and tree growth: A basin-wide analysis. *Global change biology*, *10*(5), 704-717.

Norman, J. M., & Becker, F. (1995). Terminology in thermal infrared remote sensing of natural surfaces. *Remote Sensing Reviews, 12(3-4), 159-173.*

Oberg, J. W., & Melesss, A. M. (2006). Evapotranspiration dynamics at an ecohydrological restoration site: an energy balance and remote sensing approach 1. *JAWRA Journal of the American Water Resources Association*, *42*(3), 565-582.

Paul, G., Gowda, P. H., Prasad, P. V., Howell, T. A., Aiken, R. M., & Neale, C. M. (2014). Investigating the influence of roughness length for heat transport (zoh) on the performance of SEBAL in semi-arid irrigated and dryland agricultural systems. *Journal of hydrology*, *509*, 231-244.

Porter, D., Gowda, P., Marek, T., Howell, T., Moorhead, J., & Irmak, S. (2012). Sensitivity of grass-and alfalfa-reference evapotranspiration to weather station sensor accuracy. *Applied engineering in agriculture*, *28*(4), 543-549.

Roerink, G. J., Su, Z., & Menenti, M. (2000). S-SEBI: A simple remote sensing algorithm to estimate the surface energy balance. *Physics and Chemistry of the Earth, Part B: Hydrology, Oceans and Atmosphere*, *25*(2), 147-157.

Samani, Z., Bawazir, A. S., Skaggs, R. K., Bleiweiss, M. P., Piñon, A., & Tran, V. (2007). Water use by agricultural crops and riparian vegetation: an application of remote sensing technology. *Journal of Contemporary Water Research & Education*, *137*(1), 8-13.

Santos, C., Lorite, I. J., Tasumi, M., Allen, R. G., & Fereres, E. (2010). Performance assessment of an irrigation scheme using indicators determined with remote sensing techniques. *Irrigation Science*, *28*(6), 461-477.

Senay, G. B., Bohms, S., Singh, R. K., Gowda, P. H., Velpuri, N. M., Alemu, H., & Verdin, J. P. (2013). Operational evapotranspiration mapping using remote sensing and weather datasets: A new parameterization for the SSEB approach. *JAWRA Journal of the American Water Resources Association*, *49*(3), 577-591.

Senay, G. B., Friedrichs, M., Singh, R. K., & Velpuri, N. M. (2016). Evaluating Landsat 8 evapotranspiration for water use mapping in the Colorado River Basin. *Remote Sensing of Environment*, *185*, 171-185.

Singh, R. K., Liu, S., Tieszen, L. L., Suyker, A. E., & Verma, S. B. (2012). Estimating seasonal evapotranspiration from temporal satellite images. *Irrigation science*, *30*(4), 303-313.

SU, H., Wood, E. F., McCabe, M. F., & Su, Z. (2007). Evaluation of remotely sensed evapotranspiration over the CEOP EOP-1 reference sites. *Journal of the Meteorological Society of Japan. Ser. II*, *85*, 439-459.

Su, Z. (2002). The Surface Energy Balance System (SEBS) for estimation of turbulent heat fluxes. *Hydrology and earth system sciences*, *6*(1), 85-100.

Su, Z., Schmugge, T., Kustas, W. P., & Massman, W. J. (2001). An evaluation of two models for estimation of the roughness height for heat transfer between the land surface and the atmosphere. *Journal of applied meteorology*, *40*(11), 1933-1951.

Svoboda, M., LeComte, D., Hayes, M., Heim, R., Gleason, K., Angel, J., Rippey, B., Tinker, R., Palecki, M., Stooksbury, D., Miskus, D., & Stephens, S. (2002). The drought monitor. *Bulletin of the American Meteorological Society*, *83*(8), 1181-1190.

Taghvaeian, S., & Neale, C. M. (2011). Water balance of irrigated areas: a remote sensing approach. *Hydrological Processes*, *25*(26), 4132-4141.

Taghvaeian, S., Neale, C. M., Osterberg, J. C., Sritharan, S. I., & Watts, D. R. (2018). Remote Sensing and GIS Techniques for Assessing Irrigation Performance: Case Study in Southern California. *Journal of Irrigation and Drainage Engineering*, *144*(6), 05018002.

Taghvaeian, S., Neale, C. M., Osterberg, J., Sritharan, S. I., & Watts, D. R. (2014). Water use and stream-aquifer-phreatophyte interaction along a Tamarisk-dominated segment of the Lower Colorado River. *Remote Sensing of the Terrestrial Water Cycle; John & Sons, Inc.: Hoboken, NJ, USA*, 95-113.

Teixeira, A. D. C., Bastiaanssen, W. G., Ahmad, M. U. D., & Bos, M. G. (2009). Reviewing SEBAL input parameters for assessing evapotranspiration and water productivity for the Low-Middle Sao Francisco River basin, Brazil: Part A: Calibration and validation. *agricultural and forest meteorology*, *149*(3-4), 462-476.

Timmermans, W. J., Kustas, W. P., Anderson, M. C., & French, A. N. (2007). An intercomparison of the surface energy balance algorithm for land (SEBAL) and the two-source energy balance (TSEB) modeling schemes. *Remote Sensing of Environment*, *108*(4), 369-384.

Trezza, R. (2002). Evapotranspiration using a satellite-based surface energy balance with standardized ground control.

Trezza, R., Allen, R. G., & Tasumi, M. (2013). Estimation of actual evapotranspiration along the Middle Rio Grande of New Mexico using MODIS and landsat imagery with the METRIC model. *Remote Sensing*, *5*(10), 5397-5423.

Twine, T. E., Kustas, W. P., Norman, J. M., Cook, D. R., Houser, P., Meyers, T. P., ... & Wesely, M. L. (2000). Correcting eddy-covariance flux underestimates over a grassland. *Agricultural and Forest Meteorology*, *103*(3), 279-300.

Van der Kwast, J., Timmermans, W., Gieske, A., Su, Z., Olioso, A., Jia, L., Elberts, J., Karssenverg, D., de Jong, S., de Jong, Steven. (2009). Evaluation of the Surface Energy Balance System (SEBS) applied to ASTER imagery with flux-measurements at the SPARC 2004 site (Barrax, Spain). *Hydrology and Earth System Sciences Discussions*, *6*(1), 1165-1196.

Vermote, E., & Wolfe, R. (2015). MOD09GA MODIS/Terra Surface Reflectance Daily L2G Global 1 km and 500 m SIN Grid V006. *NASA EOSDIS Land Processes DAAC. Available online: https://lpdaac. usgs. gov/dataset_ discovery/modis/modis_products_table/mod09ga_v006 (accessed on 16 October 2016)*.

Vinukollu, R. K., Wood, E. F., Ferguson, C. R., & Fisher, J. B. (2011). Global estimates of evapotranspiration for climate studies using multi-sensor remote sensing data: Evaluation of three process-based approaches. *Remote Sensing of Environment*, *115*(3), 801-823.

Wan, Z., Hook, S., & Hulley, G. (2015). MOD11A2 MODIS/Terra Land Surface Temperature/Emissivity 8-Day L3 Global 1km SIN Grid V006. *NASA EOSDIS Land Processes DAAC*, *10*.

Wang, Y., Li, X., & Tang, S. (2013). Validation of the SEBS-derived sensible heat for FY3A/VIRR and TERRA/MODIS over an alpine grass region using LAS measurements. *International Journal of Applied Earth Observation and Geoinformation*, *23*, 226-233.

Webster, E., Ramp, D., & Kingsford, R. T. (2016). Spatial sensitivity of surface energy balance algorithms to meteorological data in a heterogeneous environment. *Remote Sensing of Environment*, *187*, 294-319.

WMO. (2008). Guide to Hydrological Practices. Volume I. Hydrology–From Measurement to Hydrological Information.

Yang, Y., Long, D., & Shang, S. (2013). Remote estimation of terrestrial evapotranspiration without using meteorological data. *Geophysical Research Letters*, *40*(12), 3026-3030.

Yang, Z., Zhang, Q., Yang, Y., Hao, X., & Zhang, H. (2016). Evaluation of evapotranspiration models over semi- arid and semi- humid areas of China. *Hydrological Processes*, *30*(23), 4292-4313.

Yao, Y., Liang, S., Qin, Q., & Wang, K. (2010). Monitoring drought over the conterminous United States using MODIS and NCEP Reanalysis-2 data. *Journal of Applied Meteorology and Climatology*, *49*(8), 1665-1680.

Zhang, J., Mu, Q., & Huang, J. (2016). Assessing the remotely sensed Drought Severity Index for agricultural drought monitoring and impact analysis in North China. *Ecological Indicators*, *63*, 296-309.

CHAPTER IV

MODELING EVAPOTRANSPIRATION OF WINTER WHEAT UNDER VARIABLE GRAZING AND TILLAGE MANAGEMENTS USING MULTIPLE REMOTELY SENSED SURFACE ENERGY BALANCE MODELS

Abstract: Remotely-sensed surface energy balance (RSEB) models are being widely used to map winter wheat (*Triticum aestivum* L.) evapotranspiration (ET) across the globe. However, RSEB models' ability to capture ET from rainfed winter wheat in Oklahoma (OK), U.S, where it is currently being managed under various grazing (grain-only, graze-grain, graze-out) and tillage (conventional tillage and no-till) conditions has not been evaluated yet. Hence, we evaluated five RSEB models: mapping evapotranspiration at high resolution with internalized calibration (METRIC), surface energy balance algorithm for land (SEBAL), triangular vegetation temperature (TVT), surface energy balance system (SEBS) and two-source energy balance (TSEB) against observed daily ET data from eight eddy covariance towers covering rainfed winter wheat fields under different management systems. Model performances based on daily ET retrieved using 28 near cloud-free Landsat image dates during the growing seasons showed wide variations among the five RSEB models. Considering all plots under all management conditions, SEBAL was found to be the best performing model (lowest root mean square error and mean absolute error) and TSEB was the poorest performing model. SEBAL results showed that grain-only wheat had the highest mean daily ET, followed by graze-grain and graze-out wheat. Among

the tillage treatments, conventional tillage had larger ET than no-till treatment. However, none of the differences among grazing and tillage practices were statistically significant (p>0.05).

1. Introduction

Evapotranspiration (ET) is a key phenomenon in the Earth's system that links water, energy, and carbon cycles (Fisher, 2017; Monteith, 1965; Wong, Cowan, & Farquhar, 1979). In agricultural systems, ET is also considered as a crop response to water availability and an indicator of agricultural productivity (Doorenbos and Kassam, 1979). Thus, accurate ET information is crucial for decision making, especially in areas with limited water resources. However, estimating ET is challenging as the process involves complex feedbacks between weather, soil, crop, and environment (Allen, Pereira, Raes, & Smith, 1998). Major limitations in the commonly used field-based ET estimation methods (e.g., eddy flux towers, sap flux, lysimeter, Bowen ratio) are their inability to accurately capture ET from large heterogeneous areas (due to small footprint) and extensive maintenance requirements. Remote sensing approaches can provide spatially distributed ET at varying temporal and spatial resolutions (Anderson et al., 2011; Gowda et al., 2007) and require no maintenance by user in case of space-borne imaging. In particular, models developed on the principle of remotely-sensed surface energy balance (RSEB) based on the thermal infrared (TIR)-derived land or radiometric surface temperature (Ts) have been promising for reliable mapping of ET (Liou and Kar, 2014). ET from RSEB models is estimated as a residual of the surface energy balance:

$$LE = \lambda ET = Rn - G - H \quad (4.1)$$

where LE is the latent heat flux (W m^{-2}), λ is latent heat of vaporization (J kg^{-1}), Rn is net radiation (W m^{-2}), G is the soil heat flux (W m^{-2}), and H is the sensible heat flux (W m-2).

Several RSEB models have been developed in the past (Allen, Tasumi, & Trezza, 2007; Anderson, Norman, Mecikalski, Otkin, & Kustas, 2007; Bastiaanssen, Menenti, Feddes & Holtslag, 1998; Jiang and Islam, 1999; Norman, Kustas, & Humes, 1995; Roerink, Su, & Menenti, 2000; Senay et al., 2013; Su, 2002). Based on the scaling of ET within an image, RSEB models can be broadly categorized into contextual-based (CB) and pixel-based (PB). The CB models use actual end-member (hot and cold) pixels or theoretical hot/dry and cold/wet surfaces representing the extreme ranges of ET within an image (Price, 1990). On the other hand, PB models are independent of the contextual information (i.e. Ts values from other pixels) within an image. Studies on the evaluation of RSEB models have shown varying performances of models across different land covers and climatic conditions (Bhattarai, Shaw, Quackenbush, Im, & Niraula, 2016; French, Hunsaker, & Torp, 2015; Losgedaragh and Rahimzadegan, 2018; Lian and Huang, 2016; Timmermans, Kustas, Anderson, & French, 2007; Wagle, Bhattarai, Gowda, & Kakani, 2017). Distributed ET information from RSEB models has been applied in a range of applications in agriculture. For example, in estimating productivities of land and water (Bastiaanssen, Thiruvangadachari, Sakthivadivel, & Modlen, 1999), predicting crop yield (Mo et al., 2005), assessing the performances of irrigation schemes (Taghvaeian, Osterberg, Sritharan, & Watts, 2018; Yang, Shang, & Jiang, 2012), and administering water rights and regulations (Allen, Tasumi, Morse, & Trezza, 2005). Field-scale ET maps can assist with developing precision irrigation scheduling and minimizing water losses in irrigated agriculture.

Wheat (Triticum aestivum L.) is one of the major crops grown worldwide. Winter wheat constitutes about 80% of global wheat production (Becker-Reshef, Vermote, Lindeman, & Justice, 2010) and between 70-80% of the wheat production in the US (Vocke and Ali, 2013). In Oklahoma (OK), winter wheat occupies about 75% of total cropland (Vitale, Godsey, Edwards, & Taylor, 2011) and is often integrated with cattle production systems for grazed forage. Grazing management practices in OK, similar to many other states in the southern Great Plains, include

three main options of no grazing (grain-only), graze-grain (dual propose), and graze-out (no-grain production) (Phillips, Alberts, Albin, & Hatfield, 1999). Grazing reduces crop biomass and canopy cover, potentially decreasing crop transpiration and increasing water loss from soil evaporation. Alternatively, grazing delays shoot biomass accumulation (Winter and Thompson, 1987), potentially reducing soil water uptake during the early season and increasing root zone water availability at the later stages of the growing season. Mapping ET over winter wheat fields can provide valuable information on crop water consumption under varying grazing managements, which is an indication of soil moisture availability for the next cropping season. The information can also be used to investigate the response of wheat systems to extreme weather events.

Previous studies (Yan and Wu, 2014; Zwart et al., 2010) have applied RSEB models for estimating ET from wheat systems. Li et al. (2008) evaluated Surface Energy Balance Algorithm for Land model (SEBAL; Bastiaanssen et al., 1998) in semi-arid and semi-humid climates in eastern China and reported that SEBAL seasonal ET estimates were within 4.3% of lysimeter measurements. Another study (Bala, Rawat, Mishra, & Srivastava, 2015) in semi-arid climates in India reported mean absolute error of 0.19 mm d^{-1} from SEBAL when compared with lysimeter. Limited studies have considered RSEB model evaluation under variable management practices. For example, French et al. (2007) evaluated the Two Source Energy Balance model (TSEB; Norman et al., 1995) using very high-resolution (0.5 m) aerial imagery in arid central Arizona, US, under variable plant densities and fertilizer managements and found a better performance of TSEB model over sparse and low-nitrogen treatments. However, model biases were up to 1.29 mm d^{-1} (36.6 W m^{-2}) when compared with ET estimates based on soil water depletion. Only limited studies, such as Tang et al. (2011) have considered multiple RSEB models in a single study. This study evaluated the performance of three RSEB models (two PB and one CB) in a semi-humid region and reported a better agreement from PB models when compared against the

estimates from large aperture scintillometer observations. The study also highlighted the higher uncertainty in H and LE from PB models with uncorrected Ts and leaf area index inputs.

Current literature on RSEB-based ET over wheat systems provides no clear evidence on which model is considered better under different management and climatic conditions. This is largely because the majority of studies on winter wheat only considered single or a few (up to 3) models, which and a single validation site across all image. Use of single-pixel validation across all images provide no clear guidance on the ability of a RSEB model to derive accurate spatially explicit ET maps, since ET varies highly across a spatial scale with response to changes in land cover and land use, soil moisture, climate, and other variables. As such, evaluation of multiple pixels over a single image can provide more useful guidance on the accuracy of spatially distributed ET maps. To the best of our knowledge, only limited studies have considered such for evaluating winter wheat ET maps. In addition, no study has evaluated RSEB models for estimating winter wheat ET under variable grazing and tillage managements. We aim to overcome these shortcomings in this study by evaluating five RSEB models over eight eddy covariance (EC) sites covering winter wheat under various tillage and grazing practices in the southern Great Plains. The major objectives of this study were to: i) identify the best RSEB model for characterizing ET from winter wheat under different tillage and grazing management practices and ii) evaluate the response of daily ET obtained from the best RSEB model to variable tillage and grazing practices in the study area.

2. Materials and Methods

2.1 Site Description

The study site was the Grazinglands Research on agroEcosystems and the ENvironment (GREEN) farm, which is part of the U.S. Department of Agriculture (USDA), Agricultural

Research Service, Grazinglands Research Laboratory and the Long-Term Agroecosystem Research (LTAR) network. The GREEN farm (35°33’29” N, 98°1’50” W, ~414 m above sea level) is located near El Reno in central Oklahoma (warm temperate climate) and has a total area of 178 ha. The primary soils are Bethany silt loams, Renfrow-Kirkland silt loams, and Norge silt loams, characterized as deep, well-drained, loamy soils with clayey or loamy subsoil (NRCS, 1999). This research farm has five zones with different exposures facing north, south, and east, as well as a rolling and undulating landscape without a dominant exposure (Wagle et al., 2018). Out of five zones in the GREEN farm, four were under four-year crop rotation of canola, grain-only wheat, graze-grain wheat, and graze-out wheat. The remaining zone was under continuous graze-out wheat. In addition, each zone was divided into two plots, one under no-till and the other under conventional tillage. This resulted in a total number of 10 experiment plots. Figure 4.1 demonstrates the location of each experimental plot along with the eddy covariance flux towers that were installed near the center of eight plots.

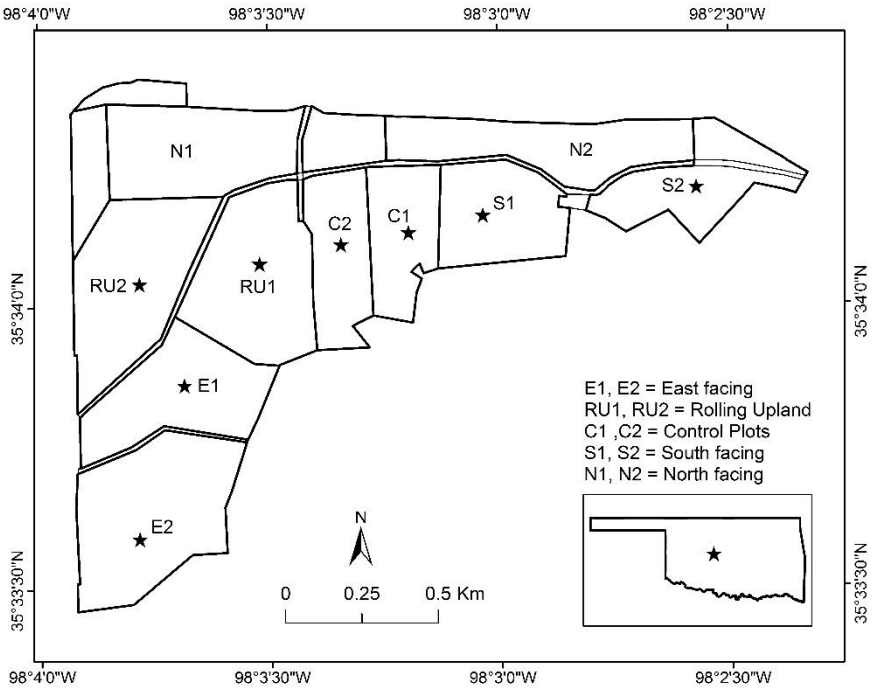

Figure 4.1. Layout of the experimental plots. The stars represent the flux towers location.

All plots were under rainfed conditions. The tillage management started in 2015 with conventional till and no-till. All conventional till experiment plots (E2, RU2, C2, S2) were tilled between 5.0 to 15.0 cm (2 to 6 inches) deep for seedbed preparation and weed control. All experimental plots were managed for fertilizer, herbicide, and pesticide using common practices in the region for a high production potential (Wagle et al., 2018). The data for this study were collected during two winter wheat/canola growing seasons (September-June) of 2016-2017 and 2017-2018. The seasonal rainfall in 2016-2017 was 741 mm, which was 20 mm greater than the normal (1981-2010) rainfall of 721 mm. The 2017-2018 season was drier with only 476 mm rainfall (36% less than normal). Graze-out wheat was planted earliest during mid-September and grazed twice. The first grazing period was from mid-November to mid-March and the second grazing period from mid-March to mid-May. The graze-grain wheat was planted next during the third week of September, grazed during mid-November to the first week of February, and harvested in the first week of June. The grazing rates were one stocker per 0.607 ha (1.5 acre) in the fall and one stocker per 0.405 ha (1 acre) in the spring. Grain-only wheat was planted in mid-October and harvested in mid-June. Both crops were planted at the approximate rate of 90 kg seeds ha^{-1} on ~19 cm (7.5 inch) row spacing with an east-west orientation. More information about the grazing and tillage practices of each plot during the study period is presented in Table 4.1.

Table 4.1. Summary of tillage and grazing management during the study period

Site ID	Area (ha)	Tillage Management	Grazing Management	
			2016-2017	2017-2018
E1	15	No-Till	Grain-only wheat	Graze-grain wheat
E2	22	Till	Grain-only wheat	Graze-grain wheat

RU1	21	No-Till	Canola	Grain-only wheat
RU2	20	Till	Canola	Grain-only wheat
C1	10	No-Till	Graze-out wheat	Graze-out wheat
C2	11	Till	Graze-out wheat	Graze-out wheat
S1	13	No-Till	Graze-grain wheat	Graze-out wheat
S2	13	Till	Graze-grain wheat	Graze-out wheat

2.2 RSEB Models

Five commonly used RSEB models were selected for evaluation in this study: three contextual-based (CB) and two pixel-based (PB) models. The selection of these models was based on their wide applicability and computational complexity. A brief explanation of each model is presented in the following sections.

2.2.1 CB Models

The three CB models included SEBAL, mapping evapotranspiration at high resolution with internalized calibration (METRIC; Allen et al., 2007) and triangle vegetation temperature (TVT; Jiang and Islam, 1999). SEBAL and METRIC use hot (minimum ET) and cold (maximum ET) pixels selected from each image to scale ET across all pixels through internal calibration of H. TVT relies on the triangular relationship between the NDVI and T_s and uses the hot and cold surfaces of the NDVI-T_s triangular structure to scale ET across all pixels without the need for calculating H. R_n is estimated by surface radiation balance as:

$$R_n = (1 - \alpha)R_s + \varepsilon_s \, \varepsilon_a \, \sigma \, T_a^4 - \varepsilon_s \, \sigma \, T_s^4 \quad (4.2)$$

where R_s is the incoming shortwave solar radiation (W m^{-2}), α is surface albedo (dimensionless) estimated using atmospheric corrections which is based on humidity data and digital elevation model (Tasumi, Allen, & Terezza, 2008), ε_s is surface emissivity (dimensionless) estimated as a function of leaf area index (LAI) for vegetation and using a normalized difference vegetation index (NDVI; Tucker, 1979) threshold (NDVI>0) for soil surface. For water and snow, ε_s was considered as a constant value (Allen et al., 2007). The LAI was estimated as a functional relationship with NDVI as described in Ershadi, McCabe, Evans, Chaney, and Wood, 2014. The ε_a is atmospheric emissivity and was estimated from atmospheric transmissivity (Bastiaanssen, 1995) which is a function of elevation (Allen et al., 1998). The T_a is air temperatures (K) and surface temperature T_s is estimated as a ratio of brightness temperature to $\varepsilon_s^{-0.25}$. σ is the Stefan-Boltzmann constant (5.67×10^{-8} W m^{-2} K^{-4}). G is estimated using empirical equations, such as given by Bastiaanssen, Menenti, Fddes, & Holtslag (1998) in relation to R_n, NDVI, and T_s.

$$\frac{G}{R_n} = \frac{(T_s - 273.15)}{\alpha}(0.0038\,\alpha + 0.0074\,\alpha^2)(1 - 0.98\,\mathrm{NDVI}^4) \qquad (4.3)$$

To estimate H, SEBAL and METRIC use hot and cold pixels as a boundary and representing opposite ET extremes within an image. The hot pixel is usually selected from the bare soil surface area within an image with smaller NDVI and larger T_s. The cold pixel is selected from well-irrigated high vigor (larger NDVI) area with smaller T_s. For the hot pixel, SEBAL assumes ET to be zero, however, METRIC uses a water balance equation (Allen et al., 1998) to account for possible residual evaporation from the hot pixel due to prior rainfall. For the cold pixel, SEBAL assumes H equal to zero, thus ET from the cold pixel is at the potential rate, whereas METRIC estimates H by rearranging equation 4.1 and assuming ET to be 5% higher than reference ET (ET_r; ASCE-EWRI, 2005). In this study, the selection of hot and cold pixels was made by an automated exhaustive search algorithm (Bhattarai, Quackenbush, Im, & Shaw, 2017). Both SEBAL and METRIC apply a linear relationship between dT (temperature difference

between two reference heights) and T_s at hot and cold pixels to estimate H by iteratively solving the equations for aerodynamic resistance (r_{ah}) and friction velocity (u_*) as shown in equation 4.5 and equation 4.6, respectively.

$$H = \frac{\rho \times c_p \times dT}{r_{ah}} \tag{4.4}$$

$$r_{ah} = \frac{1}{Ku_*}\left[\ln\left(\frac{z-d_0}{z_{0h}}\right) - \psi_{h(z-d_0)} + \psi_{h(z_{0h})}\right] \tag{4.5}$$

$$u_* = \frac{ku_b}{\ln\left(\frac{z_b}{z_{0m}}\right) - \psi_{m(z_b)}} \tag{4.6}$$

where ρ is air density (kg/m^3), c_p is air specific heat capacity (J kg^{-1} K^{-1}), K is Von Karman's constant (0.41), z is the reference height (m), d_0 is the zero-displacement height (m), u_b is the wind speed (m s^{-1}) at blending height z_b (200 m). The z_{0m} is the roughness length (m) for momentum transfer and estimated using an empirical relation with NDVI (van der Kwast et al., 2009), z_{oh} is the roughness length (m) for heat transfer. The ψ_m and ψ_h are the stability correction for momentum and heat transport, respectively. After computing H, R_n, and G, LE is estimated as a residual of the surface energy balance as shown in equation 4.1. METRIC estimates the instantaneous fraction of reference ET (ETrF) as a ratio of actual ET to ET_r and SEBAL estimates instantaneous evaporative fraction (Λ) as a ratio of LE to available energy ($R_n - G$).

Unlike the single set of hot and cold pixels in the SEBAL and METRIC models, the TVT model uses hot and cold edges derived from the NDVI-T_s triangular space to scale ET across all pixels within an image. This model uses a modified form of Priestley-Taylor's equation (Priestley and Taylor, 1972) as:

$$ET = \phi\left[\frac{\Delta}{\Delta + \gamma}\right](R_n - G) \tag{4.7}$$

where Φ (0 to 1.26) is a modified form of coefficient α and is calculated for each pixel (Φ_i) in the image using linear interpolation between maximum and minimum T_s for a given NDVI class. Readers are referred to Jiang and Islam (1999, 2003) for a detailed explanation of the model.

2.2.2 PB Models

The two PB models included TSEB and the surface energy balance system (SEBS; Su, 2002). SEBS uses a similar approach to SEBAL/METRIC in estimating R_n and G, and estimates H by solving the similarity equations for the wind speed profile (u) and the difference between the potential temperatures ($\theta_0 - \theta_a$):

$$u = \frac{u_*}{k}\left[\ln\left(\frac{z-d_0}{z_{0m}}\right) - \psi_m\left(\frac{z-d_0}{L}\right) + \psi_m\left(\frac{z_{0m}}{L}\right)\right] \quad (4.8)$$

$$\theta_0 - \theta_a = \frac{H}{Ku_*\rho_a C_p}\left[\ln\left(\frac{z-d_0}{z_{0h}}\right) - \psi_h\left(\frac{z-d_0}{L}\right) + \psi_h\left(\frac{z_{0h}}{L}\right)\right] \quad (4.9)$$

where L is the Monin-Obukhov length (m). SEBS computes H at dry (H_{dry}) and wet (H_{wet}) limits to maintain extremes for H. At the dry limit, LE is considered zero and at wet limit, it is assumed to be at a potential rate and estimated using the Penman-Monteith (P-M) equation (Monteith, 1965). After computing H, LE is estimated as the residual of SEB. After stabilization of H (see Su 2002 for details), estimated H_{dry} and H_{wet}, are used to compute relative evaporation (Λ_r), which is further used to compute Λ as:

$$\Lambda_r = 1 - \frac{H - H_{wet}}{H_{dry} - H_{wet}} \quad (4.10)$$

$$\Lambda = \frac{\Lambda_r(R_n - G - H_{wet})}{R_n - G} \quad (4.11)$$

Unlike all other models considered in this study (i.e. single-source SEB models), TSEB differentiates the canopy and soil layer and estimates R_n for each layer as:

$$R_{n,c} = H_c + LE_c \quad (4.12)$$

$$R_{n,s} = H_s + LE_s + G \quad (4.13)$$

where c and s subscripts denote canopy and soil components of each surface energy flux. $R_{n,c}$ and $R_{n,s}$ are estimated based on a method proposed by Kustas and Norman (1999). G is estimated only for the soil layer as a constant fraction of $R_{n,s}$ proposed by Choudhary, Idso, and Reginato (1987).

To estimate LE_c and LE_s, T_s is disaggregated into soil ($T_{s,s}$) and canopy ($T_{s,c}$). T_s is assumed to be linked with vegetation fraction (f_c) (Norman et al., 1995) as:

$$T_s=\left[f_c T_{s,c}^4+(1-f_c)T_{s,s}^4\right]^{1/4} \quad (4.14)$$

LE_c is estimated using the Priestley-Taylor equation (Priestly and Taylor, 1972) considering unstressed vegetation as:

$$LE_c=\alpha_{PT} f_g \left[\frac{\Delta}{\Delta+\gamma}\right] R_{n,c} \quad (4.15)$$

where α_{PT} is the Priestley-Taylor parameter, f_g is the fraction of LAI that is green (assumed to be actively transpiring), Δ is the slope of the saturation vapor pressure-temperature curve (kPa K^{-1}), and γ is the psychrometric constant (kPa K^{-1}).

Initially, α_{PT} is set to 1.26 and after estimating LE_c, H_c is estimated using series resistance network in TSEB (Norman et al., 1995). With the first estimate of $T_{s,c}$, $T_{s.s}$ is estimated from equation 4.14, and H_s and LE_s are estimated. If LE_s is negative, LE_c is reduced with an incremental decrease in α_{PT}, which increases $T_{s,c}$ and decreases $T_{s,s}$. The process is iterated until $T_{s,c}$ and $T_{s,s}$ agrees with T_s in equation 4.14, and realistic values of LE_c ($\geq$0) and LE_s ($\geq$0) are obtained. Further details are explained in Norman et al. (1995) and Kustas and Norman (1999).

2.3 Instantaneous to Daily ET

The instantaneous Λ and ETrF estimated from RSEB models during the satellite overpass was assumed to be constant for the day under clear-sky conditions (Brutsaert and Suginta, 1992; Allen et al., 2007). Thus, instantaneous Λ from SEBAL, SEBS, TVT and TSEBS was multiplied by daily R_n and a conversion factor of 86,400 and divided by λ to obtain daily ET in units of mm d^{-1}. For METRIC, instantaneous ETrF was multiplied by daily ET_r to compute daily ET.

2.4 Remote Sensing and Meteorological Data

Out of 42 Landsat images during two growing seasons, daily ET comparison was possible only for 28 days due to missing data from flux tower and filtering applied on ET data. The filtering included removing days with daily ET values less than 0.01 mm d^{-1} from flux tower or RSEB models, as well as days with potential biases in T_s estimation (T_s smaller than T_a due to the presence of thin cloud and/or cloud shadow). The at-surface reflectance, surface reflectance-based NDVI, and top-of-atmosphere (TOA) brightness temperature (T_b) images for selected dates were downloaded from the US Geological Survey Earth Resources Observation and Science Center Science Processing Architecture on Demand Interface. These products were atmospherically corrected and processed by the Landsat Ecosystem Disturbance Adaptive Processing System (LEDAPS) for Landsat 7 images (Masek et al., 2012) and the Landsat 8 Surface Reflectance Code (LaSRC) for Landsat 8 images (Vermote, Justice, Claverie, & Franch, 2016). The cloud and cloud shadow pixels from all remote sensing images were removed using the C programming language implementation of FMask algorithm (Zhu and Woodcock, 2012; Zhu, Wang, & Woodcock, 2015). The 30-m ground resolution 2011 National Land Cover Database (Homer et al., 2015) was used to identify the land covers for facilitating the selection of hot and cold pixels in SEBAL/METRIC. A common spatial subset of ~70 km×70 km covering the EC towers was used to process each Landsat image. Processing of all RSEB models except TSEB was carried out in Matlab (The Mathworks Inc., Natick, MA). TSEB was processed in Python using the algorithms available at https://github.com/hectornieto/pyTSEB.

The hourly weather data were obtained from four Oklahoma Mesonet stations (Brock et al., 1995; McPherson et al., 2007) located near the research site and within the spatial subset used in image processing. The quality assessment of hourly air temperature, solar radiation, wind speed, and relative humidity was performed as described in ASCE-EWRI (2005). The hourly ET_r was estimated following ASCE-EWRI (2005) and summed for 24-hour to obtain daily ET_r. An inverse distance weighted interpolation (power of two) was applied to create a 30-m grid equivalent to the spatial resolution of Landsat for each meteorological input parameter for use in the RSEB models.

2.5 Flux Data

The 30-min flux data were obtained from the eight eddy covariance towers installed near the center of research plots. The towers were 2.5 m tall and equipped with 3-D sonic anemometer (CSAT3, Campbell Scientific Inc., Logan, Utah, USA) and open path infrared gas analyzer (Li-7500-RS, LI-COR Inc., Lincoln, Nebraska, USA). The detailed description of the installation and instrumentation of towers is presented in Wagle et al. (2018). The energy balance closure was 0.77 during the study period. This error was corrected for 30-min data by following the constant Bowen-Ratio method of Twine et al. (2000). The corrected 30-min data were aggregated to obtain daily ET for comparison with estimates from RSEB models.

2.6 Model Evaluation

Considering the land use homogeneity around the flux tower locations, pixel subset-based analysis was conducted to evaluate the performance of RSEB models. The average ET of 3×3 pixels (90 m×90 m) centering the flux towers was used in comparison with flux tower ET. For statistical analysis mean absolute error (MAE) and root mean square error (RMSE) (Moriasi et al., 2007) were used. Linear regression lines with slope ‘a’ and intercept ‘b’ were also plotted and coefficient of determination (R2) was estimated to evaluate the fitness of models. A perfect fit is

represented by R2 equal to one, a slope of one and intercept of zero. Model performance was evaluated for all data combined. Daily ET from canola plots (RU1 and RU2 in 2016-2017) were not included for comparison.

2.7 Impacts of Grazing and Tillage on ET

After selecting the best RSEB model, the average daily ET from experimental plots were applied to evaluate the impact of grazing and tillage managements. Out of 42 available Landsat images, 33 images (15 in 2016-2017 and 18 in 2017-2018) were used for statistical analysis since some of the images were filtered as described in section 2.4. This number of images, however, was larger than the number of images used for daily ET comparisons against flux tower (28) since there was no limitation imposed by availability of flux data. The statistical evaluation of daily ET from different tillage and grazing managements was made by applying the linear mixed-effects models package (lme4) (Bates et al., 2015) in R software (R Foundation for Statistical Computing, Vienna, Austria). The evaluation was made by comparing the log-odds ratios of linear models at a significance level of 0.05 to analyze the impact on daily ET from tillage, grazing, and their interactions (main effects), considering experiment plots and growing season as random effects. Tukey's HSD test was applied to evaluate the differences among the mean daily ET from grazing and tillage managements.

3. Results and Discussion

3.1 Model Evaluation

The comparison of daily RSEB-based ET with flux towers showed an acceptable performance for all models with MAE less than 31 W m^{-2} and RMSE less than 42 W m^{-2} (Figure 4.2 and Table 4.2). METRIC and TSEB overestimated ET, whereas other models underestimated ET. SEBAL had the smallest MAE and RMSE, followed by TVT. Among all models, TSEB had

the largest MAE and RMSE. Overall, the three CB models had smaller RMSE and MAE than PB models.

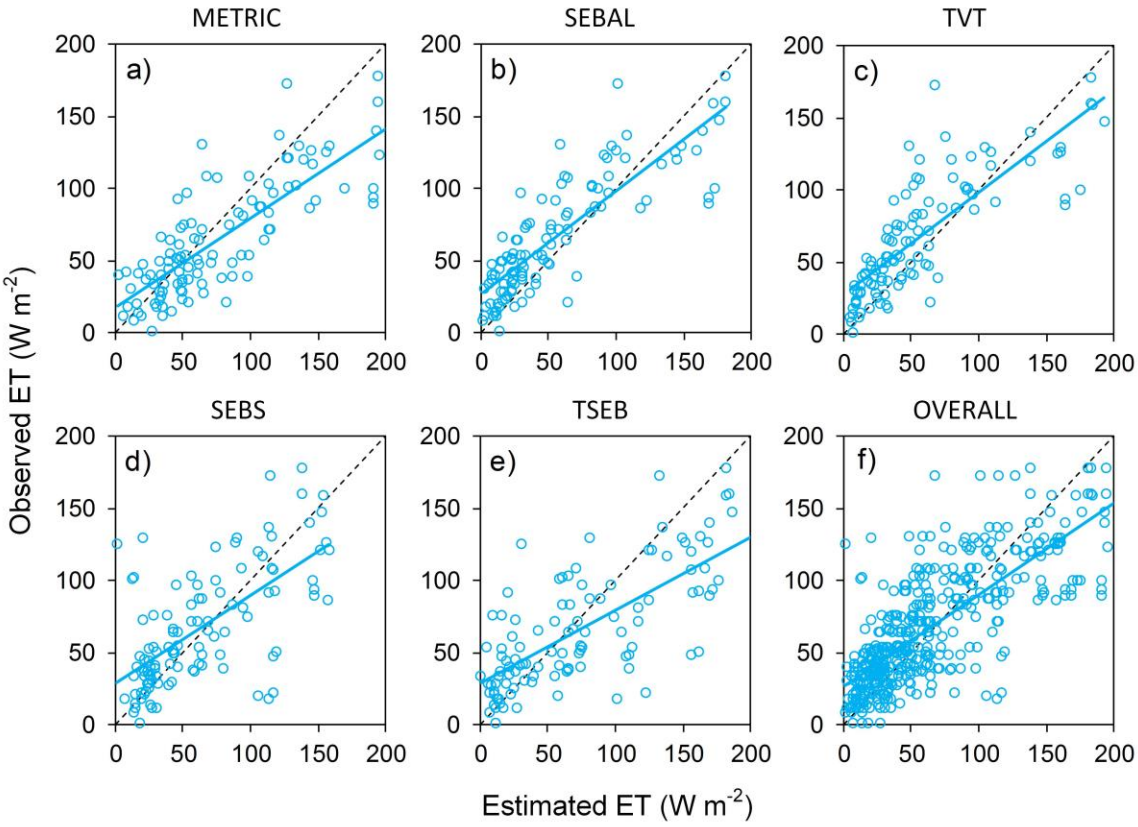

Figure 4.2. Comparison of daily ET between flux tower observations (y-axis) and RSEB models (x-axis).

Table 4.2. Statistical comparison of observed and estimated daily ET

Statistic	Contextual-Based			Pixel-Based	
	METRIC	SEBAL	TVT	SEBS	TSEB
MAE (W m^{-2})	25.8	22.5	22.8	25.2	30.5
RMSE (W m^{-2})	33.7	28.5	29.9	35.6	41.1

Based on regression lines plotted between observed and estimated daily ET, SEBAL had the largest R^2 of 0.71, followed by METRIC, TVT, TSEB, and SEBS (Table 4.3). In terms of

slope (a), SEBAL and TVT had the better fit than other models. METRIC had the smallest intercept (b) while the value of this parameter was similar for other regression models. Overall, regression lines of CB models had better fit than PB models.

Table 4.3. Slope, intercept and coefficient of determination of regression lines

Parameter	Contextual-Based			Pixel-Based	
	METRIC	SEBAL	TVT	SEBS	TSEB
a (slope)	0.62	0.71	0.71	0.61	0.51
b (intercept)	17.97	27.72	27.63	28.72	28.68
R^2	0.68	0.71	0.66	0.43	0.53

Previous studies on evaluating RSEB models have shown varying performances over different land covers and climates when compared with flux tower estimations. For example, Bhattarai et al. (2016) compared five RSEB models and reported a better performance from SEBS in daily ET estimation using Landsat images with RMSE of 20.1 W m^{-2} over multiple land covers under a humid climate of the southeast US. After SEBS, SEBAL provided the lowest RMSE of 23.5 W m^{-2}. Lian and Huang (2016) found a better performance from METRIC in the oasis-desert region of northwest China across multiple land covers with RMSE of 20.1 W m^{-2} and MBE of 12.5 W m^{-2}. In the high biomass sorghum in central Oklahoma, Wagle et al. (2017) reported the best performance (RMSE of 25.5 W m^{-2}) from Simplified Surface Energy Balance model (S-SEBI; Roerink et al., 2000), followed by SEBAL (27.5 W m^{-2}). Over native grassland and managed switchgrass in central and western Oklahoma, SEBS provided RMSE less than 50 W m^{-2} when using MODIS images (Khand et al., 2019). While the performances varied across

models, the biases from the present study are within a range of errors reported in previous studies for daily ET estimations.

RSEB models require several inputs representing crop characteristics and local weather, and the model performance differs with sensitivity to input parameters. Evaluating the models sensitivity is outside the scope of this study. However, an analysis was made to evaluate the performance of models with three main inputs representing crop characteristics, weather, and soil moisture. NDIV and/or LAI is a primary input representing crop characteristics. Results from this study show larger biases from all models at lower values of LAI (Figure 4.3a-e). When LAI was greater than 3, METRIC had the smallest mean bias of 5.4 W m^{-2}, followed by other CB models (SEBAL, TVT). These results show the inverse relation between ET estimation bias and LAI in CB models. However, such a relation did not exist for PB models.

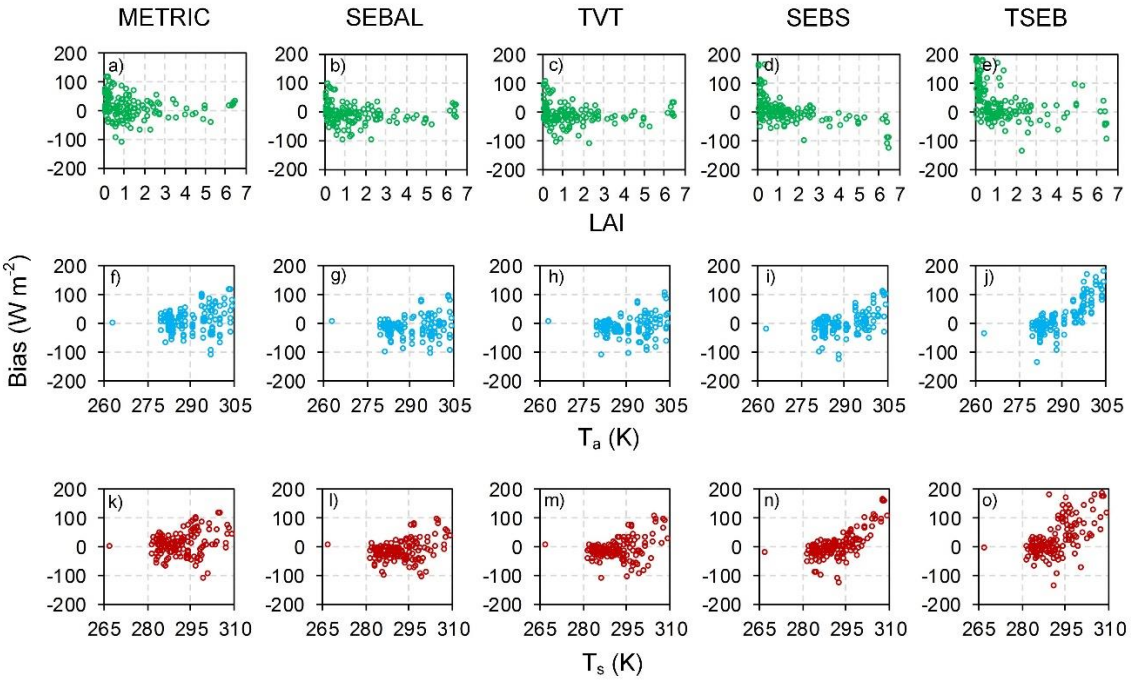

Figure 4.3. ET biases (estimated-observed) of RSEB models with respect to leaf area index (LAI, first row), instantaneous air temperature (T_a, second row), and surface temperature (T_s, third row).

PB models had a clear pattern of increasing ET bias (overestimation) with T_a, while this pattern was not as clear in the case of CB models (Figure 4.3f-j). For T_a > 300 K, TSEB showed largest mean bias of 116 W m^{-2}, followed by SEBS (74 W m^{-2}), while, mean biases from the CB models were less than 34 W m^{-2}. A similar response was observed in case of T_s, which is another key input parameter for all RSEB models. Biases from all models increased with an increase in T_s (Figure 4.3k-o), suggesting relatively poor performance of the models under drier conditions. Larger ET overestimation errors were observed from PB models (Figure 4.3n,o) at higher T_s compared to CB models (Figure 4.3k-m). The mean ET bias from PB models were up to 95 W m^{-2} (TSEB), whereas CB models provided bias within 41 W m^{-2} when T_s > 300 K.

The impact of T_s on modeled ET estimates could arise from uncertainties associated with T_s derivation or the approaches and assumptions made in the RSEB models to derive extreme surfaces (hot and cold pixels/edges). All three CB models are highly sensitive to the selection of domain (Long et al., 2011; Tang et al., 2013; Xia et al., 2016), as it could change the values (and locations) of extreme pixels used in these models. A different set of hot and cold pixels in SEBAL and METRIC produces completely different ET results for all other pixels in the image, if the T_s values of the new hot/cold pixels were significantly different (Tang et al., 2013). Long et al. (2011) reported that H might be biased by up to 25 W m^{-2} for a 2 K bias in the selected hot/cold pixel in SEBAL. Antecedent soil moisture at the bare ground or fallow agricultural land could induce biases in ET estimates from CB models, as LE may not be zero due to residual evaporation. Though METRIC uses the water balance to account residual evaporation from hot pixel (ETrFhot), ET estimation biases may increase if the maximum value for ETrFhot is not limited (Choi, Kustas, Anderson, & Allen, 2009). There might be cases when dry and wet surfaces are not well represented within an image, which could lead to biased ET estimates across a pixels from CB models. Xia et al. (2016) highlighted the sensitivity of the triangular ET model to spatial domain size and potential non- representation of dry and wet surfaces within the image.

Unlike CB models, PB models such as SEBS and TSEB use pixel level LAI and T_s information to scale ET for each pixel independent of ET values across the neighboring pixels. However, this makes the model more sensitive to the absolute values of LAI/T_s. For example, the characterization of aerodynamic conductance in SEBS is based on excess resistance parameter (kB^{-1}) based on LAI and surface roughness. Hence, any errors in these parameters will propagate to kB^{-1} and consequently H and LE. SEBS uses kB^{-1} to account for the difference between T_s and aerodynamic temperature (T_o), which is impossible to measure through remote sensing. This is semi-empirical in nature and could induce additional uncertainty in ET estimates (Bhattarai, Mallick, Brunsell, Sun, & Jian, 2018). TSEB relies on the Priestley-Taylor coefficient, which is variant with space and time (Komatsu, 2003; Yang et al., 2015) and is a major source of uncertainty (Colaizzi et al., 2012; Song et al., 2018). Apart from the uncertainties in the RSEB models, some errors are associated with flux tower observations and this should be considered when comparing the results with estimates of RSEB models. For example, flux tower data often lag the energy closure in order of 20% (Wilson et al., 2002) and the performance of RSEB models may vary depending on the energy balance closing approach used (Xia et al., 2016).

3.2 Impacts of Grazing and Tillage on ET

The mean daily ET from the two grazing managements (graze-grain and graze-out) are plotted versus daily ET from grain-only for each day of available Landsat imagery (Figure 4.4a). As this scatterplot shows, the ET from grain-only wheat was larger, especially for daily ET estimates larger than 2.0 mm d^{-1}. Daily ET from tilled wheat is also plotted against no-till ET in Figure 4.4b. Although a difference between the two tillage managements appeared to exist at daily ET estimates larger than 2.0 mm d^{-1}, the overall difference between tillage practices was considerably smaller than the difference between grazing practices. To demonstrate ET differences on a distributed basis, one ET map from mid-March of each growing seasons is also presented in Figure 4.5. These maps show the potential impacts of grazing managements as this

time is closer to the end of first grazing (mid-March) at graze-out plots and the end of grazing (first week of February) at graze-grain plots. As expected, the daily ET rates were higher from grain-only plots (E1 and E2 in 2016-2017 and RU1 and RU2 in 2017-2018). The impact of grazing on wheat ET may vary depending on grazing intensity and duration. Grazing reduces canopy cover and exposes the soil surface for more evaporation; however, transpiration may be lowered due to reduced biomass. Thus, the combined impact of evaporation and transpiration may increase or decrease ET. A study (Harrison, Evans, Dove, & Moore, 2012) in south-eastern Australia reported both increase and decrease in ET based on grazing intensity and duration. Grazing may also decrease water stress in rainfed winter wheat and enhance leaf photosynthesis (Harrision, Kelman, Moore, & Evans, 2010), which may increase transpiration rates when sufficient soil moisture is available in the root zone.

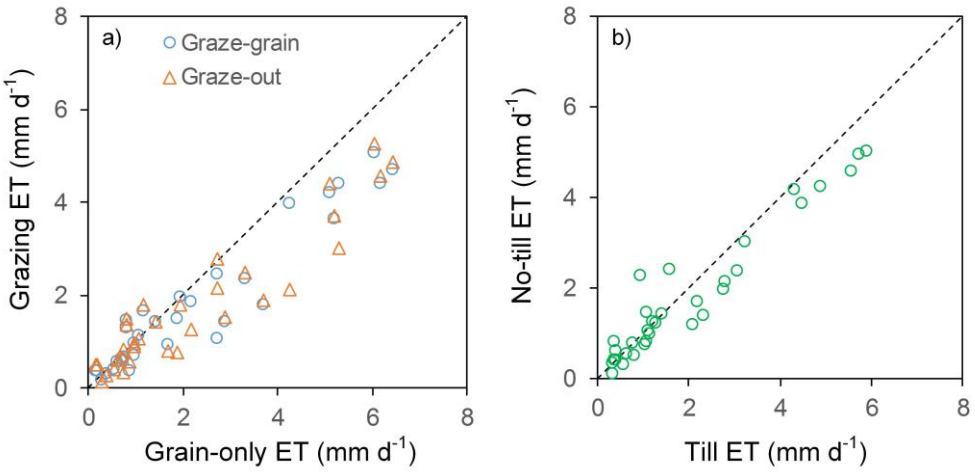

Figure 4.4. Mean daily ET comparison form grazing (a) and tillage (b) managements

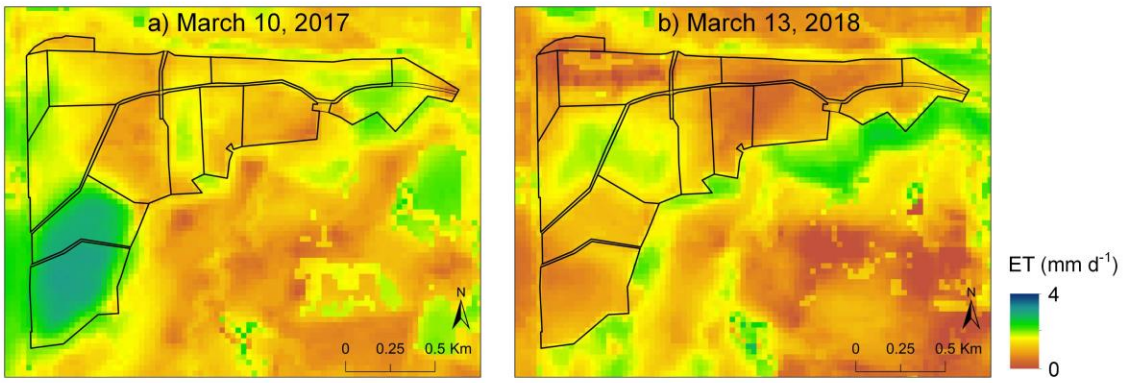

Figure 4.5. Daily ET maps of experiment plots during early March of 2016-2017 (a) and 2017-2018 (b) growing seasons.

When averaged over all overpass dates in the two studied seasons, the mean daily ET was higher from grain-only wheat, followed by graze-grain wheat and graze-out wheat (Table 4.4). Grain-only mean daily ET was 2.25 mm d^{-1}, which was 26% greater than graze-grain and 49% greater than graze-out. Statistical analysis, however, indicated the differences in mean daily ET from grazing managements were not significantly different (Table 4.4). The mean daily ET from tilled plots was 12% higher than no-till plots, but these mean ET were not statistically different either (Table 4.5). It should be noted that no significant interactions between grazing and tillage managements were found (p=0.824).

Table 4.4. Mean daily ET from grain-only, graze-grain and graze-out winter wheat. The different letters following the mean daily ET represent statistically significant differences at the 0.05 level.

Grazing managements	Grain-only	Graze-grain	graze-out
ET (mm d^{-1})	2.25a	1.79a	1.51a

Table 4.5. Mean daily ET from till and no-till winter wheat. The different letters following the mean daily ET represent statistically significant differences at the 0.05 level.

Tillage managements	Till	No-till
ET (mm d^{-1})	1.90a	1.70a

4. Conclusions

Five RSEB models were evaluated to estimate daily ET from rainfed winter wheat under variable grazing (grain-only, graze-grain, graze-out) and tillage (till, no-till) management. The study was conducted for two winter wheat growing seasons (2016-2017 and 2017-2018) in central Oklahoma, U.S. All RSEB models provided reasonably good performance, with SEBAL being the best performing model (MAE=22.5 W m^{-2}, RMSE=28.5 W m^{-2}) when compared with flux tower estimations. The daily ET from SEBAL model was then used to evaluate the impact of variable grazing and tillage managements on ET. On average, daily ET from grain-only wheat was 2.25 mm d^{-1}, which was 26% greater than graze-grain and 49% greater than graze-out 27%. However, these differences were not statistically significant. Mean daily ET from tilled plots was 1.90 mm d^{-1}, which was 12% more than that from no-till plots. This difference was not statistically significant either. The study showed the potential application of RSEB models for capturing field-scale ET variations from different grazing/tillage management.

References

Allen, R. G., Pereira, L. S., Raes, D., & Smith, M. (1998). Crop Evapotranspiration-Guidelines for computing crop water requirements-FAO Irrigation and drainage paper 56. Fao, Rome, 300(9), D05109.

Allen, R. G., Tasumi, M., & Trezza, R. (2007). Satellite-based energy balance for mapping evapotranspiration with internalized calibration (METRIC)—Model. *Journal of irrigation and drainage engineering*, *133*(4), 380-394.

Allen, R. G., Tasumi, M., Morse, A., & Trezza, R. (2005). A Landsat-based energy balance and evapotranspiration model in Western US water rights regulation and planning. *Irrigation and Drainage systems*, *19*(3-4), 251-268.

Anderson, M. C., Hain, C., Wardlow, B., Pimstein, A., Mecikalski, J. R., & Kustas, W. P. (2011). Evaluation of drought indices based on thermal remote sensing of evapotranspiration over the continental United States. *Journal of Climate*, *24*(8), 2025-2044.

Anderson, M. C., Norman, J. M., Mecikalski, J. R., Otkin, J. A., & Kustas, W. P. (2007). A climatological study of evapotranspiration and moisture stress across the continental United States based on thermal remote sensing: 1. Model formulation. *Journal of Geophysical Research: Atmospheres*, *112*(D10).

ASCE-EWRI. (2005). The ASCE Standardized Reference Evapotranspiration Equation. Environmental and Water Resources Institute of the ASCE, Report by the Task Committee on Standardization of Reference Evapotranspiration.

Bala, A., Rawat, K. S., Misra, A. K., & Srivastava, A. (2016). Assessment and validation of evapotranspiration using SEBAL algorithm and Lysimeter data of IARI agricultural farm, India. *Geocarto International*, *31*(7), 739-764.

Bastiaanssen W. G., Menenti, M., Feddes, R. A., & Holtslag, A. A. M. (1998). A remote sensing surface energy balance algorithm for land (SEBAL). 1. Formulation. *Journal of - hydrology*, *212*, 198-212.

Bastiaanssen, W. G. M. (1995). *Regionalization of surface flux densities and moisture indicators in composite terrain: A remote sensing approach under clear skies in Mediterranean climates*. SC-DLO.

Bastiaanssen, W. G., Thiruvengadachari, S., Sakthivadivel, R., & Molden, D. J. (1999). Satellite remote sensing for estimating productivities of land and water. *International Journal of Water Resources Development*, *15*(1-2), 181-194.

Bates, D., Maechler, M., Bolker, B., Walker, S., Christensen, R. H. B., Singmann, H., Dai, B., Grothendieck, G., & Green, P. (2015). Package 'lme4'. *Convergence*, *12*(1).

Becker-Reshef, I., Vermote, E., Lindeman, M., & Justice, C. (2010). A generalized regression-based model for forecasting winter wheat yields in Kansas and Ukraine using MODIS data. *Remote sensing of environment*, *114*(6), 1312-1323.

Bhattarai, N., Mallick, K., Brunsell, N.A., Sun, G., & Jain, M. (2018). Regional evapotranspiration from an image-based implementation of the Surface Temperature Initiated Closure (STIC1.2) model and its validation across an aridity gradient in the conterminous US. *Hydrology and Earth System Science*, *22*, 2311-2341.

Bhattarai, N., Quackenbush, L. J., Im, J., & Shaw, S. B. (2017). A new optimized algorithm for automating endmember pixel selection in the SEBAL and METRIC models. *Remote sensing of environment*, *196*, 178-192.

Bhattarai, N., Shaw, S. B., Quackenbush, L. J., Im, J., & Niraula, R. (2016). Evaluating five remote sensing based single-source surface energy balance models for estimating daily evapotranspiration in a humid subtropical climate. *International journal of applied earth observation and geoinformation*, *49*, 75-86.

Brock, F. V., Crawford, K. C., Elliott, R. L., Cuperus, G. W., Stadler, S. J., Johnson, H. L., & Eilts, M. D. (1995). The Oklahoma Mesonet: a technical overview. *Journal of Atmospheric and Oceanic Technology*, *12*(1), 5-19.

Brutsaert, W., & Sugita, M. (1992). Application of self-preservation in the diurnal evolution of the surface energy budget to determine daily evaporation. *Journal of Geophysical Research: Atmospheres*, *97*(D17), 18377-18382.

Choi, M., Kustas, W. P., Anderson, M. C., Allen, R. G., Li, F., & Kjaersgaard, J. H. (2009). An intercomparison of three remote sensing-based surface energy balance algorithms over a corn and soybean production region (Iowa, US) during SMACEX. *Agricultural and Forest Meteorology*, *149*(12), 2082-2097.

Choudhury, B. J., Idso, S. B., & Reginato, R. J. (1987). Analysis of an empirical model for soil heat flux under a growing wheat crop for estimating evaporation by an infrared-temperature based energy balance equation. *Agricultural and Forest Meteorology*, *39*(4), 283-297.

Colaizzi, P.D., Kustas, W.P., Anderson, M.C., Agam, N., Tolk, J.A., Evett, S.R., Howell, T.A., Gowda, P.H., & O'Shaughnessy, S.A. (2012). Two-source energy balance model estimates of evapotranspiration using component and composite surface temperatures. *Advances in water resources*, *50*, 134-151.

Doorenbos, J., & Kassam, A. H. (1979). Yield response to water. *Irrigation and drainage paper*, *33*, 257.

Ershadi, A., McCabe, M. F., Evans, J. P., Chaney, N. W., & Wood, E. F. (2014). Multi-site evaluation of terrestrial evaporation models using FLUXNET data. *Agricultural and Forest Meteorology*, *187*, 46-61.

Fisher, J. B., Melton, F., Middleton, E., Hain, C., Anderson, M., Allen, R., McCabe, M. F., Hook, S., Baldocchi, D., Townsend, P. A., Kilic, A., Tu, K., Miralle, D. D., Parret, J., Lagouarde, J. Waliser, D., Purdy, A. J., French, A., Schimel, D., Famiglietti, J. S.,

Stephens, G., & Wood, E. F. (2017). The future of evapotranspiration: Global requirements for ecosystem functioning, carbon and climate feedbacks, agricultural management, and water resources. *Water Resources Research*, *53*(4), 2618-2626.

French, A. N., Hunsaker, D. J., & Thorp, K. R. (2015). Remote sensing of evapotranspiration over cotton using the TSEB and METRIC energy balance models. *Remote Sensing of Environment*, *158*, 281-294.

French, A. N., Hunsaker, D. J., Clarke, T. R., Fitzgerald, G. J., Luckett, W. E., & Pinter Jr, P. J. (2007). Energy balance estimation of evapotranspiration for wheat grown under variable management practices in central Arizona. *Transactions of the ASABE*, *50*(6), 2059-2071.

Gowda, P. H., Chavez, J. L., Colaizzi, P. D., Evett, S. R., Howell, T. A., & Tolk, J. A. (2007). Remote sensing based energy balance algorithms for mapping ET: Current status and future challenges. *Transactions of the ASABE*, *50*(5), 1639-1644.

Harrison, M. T., Evans, J. R., Dove, H., & Moore, A. D. (2012). Recovery dynamics of rainfed winter wheat after livestock grazing 1. Growth rates, grain yields, soil water use and water-use efficiency. *Crop and Pasture Science*, *62*(11), 947-959.

Harrison, M. T., Kelman, W. M., Moore, A. D., & Evans, J. R. (2010). Grazing winter wheat relieves plant water stress and transiently enhances photosynthesis. *Functional Plant Biology*, *37*(8), 726-736.

Homer, C., Dewitz, J., Yang, L., Jin, S., Danielson, P., Xiang, G., Coulston, J. Herold, N., Wickham, J. (2015). National Landcover Database 2001 (NLCD 2001). *Multi-Resolution Land Characteristics Consortium*.

Jiang, L., & Islam, S. (1999). A methodology for estimation of surface evapotranspiration over large areas using remote sensing observations. *Geophysical research letters*, *26*(17), 2773-2776.

Jiang, L., & Islam, S. (2003). An intercomparison of regional latent heat flux estimation using remote sensing data. *International Journal of Remote Sensing*, *24*(11), 2221-2236.

Khand, K., Taghvaeian, S., Gowda, P., & Paul, G. (2019). A Modeling Framework for Deriving Daily Time Series of Evapotranspiration Maps Using a Surface Energy Balance Model. *Remote Sensing*, *11*(5), 508.

Komatsu, T. S. (2003). Toward a robust phenomenological expression of evaporation efficiency for unsaturated soil surfaces. *Journal of Applied Meteorology*, *42*(9), 1330-1334.

Kustas, W. P., & Norman, J. M. (1999). Evaluation of soil and vegetation heat flux predictions using a simple two-source model with radiometric temperatures for partial canopy cover. *Agricultural and Forest Meteorology*, *94*(1), 13-29.

Li, H., Zheng, L., Lei, Y., Li, C., Liu, Z., & Zhang, S. (2008). Estimation of water consumption and crop water productivity of winter wheat in North China Plain using remote sensing technology. *Agricultural Water Management*, *95*(11), 1271-1278.

Lian, J., & Huang, M. (2016). Comparison of three remote sensing based models to estimate evapotranspiration in an oasis-desert region. *Agricultural Water Management*, *165*, 153-162.

Liou, Y. A., & Kar, S. K. (2014). Evapotranspiration estimation with remote sensing and various surface energy balance algorithms—A review. *Energies*, *7*(5), 2821-2849.

Long, D., Singh, V. P., & Li, Z. L. (2011). How sensitive is SEBAL to changes in input variables, domain size and satellite sensor?. *Journal of Geophysical Research: Atmospheres*, *116*(D21).

Losgedaragh, S. Z., & Rahimzadegan, M. (2018). Evaluation of SEBS, SEBAL, and METRIC models in estimation of the evaporation from the freshwater lakes (Case study: Amirkabir dam, Iran). *Journal of Hydrology*, *561*, 523-531.

Masek, J. G., Vermote, E. F., Saleous, N., Wolfe, R., Hall, F. G., Huemmrich, K. F., Gao, F., Kutler, J., Lim, T. K. (2012). LEDAPS Landsat calibration, reflectance, atmospheric correction preprocessing code. *ORNL DAAC*.

McPherson, R. A., Fiebrich, C. A., Crawford, K. C., Kilby, J. R., Grimsley, D. L., Martinez, J. E., Basara, J. B., Illston, B. G., Morris, D. A., Kloesel, K. A., Melvin, A. D., Sirvantava, H., WOolfinbarger, M., Bostic, J.P., & Demko, D. B. (2007). Statewide monitoring of the mesoscale environment: A technical update on the Oklahoma Mesonet. *Journal of Atmospheric and Oceanic Technology*, *24*(3), 301-321.

Mo, X., Liu, S., Lin, Z., Xu, Y., Xiang, Y., & McVicar, T. R. (2005). Prediction of crop yield, water consumption and water use efficiency with a SVAT-crop growth model using remotely sensed data on the North China Plain. *Ecological Modelling*, *183*(2-3), 301-322.

Monteith, J. L. (1965). Evaporation and environment. In *Symp. Soc. Exp. Biol.*, *19*, 205-23.

Moriasi, D. N., Arnold, J. G., Van Liew, M. W., Bingner, R. L., Harmel, R. D., & Veith, T. L. (2007). Model evaluation guidelines for systematic quantification of accuracy in watershed simulations. *Transactions of the ASABE*, *50*(3), 885-900.

Norman, J. M., Kustas, W. P., & Humes, K. S. (1995). Source approach for estimating soil and vegetation energy fluxes in observations of directional radiometric surface temperature. *Agricultural and Forest Meteorology*, *77*(3-4), 263-293.

NRCS (Natural Resources Conservation Service), USDA. 1999. Soil survey of Canadian county, Oklahoma. USDA-NRCS and Okla. Agric. Exp. Stn., Stillwater, OK.

Phillips, W. A., Albers, R., Albin, R., & Hatfield, E. E. (1999). The effect of herbicide application during the winter on forage production, animal performance, and grain yield of winter wheat. *The Professional Animal Scientist*, *15*(2), 141-147.

Price, J. C. (1990). Using spatial context in satellite data to infer regional scale evapotranspiration. *IEEE transactions on Geoscience and Remote Sensing*, *28*(5), 940-948.

Priestley, C. H. B., & Taylor, R. J. (1972). On the assessment of surface heat flux and evaporation using large-scale parameters. *Monthly weather review*, *100*(2), 81-92.

Roerink, G. J., Su, Z., & Menenti, M. (2000). S-SEBI: A simple remote sensing algorithm to estimate the surface energy balance. *Physics and Chemistry of the Earth, Part B: Hydrology, Oceans and Atmosphere*, *25*(2), 147-157.

Senay, G. B., Bohms, S., Singh, R. K., Gowda, P. H., Velpuri, N. M., Alemu, H., & Verdin, J. P. (2013). Operational evapotranspiration mapping using remote sensing and weather datasets: A new parameterization for the SSEB approach. *JAWRA Journal of the American Water Resources Association*, *49*(3), 577-591.

Song, L., Liu, S., Kustas, W.P., Nieto, H., Sun, L., Xu, Z., Skaggs, T.H., Yang, Y., Ma, M., & Xu, T. (2018). Monitoring and validating spatially and temporally continuous daily evaporation and transpiration at river basin scale. *Remote sensing of Environment*, *219*, 72-88.

Su, Z. (2002). The Surface Energy Balance System (SEBS) for estimation of turbulent heat fluxes. *Hydrology and earth system sciences*, *6*(1), 85-100.

Taghvaeian, S., Neale, C. M., Osterberg, J. C., Sritharan, S. I., & Watts, D. R. (2018). Remote Sensing and GIS Techniques for Assessing Irrigation Performance: Case Study in Southern California. *Journal of Irrigation and Drainage Engineering*, *144*(6), 05018002.

Tang, R., Li, Z. L., Chen, K. S., Jia, Y., Li, C., & Sun, X. (2013). Spatial-scale effect on the SEBAL model for evapotranspiration estimation using remote sensing data. *Agricultural and Forest Meteorology*, *174*, 28-42.

Tang, R., Li, Z. L., Jia, Y., Li, C., Sun, X., Kustas, W. P., & Anderson, M. C. (2011). An intercomparison of three remote sensing-based energy balance models using Large Aperture Scintillometer measurements over a wheat–corn production region. *Remote Sensing of Environment*, *115*(12), 3187-3202.

Tasumi, M., Allen, R. G., & Trezza, R. (2008). At-surface reflectance and albedo from satellite for operational calculation of land surface energy balance. *Journal of hydrologic engineering*, *13*(2), 51-63.

Timmermans, W. J., Kustas, W. P., Anderson, M. C., & French, A. N. (2007). An intercomparison of the surface energy balance algorithm for land (SEBAL) and the two-source energy balance (TSEB) modeling schemes. *Remote Sensing of Environment*, *108*(4), 369-384.

Tucker, C. J. (1979). Red and photographic infrared linear combinations for monitoring vegetation. *Remote Sensing of Environment*, *8*(2), 127-150.

Twine, T. E., Kustas, W. P., Norman, J. M., Cook, D. R., Houser, P., Meyers, T. P., Prueger, J. H., Starks, P. J., & Wesely, M. L. (2000). Correcting eddy-covariance flux underestimates over a grassland. *Agricultural and Forest Meteorology*, *103*(3), 279-300.

Van der Kwast, J., Timmermans, W., Gieske, A., Su, Z., Olioso, A., Jia, L., Elberts, J., Karssenberg, D., de Jong, S., de Jong, Steven (2009). Evaluation of the Surface Energy Balance System (SEBS) applied to ASTER imagery with flux-measurements at the SPARC 2004 site (Barrax, Spain). *Hydrology and Earth System Sciences Discussions*, *6*(1), 1165-1196.

Vermote, E., Justice, C., Claverie, M., & Franch, B. (2016). Preliminary analysis of the performance of the Landsat 8/OLI land surface reflectance product. *Remote Sensing of Environment*, *185*, 46-56.

Vitale, J. D., Godsey, C., Edwards, J., & Taylor, R. (2011). The adoption of conservation tillage practices in Oklahoma: Findings from a producer survey. *Journal of Soil and Water Conservation*, *66*(4), 250-264.

Vocke, G., & Ali, M. (2013). *US wheat production practices, costs, and yields: Variations across regions* (No. 1476-2017-3890).

Wagle, P., Bhattarai, N., Gowda, P. H., & Kakani, V. G. (2017). Performance of five surface energy balance models for estimating daily evapotranspiration in high biomass sorghum. *ISPRS Journal of Photogrammetry and Remote Sensing*, *128*, 192-203.

Wagle, P., Gowda, P. H., Northup, B. K., Turner, K. E., Neel, J. P., Manjunatha, P., & Zhou, Y. (2018). Variability in carbon dioxide fluxes among six winter wheat paddocks managed under different tillage and grazing practices. *Atmospheric Environment*, *185*, 100-108.

Wilson, K., Goldstein, A., Falge, E., Aubinet, M., Baldocchi, D., Berbigier, P., Brenhofer, C., Ceulemans, R., Dolman, H., Field, C., Grelle, A., Ibrom, A., Law, B. E., Kowalski, A., Meyers, T., Moncerieff, J., Monson, R., Oechel, W., Tenhunen, J., Valentini, R., & Verma, S. (2002). Energy balance closure at FLUXNET sites. *Agricultural and Forest Meteorology*, *113*(1-4), 223-243.

Winter, S. R., & Thompson, E. K. (1987). Grazing Duration Effects on Wheat Growth and Grain Yield 1. *Agronomy Journal*, *79*(1), 110-114.

Wong, S. C., Cowan, I. R., & Farquhar, G. D. (1979). Stomatal conductance correlates with photosynthetic capacity. *Nature*, *282*(5737), 424.

Xia, T., Kustas, W. P., Anderson, M. C., Alfieri, J. G., Gao, F., McKee, L., Prueger, J.H., Geli, H. M. E., Neale, C. M. U., Sanchez, L., Alsina, M. M., & Wang, Z. (2016). Mapping evapotranspiration with high-resolution aircraft imagery over vineyards using one-and two-source modeling schemes. *Hydrology and Earth System Sciences*, *20*(4), 1523.

Yan, N., & Wu, B. (2014). Integrated spatial–temporal analysis of crop water productivity of winter wheat in Hai Basin. *Agricultural Water Management*, *133*, 24-33.

Yang, Y., Long, D., Guan, H., Liang, W., Simmons, C., & Batelaan, O. (2015). Comparison of three dual-source remote sensing evapotranspiration models during the MUSOEXE-12 campaign: Revisit of model physics. *Water resources research*, *51*(5), 3145-3165.

Yang, Y., Shang, S., & Jiang, L. (2012). Remote sensing temporal and spatial patterns of evapotranspiration and the responses to water management in a large irrigation district of North China. *Agricultural and Forest Meteorology*, *164*, 112-122.

Zhu, Z., & Woodcock, C. E. (2012). Object-based cloud and cloud shadow detection in Landsat imagery. *Remote sensing of environment*, *118*, 83-94.

Zhu, Z., Wang, S., & Woodcock, C. E. (2015). Improvement and expansion of the Fmask algorithm: Cloud, cloud shadow, and snow detection for Landsats 4–7, 8, and Sentinel 2 images. *Remote Sensing of Environment*, *159*, 269-277.

Zwart, S. J., Bastiaanssen, W. G., de Fraiture, C., & Molden, D. J. (2010). WATPRO: A remote sensing based model for mapping water productivity of wheat. *Agricultural Water Management*, *97*(10), 1628-1636.

CHAPTER V

CONCLUSIONS

Vegetation index (VI)-based and remotely sensed surface energy balance (RSEB) models were evaluated and a framework was developed to construct daily time series of ET maps using a RSEB model. The study showed the application of a simple VI-based model using a single Landsat image for mapping annual riparian ET within good accuracy, which can be useful for rapid assessment of interannual variation in riparian ET with fewer data and resources. The daily and annual ET maps from the modeling framework captured the spatial and temporal variability of ET across nine climate divisions of Oklahoma. The study highlighted a range of applications of the modeling framework, such as for identifying water-scarce regions and areas with larger impact of drought on crop water use, and for integration in decision and policy making. Evaluation of five RSEB models in central Oklahoma identified the best performing RSEB model that can capture field-scale ET variability of rainfed winter wheat under variable grazing and tillage managements.

VITA

Kul Bikram Khand

Candidate for the Degree of

Doctor of Philosophy

Thesis: ASSESSMENT AND DEVELOPMENT OF REMOTELY SENSED EVAPOTRANSPIRATION MODELING APPROACHES

Major Field: Biosystems and Agricultural Engineering

Biographical:

Education:

Completed the requirements for the Doctor of Philosophy in Biosystems Engineering at Oklahoma State University, Stillwater, Oklahoma in May, 2019.

Completed the requirements for the Master of Science in Agricultural and Biosystems Engineering at South Dakota State University, Brookings, South Dakota in 2014.

Completed the requirements for the Bachelor of Science in Agricultural Engineering at Tribhuvan University, Kathmandu, Nepal in 2010.

Experience:

Graduate Research Assistant 2016-2019
Oklahoma State University, Stillwater, Oklahoma

Research Assistant 2014-2016
Geospatial Sciences Center of Excellence, South Dakota State University, Brookings South Dakota

Graduate Research Assistant 2012-2014
South Dakota State University, Brookings, South Dakota

Energy and Environment Officer 2010-2012
Office of District Development Committee, Dang, Government of Nepal

Professional Memberships:

United States Committee on Irrigation and Drainage 2016-present
American Geophysical Union 2014-present
American Society of Agricultural and Biological Engineers 2012-present